THE UNIVERSITY
of EDINBURGH

Resolving fingerprints of unconventional gas resources and methane rich groundwaters in the UK.

Rebecca Marie Chambers

Thesis submitted for the degree of Doctor of Philosophy

School of GeoSciences

University of Edinburgh

2024

Author Declaration

I declare that all work in this thesis, unless otherwise referenced or acknowledged, is entirely my own. None of this work has been submitted for any degree or professional qualification other than that specified on the title page.

The work presented in Chapter 3 was previously published in the Earth Science, Systems and Society Journal as "Constraining the Geochemical Fingerprints of Gases from the UK Carboniferous Coal Measures at the Glasgow Geoenergy Observatories Field Site, Scotland" by myself and co-authors Stuart Gilfillan, Gareth Johnson, and Adrian Boyce. This study was conceived by all authors. I carried out the data analysis, visualisation, and lead writing of the paper.

Rebecca M Chambers

January 2024

Abstract

Interest in the utilisation of subsurface geoenergy technologies (such as geothermal or unconventional gas extraction) has increased in recent years, as they are considered key in achieving Net Zero carbon emissions targets. 90% of UK homes used (predominantly gas) fossil fuels for heating, cooking, and hot water in 2020; with heating and cooling accounting for 51% of the energy demand in 2018 globally. However, there are several manageable, but significant techno-societal risks associated with the usage of the subsurface that has to be reduced, such as resource sustainability and efficiency, reservoir quality, operation maintenance, ground gases and environmental change. Determining the presence, magnitude, and origin of subsurface gases, and how their geochemical fingerprints evolve within the shallow subsurface is vital to developing an understanding of how to manage the risk posed by ground gases in geoenergy technology development. One of the risk factors in the development of such technologies is the potential for contamination of potable groundwater resources. As such, it is key to establish whether deep gas that is released by changes to the subsurface can be categorically identified at shallow depths; and distinguished from shallow biogenically derived methane sources. This thesis aims to characterise the subsurface geochemical conditions of potential geoenergy technology sites using a range of geochemical fingerprinting techniques.

The UK Geoenergy Observatory in Glasgow is a unique facility for investigating shallow, low-temperature mine water thermal energy within abandoned and flooded workings. Here, the first CH_4 and CO_2 concentration-depth profiles and stable isotope ($\delta^{13}C_{CH4}$, $\delta^{13}C_{CO2}$, and δD_{CH4}) profiles obtained from UK mine workings are presented, through analysis of headspace gas samples degassed from cores and chippings collected during construction. These are used to investigate the variability of gas fingerprints with depth within unmined Carboniferous coal measures and Glasgow coal mine workings. Stable isotope compositions of CH_4 provide evidence of a biogenic source, with carbonate reduction being the primary pathway of CH_4 production. Gas samples collected at depths of 63 to 79m exhibit enrichments in $^{13}C_{CH4}$ and ^{2}H, indicating the oxidative consumption of CH_4. This correlates with their proximity to the Glasgow Ell mine workings, which will have increased exposure to O_2 from the atmosphere as

a result of mining activities. CO_2 gas is more abundant than CH_4 throughout the succession in all three boreholes, exhibiting high $\delta^{13}C_{CO2}$ values relative to the CH_4 present. $\delta^{13}C_{CO2}$ values become progressively lower at shallower depths (above 90m), which can be explained by the increasing influence of shallow groundwaters containing a mixture of dissolved marine carbonate minerals (~0‰) and soil gas CO_2 (-26‰) as depth decreases. These findings provide an insight into the variability of mine derived gases within 200m of the surface and provide an important 'time-zero' record of the site.

The Vale of Pickering was first identified as a potential target for exploitation of unconventional gas resources, and whilst such exploration has ceased within the UK at present, the Vale of Pickering site is now being considered for potential geoenergy technology development. Groundwater and gas samples collected from the region provide an opportunity to establish how geochemical tracers, such as stable isotopes and noble gases, can be used to distinguish hydrocarbon source rocks and identify potential migration of deep gas to shallow aquifer bodies. Stable isotope compositions of CH_4 provide evidence of two distinct methane sources, with methane in both the shallow superficial and Corallian groundwater samples being produced biogenically by CO_2 reduction; and methane within the Third Energy gas samples exhibiting a distinct thermogenic gas signature. Both $^3He/^4He$ and $^4He/^{20}Ne$ ratios are elevated in comparison to atmospheric values, and evidence potential mixing between deep gases (KM5) and the atmosphere. From ^4He generation calculations, it is evident that measured ^4He concentrations cannot be generated from the in-situ decay of U and Th within the Vale of Pickering stratigraphy alone. Therefore, ^4He must be sourced from an external radiogenic flux. In order to further investigate how ^4He noble gas signatures change with depth within the subsurface, a coupled a hydro-chemical model of the Vale of Pickering was developed and is outlined in this thesis. From this, a better understanding of the migration of deep sourced methane to the shallow groundwaters in the Vale of Pickering is resolved, incorporating the likely evolution of gas signatures through migration.

The use of noble gas geochemistry alongside gas composition and stable isotope ratio allows for the better characterisation of geochemical signatures of ground gases, and the

identification of different methane sources within the subsurface. This thesis highlights the need for an understanding of the fluid migration pathways and their associated geochemical signatures of ground gases, and establishes key environmental baselines in the event of future geoenergy technology development of the sites.

Lay Summary

In order to achieve net zero climate goals of reducing global heating to within 2°C by 2050, there is a real need for a rapid 'energy transition'. Globally, energy is still primarily generated through the combustion of fossil fuels, with energy related CO_2 emissions at their highest recorded levels in 2022. As such, in order to de-carbonise, there is a need for new low carbon 'geoenergy' technologies to extract and store energy (for example, geothermal energy and carbon capture and storage). As these geoenergy technologies use the subsurface either at shallow or increasing depths, there are a number of technical and societal risks associated with their development and use, which need to be addressed if they are to become key to tackling climate change.

One risk associated with using the subsurface is the risk of mobilising ground gases during development of the site, resulting in the potential for contamination of groundwater resources or gas leakage into infrastructures. In order to reduce the risk of contamination, and to increase public acceptance, it is necessary to establish an environmental baseline prior to the site being developed. By identifying the sources of gas within the ground, and what their geochemical signature is like, confidence in detecting any future gas contamination increases.

The aim of this research is to identify the presence and origin of different sources of subsurface gases (such as methane) and investigate how its signature changes as it moves through the ground to the surface. This thesis aims to understand the geochemical signature of methane within two potential geoenergy sites (the Geoenergy Observatory, Glasgow and the Vale of Pickering, Yorkshire) using a range of geochemical fingerprinting techniques.

By using a combination of different geochemical tools (such as stable isotope and noble gases) in establishing environmental baselines, the origin and movement of methane within the subsurface can be better characterised.

Acknowledgments

Firstly, I would like to thank my supervisory team, Stuart Gilfillan, Chris McDermott, and Pauline Smedley. Thank you for supporting me throughout my PhD, for your guidance, feedback, and encouragement when the finish line seemed so far from sight. Thanks to Katriona Edlmann, for providing a listening ear and support whenever I needed it. Thanks also to the BGS for allowing me to tag along on your quarterly monitoring rounds. Thank you to Terry Donnelly at SUERC, for showing me the ropes of the methane line. I hope you are finally enjoying your well-deserved retirement.

A big thank you goes to all the friends I've made on this PhD journey. To everyone in the Grant Institute- thank you for all the laughs over 11am coffees and Pub Fridays. A shout out to booth buddies, past and present, thank you for putting up with my venting, frequent sighing, and Christmas decorations. You have all been a big support. A special thanks must go to a few people whose support and friendship has got me through the last few years. To Mylène, thank you for being such a good friend and for your endless support. Thank you for never saying no to a late-night stress walk. Dylan, thank you for grounding me to reality when my stress got too much, and for all the support and laughs over the last few years. We got there, and we done it. Fiona, thank you for your support and advice over PhD, jobs, life, and everything in between. Sophie, thanks for the laughs, the wine nights, and allowing me to stress-cry on your couch. Gina, thank you for being a constant friend, even from the other side of the world. For always lending an ear, whether over cocktail evenings or on a beach in Hawaii.

A massive thank you goes to my family and friends, whose constant support and encouragement got me to the finish line. Mum and Dad, thank you for always believing in me and being my biggest supporters. Your unwavering support, constant encouragement and even (on the odd occasion) being my data assistant, have been key to me being where I am today. Thank you for never doubting me, even when I doubted myself. You have picked me up, dusted me off, and got me back on my feet more times than I can count. It means more than you will ever know. Eve and Jordan, thank you for the endless Facetime calls, pick me ups, and encouragement. I could not have done it without both of your support. To my wee Grans, who despite not quite understanding whether a PhD was 'a real job' or not, were

always there to listen and provide a well needed cuppa. I'm glad I can tell you both I've finally finished. Jacqueline, thank you for listening and supporting me whenever I felt I could not do it. You truly are the best friend a person could have. Finally, to Anthony, thank you for your never-ending belief that I could do it. Thank you for your patience through the late-night stress writing, the imposter syndrome, and bad moods. You always managed to combat them with laughs, hugs, and de-stress dances. Thank you for the countless meals cooked when I'd forgotten to eat when writing. Despite you 'not having a clue' about my PhD, this thesis would 100% not have been finished without you. Thank you.

Table of Contents

Author Declaration ..... *v*

Abstract ..... *vii*

Lay Summary ..... *xi*

Acknowledgments ..... *xiii*

Table of Contents ..... *xv*

Table of Figures ..... *xviii*

1 Introduction *1*

1.1 Establishing environmental baselines for UK geoenergy technology sites **1**

1.2 Methane and unconventional gas extraction **1**

1.3 Gas monitoring **3**

1.4 Sources of methane in the subsurface **4**

1.4.1 Biogenic methane 5

1.4.2 Thermogenic methane 6

1.4.3 Abiogenic methane 7

1.5 Distinguishing methane sources **7**

1.5.1 Hydrocarbon abundance and stable isotopes 7

1.5.2 Noble gases 8

1.6 Potential hazards of subsurface gases **11**

1.6.1 Risks of methane and CO_2 in the subsurface 11

1.6.2 Methane and groundwater 11

1.7 Subsurface methane and the methane budget **12**

1.8 Research Aims **13**

1.9 Thesis Outline: **13**

1.10 References **15**

2 Techniques and Methodology *21*

2.1 Chapter Overview **21**

2.2 Study Locations **21**

2.2.1 The Glasgow Geoenergy Observatory Field Site 21

2.2.2 The Vale of Pickering, Yorkshire 22

2.3 Sample collection **22**

2.3.1 Sample collection for Glasgow UKGEOS site 22

2.3.2 Sample collection for Vale of Pickering site 23

2.4 Analytical procedures **25**

2.4.1 Major gas concentrations 25

2.4.2 Stable isotope analysis 25

2.4.3 Noble gas analysis 27
2.5 Numerical Modelling 28
2.5.1 Modelling approach and code 28
2.5.2 Numerical modelling overview 28
2.6 References 31
3 Constraining the geochemical fingerprints of gases from the UK Carboniferous Coal Measures at the Glasgow Geoenergy Observatories Field Site, Scotland. 33
3.1 Chapter Overview 33
3.2 Introduction 34
3.3 Setting of the UK Geoenergy Observatory in Glasgow, Scotland 36
3.4 Materials and Methods 38
3.5 Results 41
3.5.1 CH_4 and CO_2 Gas Concentrations from Core and Cutting Samples 41
3.5.2 CH_4 and CO_2 Stable Isotope Values 43
3.6 Discussion 44
3.6.1 Subsurface CH_4 Sources at the Glasgow Observatory 44
3.6.2 CO_2 Signatures 46
3.6.3 Stable Isotope Profiles with Depth 48
3.6.4 Lessons for the monitoring of minewater geothermal sites 50
3.7 Conclusions 51
3.8 References 53
4 Stable isotope and noble gas characterisation of subsurface methane from the Vale of Pickering, Yorkshire 59
4.1 Chapter Overview 59
4.2 Introduction 59
4.3 Geological setting of the Vale of Pickering 61
4.4 Sampling and analytical techniques 64
4.4.1 Sample collection 64
4.4.2 Sample analysis 64
4.5 Results 66
4.5.1 Major gas compositions 66
4.5.2 Stable isotope ratios 66
4.5.3 Noble gas compositions- Gas samples 67
4.5.4 Noble gas compositions- Groundwater samples 73
4.6 Discussion 74
4.6.1 Subsurface CH_4 sources at the Vale of Pickering 74
4.6.2 Origin of noble gases 76
4.6.3 Geochemical integration for subsurface characterisation 80
4.7 Conclusions 83
4.8 References 85

5 Hydrogeological and mass transport modelling of radiogenic ^{4}He noble gas within the Vale of Pickering subsurface 91

5.1 Chapter Overview 91

5.2 Introduction 91

5.3 Gas signatures of the Vale of Pickering 94

5.4 Conceptual model 96

5.5 Modelling approach 97

5.5.1 Model parameterisation 98

5.5.2 Model assumptions and simplifications 103

5.6 Modelling Results 105

5.6.1 He migration via diffusion and dispersion of thermogenic gas 105

5.6.2 Effect of groundwater flushing 106

5.6.3 Model limitations and future work 110

5.7 Discussion 112

5.7.1 Implications for the use of modelling and geochemical fingerprinting techniques 112

5.8 Conclusions 113

5.9 References 114

6 Summary and Future work 119

6.1 Chapter 3: Constraining the Geochemical Fingerprints of Gases from the UK Carboniferous Coal Measures at the Glasgow Geoenergy Observatories Field Site, Scotland. . 119

6.1.1 Chapter summary 119

6.1.2 Future work 121

6.2 Chapter 4: Stable isotope and noble gas characterisation of subsurface methane from the Vale of Pickering, Yorkshire 122

6.2.1 Chapter summary 122

6.2.2 Future work 123

6.3 Chapter 5: Hydrogeological and mass transport modelling of radiogenic ^{4}He noble gas within the Vale of Pickering subsurface 124

6.3.1 Chapter summary 124

6.3.2 Future work 125

6.4 References 126

Appendix A- Full gas composition and stable isotope results 127

Appendix B Model Theory 137

B1 Empirical Process Laws 137

B.1.1 Groundwater flow 137

B1.2 Mass transport 138

B.2 Groundwater flow equation derivation 139

Table of Figures

Figure 1-1: Schematic diagram illustrating the different types of methane sources within the subsurface (Bell et al., 2017). 4
Figure 1-2: Classification of methane sources plot highlighting the different methane signatures (SM= secondary methane), as well as the influence of methane source mixing, oxidation, and sulphate reduction on isotopic signatures. Plot adapted from Whiticar, 1999 and Milkov and Etiope 2018. 8
Figure 1-3: Diagram highlighting the different sources of noble gases within the subsurface: atmosphere, crustal, and mantle (Byrne et al., 2017). 9
Figure 2-1: Relative methane concentrations with depth for de-ionised and N_2 stored samples, highlighting higher exsolved gas concentrations from de-ionised water storage. 23
Figure 2-2: A shows the isojars used to collect the Glasgow UKGEOS core and cutting samples, which were filled either with N_2 gas or de-ionised water and sealed shut. B is a diagram of the copper tube sampling system, highlighting the steel clamps which form the cold weld seal. C shows the copper tube sampling set up in the field. 24
Figure 2-3: Gas combustion line at SUERC, which was used for methane and CO_2 gas stable isotope analysis. Photo shows the Glasgow UKGEOS Isojars connected directly to the extraction inlet for the line. 26
Figure 3-1:The UK Geoenergy Observatory is located in the Eastern side of Glasgow, the largest city in Scotland, located next to the River Clyde, in the Midland Valley of Scotland. The site consists of 12 boreholes, located at five sites, four of these are located within the Cuningar Loop formed by a meander of the River Clyde, with the GGC01 borehole located at site 10 in the Dalmarnock area. Contains Ordnance Survey data © Crown copyright and database rights. All rights reserved [2021] Ordnance Survey (100025252). 37
Figure 3-2: Composite logs of GGC01, GGA05, and GGA08 boreholes, and the depths of the core and cutting samples that were obtained for stable isotope analysis. The borehole logs indicate the major coal seams (Glasgow Upper, Glasgow Ell Index, Glasgow Ell, Glasgow Main), with Glasgow Ell and Glasgow Main coal seams have been mined in the shallow GGA05 and GGA08 boreholes. These seams can be correlated to unmined coal seams in GGC01. 39
Figure 3-3: Stratigraphic log of BH GGC01 and CH_4 and CO_2 concentrations with depth (black dashed lines indicate coal seams). The figure highlights that increased concentrations of CH_4 gas correlate to areas immediately surrounding the unmined coal seams in the subsurface. The highest CO_2 concentrations occurred in samples with lowest CH_4 concentrations, or where CH_4 was absent. 41
Figure 3-4: Stratigraphic log of BH GGA05 and CH_4 and CO_2 concentrations with depth (black dashed lines indicate coal seams and grey dashed boxes indicate coal mine workings). CH_4 was solely detected at 57 to 67m depth in a cluster of samples, in the succession directly above the Glasgow Ell mine workings. The CO_2 gas did not show the same trend, and was present throughout the stratigraphic succession. 42
Figure 3-5: Stratigraphic log of BH GGA08 and CH_4 and CO_2 concentrations with depth black dashed lines indicate coal seams and grey dashed boxes indicate coal mine workings). CH_4 was identified at four stratigraphic depths; all of which correspond to areas of coal seams or mine workings. Conversely, CO_2 was present throughout the entire stratigraphic sequence, and generally present in higher concentrations than CH_4. 43
Figure 3-6: Plot of δD_{CH4} and $\delta^{13}C_{CH4}$ stable isotopic analyses of CH_4 gas exsolved from core and cutting samples from GGC01, GGA05, and GGA08 boreholes. (Secondary CH_4 (SM) boundary indicated in green and thermogenic CH_4 boundary indicated in purple). Processes that affect the isotopic and molecular composition are highlighted (oxidation and thermochemical sulphate

reduction). Mixing of microbial gases produced through carbonate reduction and methyl fermentation is indicated by the blue mixing arrow, with mixing of thermogenic and microbial methane indicated by the purple mixing arrow. The majority of samples plot within the biogenic CH_4 zone, with a potential mixing of both carbonate reduction and methyl type fermentation sources. Enriched samples plotting outside of biogenic origin fields are a result of CH_4 oxidation. The classification areas of biogenic and thermogenic CH_4 sources are adapted from Whiticar, 1999, and the plot is adapted from Milkov and Etiope, 2018. 45
Figure 3-7: Isotope combination plot of $\delta^{13}C_{CH4}$ and $\delta^{13}C_{CO2}$ data from GGC01, GGA05, and GGA08 boreholes; with isotope fractionation lines and partitioning trajectories as a result of CH_4 formation and oxidation processes. The majority of samples exhibit greater ^{12}C enrichment with an isotopic fractionation indicative of CH_4 production by carbonate reduction. The three enriched samples that plot around 5% isotope fractionation indicate CH_4 oxidation, as ^{12}C is preferentially removed resulting in a decrease in isotopic fractionation between $^{13}C_{CH4}$ relative to $^{13}C_{CO2}$. Isotope plot adapted from Whiticar, 1999. 46
Figure 3-8: Isotopic depth plots of CH_4 and CO_2 $\delta^{13}C$ values from GGC01, GGA05, and GGA08 boreholes; with the corresponding stratigraphy. CH_4 stable isotopes have no clear correlation with depth, with a consistent biogenic signature present, and a distinct zone of enriched CH_4 in the area surrounding the Glasgow Ell mine workings. CO_2 gas exhibits a consistent depleted $^{13}C_{CO2}$ signature with shallower depth, highlighting the increasing influence of shallow groundwater within the subsurface. 49
Figure 4-1: Geological map of the Vale of Pickering, highlighting the bedrock geology, faults, and the Kirby Misperton well site (blue square) (Ward et al., 2019). BGS and Third Energy sample locations are highlighted as blue circles, with the KMA well site containing both KM5 and BHE sample localities. 62
Figure 4-2: Bernard plot of gas dryness (C_1/C_2+C_3) versus $\delta^{13}C_{CH4}$ (Bernard et al., 1976). All groundwater samples plot distinctly within the biogenic methane field, with the deep gas samples plotting within the thermogenic gas range. 67
Figure 4-3: $^{20}Ne/^{22}Ne$ vs $^{21}Ne/^{22}Ne$ plot with air, with solid black lines showing air-MORB and air-crust mixing. Dashed black line shows mass fractionation processes, with all Vale of Pickering samples falling on or near the mass fractionation line. Errors are 1s. 69
Figure 4-4: Plot of δD_{CH4} and $\delta^{13}C_{CH4}$ stable isotopic analyses of CH_4 gas from Vale of Pickering samples. (Secondary CH_4 (SM) boundary indicated in green and thermogenic CH_4 boundary indicated in purple). Processes that affect the isotopic and molecular composition are highlighted (oxidation). Mixing of microbial gases produced through carbonate reduction and methyl fermentation is indicated by the blue mixing arrow, with mixing of thermogenic and microbial methane indicated by the purple mixing arrow. All groundwater samples plot within the biogenic CH_4 zone, within the carbonate reduction pathway, with the deep gas samples plotting firmly within the thermogenic methane zone. The classification areas of biogenic and thermogenic CH_4 sources are adapted from Whiticar, 1999, and the plot is adapted from Milkov and Etiope, 2018. 75
Figure 4-5: Isotope combination plot of $\delta^{13}C_{CH4}$ and $\delta^{13}C_{CO2}$ data from BGS groundwater samples from sites 15 and 42 (Smedley et al., in review); with isotope fractionation lines and partitioning trajectories as a result of CH_4 formation and oxidation processes. The majority of samples exhibit greater ^{12}C enrichment with an isotopic fractionation indicative of CH_4 production by carbonate reduction. There are two slightly enriched samples that may potentially indicate methane oxidation. Isotope plot adapted from Whiticar, 1999. 76
Figure 4-6: $^{3}He/^{4}He$ vs $^{4}He/^{20}Ne$ plot for Vale of Pickering samples. The mixing trajectory between the deep gas Pickering sample and ASW is shown (dashed black line). It is evident that samples fall along a trend of mixing between shallow ASW like groundwater and a deep, radiogenic ^{4}He signature,

highlighting the potential for the migration of radiogenic ^{4}He from depth. From the mixing line, it can be estimated that approximately 2 to 50 % of ^{4}He is sourced from depth. 1s error bars are smaller than symbols. 77
Figure 4-7: Theoretical concentration profiles of ^{4}He against depth for the Kirkham Abbey Fm, Sherwood Sandstone, Corallian, and Kimmeridge Clay units, modelled after Andrews et al., 1991 for the diffusion coefficient of water ($D=0.0315 m^2/a$). ^{4}He concentration data for groundwater and gas samples are also plotted with depth and highlight samples do not fit any of the modelled stored ^{4}He profiles, with all groundwater and gas samples having an additional ^{4}He contribution. 80
Figure 4-8: *$^{84}Kr/^{36}Ar$ vs $^{20}Ne/^{36}Ar$ (**A**) and $^{132}Xe/^{36}Ar$ vs $^{20}Ne/^{36}Ar$ (**A**) plots for the Vale of Pickering samples. The $^{84}Kr/^{36}Ar$ vs $^{20}Ne/^{36}Ar$ (**A**) plot highlights that groundwater samples exhibit a signature characteristic of mixing between Air and ASW, with the exception of BGS site 38 which is enriched in $^{84}Kr/^{36}Ar$ relative to ASW. Again, the Third Energy samples plot distinctly separate from groundwater samples. Batch and Rayleigh fractionation lines (batch mixing= black, Rayleigh fractionation of degassed water-gas= red, and Rayleigh fractionation (water)=blue) plotted highlight that high $^{20}Ne/^{36}Ar$ ratios can be accounted for through the re-dissolution of noble gases into a degassed groundwater.* 82
Figure 4-9: $^{4}He/^{20}Ne$ vs. $CH_4/^{36}Ar$ plot for the Vale of Pickering groundwater samples. The trend of increasing $^{4}He/^{20}Ne$ and $CH_4/^{36}Ar$ shows groundwater equilibration with a methane rich source at greater depths, with all groundwater samples exceeding ASW values. During biogenic methanogenesis, there is no mechanism for He, Ne, or Ar production, and so values expected are $CH_4/^{36}Ar < CH_4$ solubility and $^{4}He/^{20}Ne$=ASW (blue square) (Darrah et al., 2015). All samples exceed these values, with all samples except the groundwater sample collected from BGS site 15 plotting above CH_4 saturation. As such, elevated ^{4}He values must be from an exogeneous and non-biogenic source (Darrah et al., 2015). 1s error bars are smaller than symbols. 83
Figure 5-1: Conceptual diagram highlighting noble gas sources within the subsurface and groundwater systems (Lollar and Ballentine, 2009). 93
Figure 5-2: Conceptual diagram of Vale of Pickering subsurface, highlighting the hydraulically disconnected Corallian aquifer and unconfined, shallow superficial aquifer. The two identified methane sources are highlighted, with methane produced biogenically in shallower depths, and thermogenic methane within the primary reservoir of the Kirkham Abbey Formation. The migration of a crustal radiogenic ^{4}He signature from depth is shown, which is lost in the superficial aquifer due to shallow groundwater flushing. 95
Figure 5-3: Representative 400m wide geological section of the Vale of Pickering stratigraphic units. 100
Figure 5-4: *Mesh (with a density of 40m) of the modelled section of the Vale of Pickering subsurface, with boundary conditions highlighted in red. At the base of the model, a boundary condition of 60m hydraulic head and He noble gas concentration (N.G.) of 100% is set. At the surface, a 30m hydraulic head is set up, to simulate an upward hydraulic gradient. The two locations of the groundwater flushing scenarios are highlighted (Sherwood Sandstone and superficial deposits), with their associated ASW He concentrations and heads set as boundary conditions. Model results are obtained from the green centre polyline.* 104
Figure 5-5: Modelled He concentration profiles in the subsurface over five time-steps as a result of diffusion and dispersion, with fluid velocity vectors highlighted. 105
Figure 5-6: Modelled result of ^{4}He concentration profile with depth via diffusion/dispersion. Measured ^{4}He concentrations collected from the Vale of Pickering (purple) are plotted for comparison. It is evident that the modelled ^{4}He results do not correlate to measured ^{4}He values. .106
Figure 5-7: Modelled He concentration profiles in the subsurface over the five modelled time steps with fluid velocity vectors highlighted. The model presents the diffusion and dispersion of ^{4}He from

thermogenic gas from depth, with groundwater flushing occurring at 1150m, releasing an ASW He signature into the model. 107
Figure 5-8: Modelled result of ^{4}He concentration profile with depth via diffusion/dispersion of thermogenic gas (blue). Groundwater flushing is simulated at 1150m depth in the Sherwood Sandstone units, releasing an ASW signature into the subsurface (green). Measured ^{4}He concentrations collected from the Vale of Pickering (purple) are plotted for comparison. It is evident groundwater flushing has an impact on He concentration, with ^{4}He concentrations declining within 100m of the flushing to an ASW signature. Modelled superficial values, are more reflective of a groundwater flushing signal, though are still higher than measured concentrations. The high ^{4}He signature observed in the Corallian aquifer cannot be accounted for through diffusion and groundwater flushing of the KMB thermogenic gas. Due to the confined nature of the Corallian unit, it is thought to be hydraulically disconnected from the overlying and underlying aquifer units. 108
Figure 5-9: Modelled He concentration profiles in the subsurface over the five modelled time steps with fluid velocity vectors highlighted. The model presents the diffusion and dispersion of ^{4}He from thermogenic gas from depth, with groundwater flushing occurring within the shallow superficial deposits, within 100m of the surface (highlighted by the black line). 109
Figure 5-10: Modelled result of ^{4}He concentration profile with depth via diffusion/dispersion of thermogenic gas. Groundwater flushing is simulated in the shallow superficial deposits, within 100m of the surface. Measured ^{4}He concentrations collected from the Vale of Pickering (purple) are plotted for comparison. Shallow groundwater flushing within the superficial deposits closely match the measured ^{4}He concentrations in the Vale of Pickering groundwater. As such, it is thought that a deep ^{4}He external source is migrating from depth before shallow groundwater flushing results in a decrease in concentration to near ASW values. 110
Figure 5-11: Modelled diffusion profile with reduced Kimmeridge Clay thickness (light blue dots) plotted against depth, alongside previous diffusive profile of increased Kimmeridge Clay thickness (blue line). As highlighted, there is no effect on the diffusive ^{4}He signature. Measured ^{4}He concentrations collected from the Vale of Pickering (purple) are plotted for comparison. 111

1 Introduction

1.1 Establishing environmental baselines for UK geoenergy technology sites

In order to meet Net Zero carbon emissions targets and tackle climate change, interest in the development of geoenergy technologies that harness the subsurface has increased. Technical aspects of utilising the subsurface span multiple disciplines (e.g., geoscience, engineering, social science etc.), with the associated risks and uncertainties involving geoenergy technologies requiring better understanding in order to increase both their development and their social acceptance (Monaghan et al., 2022). Through the development of onshore geoenergy technologies, including hydraulic fracturing of unconventional hydrocarbon systems onshore, concerns over the potential contamination of groundwater aquifers and surface water bodies have increased. Such concerns have arisen as a result of allegations of contamination of drinking water wells near shale gas extraction sites in the US (Jackson et al., 2013; Osborn et al., 2011). However, constraint of the definitive origin of alleged groundwater contamination within unconventional hydrocarbon extraction areas in the US and Canada has proven difficult, primarily due to a lack of pre-extraction environmental baseline data (Hendry et al., 2016; Hendry et al., 2017; Humez et al., 2019). Hence, the establishment of environmental baselines for groundwater bodies before implementation of any future geoenergy technology utilising the subsurface are essential in creating a protocol for the protection of potable water sources.

1.2 Methane and unconventional gas extraction

The surge of North American unconventional gas production has transformed the global energy landscape, with the use of hydraulic fracturing techniques allowing for previously inaccessible gas-bearing tight rock formations, such as shales, to be exploited (Cahill et al., 2023; Jackson et al., 2013; Kerr, 2010). Production of such unconventional oil and gas resources rapidly increased in the early 2000's, as directional drilling technologies were combined with hydraulic fracturing techniques (U.S EPA, 2016), with global estimates of

natural gas reserves in unconventional shales approximately 716 trillion m^3 (Vengosh et al., 2014).

However, despite the economic benefits and resource potential of the shale gas industry within the US, the increased expansion of the sector has resulted in considerable public debate and scrutiny over the potential for environmental and human health impacts, with a key concern being the contamination of shallow groundwater resources (Cahill et al., 2023; Hendry et al., 2016; Hendry et al., 2017; Humez et al., 2016; Jackson et al., 2013; Vengosh et al., 2014). It was estimated between 2000 and 2013, approximately 3900 public water systems were within one mile of at least one hydraulically fractured well, which serviced over 8.6 million people in 2013 (U.S EPA, 2016). As a result of increased environmental concerns, the need for establishing environmental baselines was identified in order to investigate potential well leakage, fugitive gas migration, and well integrity failure (Cahill et al., 2023; Hendry et al., 2016; Jackson et al., 2013). However, due to many shale gas locations failing to establish environmental baseline prior to drilling, multiple cases of environmental impacts that have been investigated (Jackson et al., 2013; Osborn et al., 2011) have resulted in controversy and various regional moratoria (Cahill and Jakobsen, 2015).

The rapid expansion of the US unconventional gas extraction sector that has resulted in the U.S. becoming independent in meeting their gas demands (Stephenson, 2015) has prompted other nations to investigate the potential of their unconventional gas resources. Whilst the use of hydraulic fracturing (fracking) in the UK is not a new technique; with fracking offshore in the North Sea occurring regularly since the 1970's (Priestley, 2018), to date it has been undertaken in conventional reservoirs, usually in vertical or deviated wells in order to improve their permeability. In the 1980's, investigations began into the viability of onshore shale gas extraction (Priestley, 2018); and in 2010, a 2700m exploratory borehole was drilled into the Bowland Shale, near Blackpool (Stuart, 2012). Hydraulic fracturing of the Bowland Shale began in March 2011; however, work was halted as two minor earthquakes of approximately 2.3 ML and 1.5ML were detected (Priestley, 2018; Stuart, 2012). Subsequent investigations highlighted that such earthquakes were the result of fluid injection from the hydraulic

fracturing process reactivating a nearby fault zone, through the migration of the fluid along bedding planes in the shale being targeted, resulting in a series of minor tremors (Stuart, 2012). These events caused a halt in all onshore hydraulic fracturing until December 2012 (Priestley, 2018). Exploitation of unconventional gas in the UK is highly controversial, with diverse public and political opinions on the process. Currently, a moratorium on unconventional gas extraction is in place in the UK.

1.3 Gas monitoring

To provide a robust monitoring regime of any proposed geoenergy technology, it is essential that baseline monitoring of groundwater near to proposed sites is established before development of the subsurface occurs. Such monitoring is key, as failure to determine baseline levels for sites in the US before unconventional hydrocarbon extraction occurred, has resulted in uncertainty over whether methane being detected in groundwater near sites is due to extraction; or was present as part of the 'natural baseline' (Bell et al., 2017). As a result, for certain sites in the US where hydraulic fracturing is occurring, the ability of definitively proving if high methane concentrations are as a result of shale gas extraction is difficult.

The British Geological Survey (BGS) have primarily been establishing this baseline for groundwater bodies in the UK, with a focus being on potential shale gas extraction sites and major aquifer bodies (Bell et al., 2017; Ward et al., 2019). One such investigation into the methane concentrations of major aquifers in the UK has reported that out of a total of 343 sites, 96% had a total dissolved methane concentration of less than 100μg/l (Bell et al., 2017); with methane concentrations ranging from 0.5 to 4,700μg/l (Bell et al., 2017). Furthermore, no site investigated had methane concentrations near the potential hazard threshold of 10,000 μg/l (Bell et al., 2017). Such an investigation highlights that whilst methane concentrations in the major aquifer systems are low; methane occurring in groundwater 'naturally' is common. Therefore, determining the presence, magnitude, and origin of subsurface gases, and how their geochemical fingerprints evolve within the shallow

subsurface is vital to developing an understanding of how to manage the risk posed by subsurface gases in the development of geoenergy technologies.

1.4 Sources of methane in the subsurface

Methane can be derived from several sources within the subsurface, though there are two predominant organic sources: biogenic methane, formed through bacterial activity at shallow depths (USGS, 2018); and thermogenic methane, produced by the thermal breakdown of organic matter (Stolper et al., 2015) commonly formed at depths exceeding 1000m (Floodgate and Judd, 1992). There is also evidence that methane can be formed in the subsurface abiogenically, through inorganic reactions (Schoell, 1988) termed abiogenic methane.

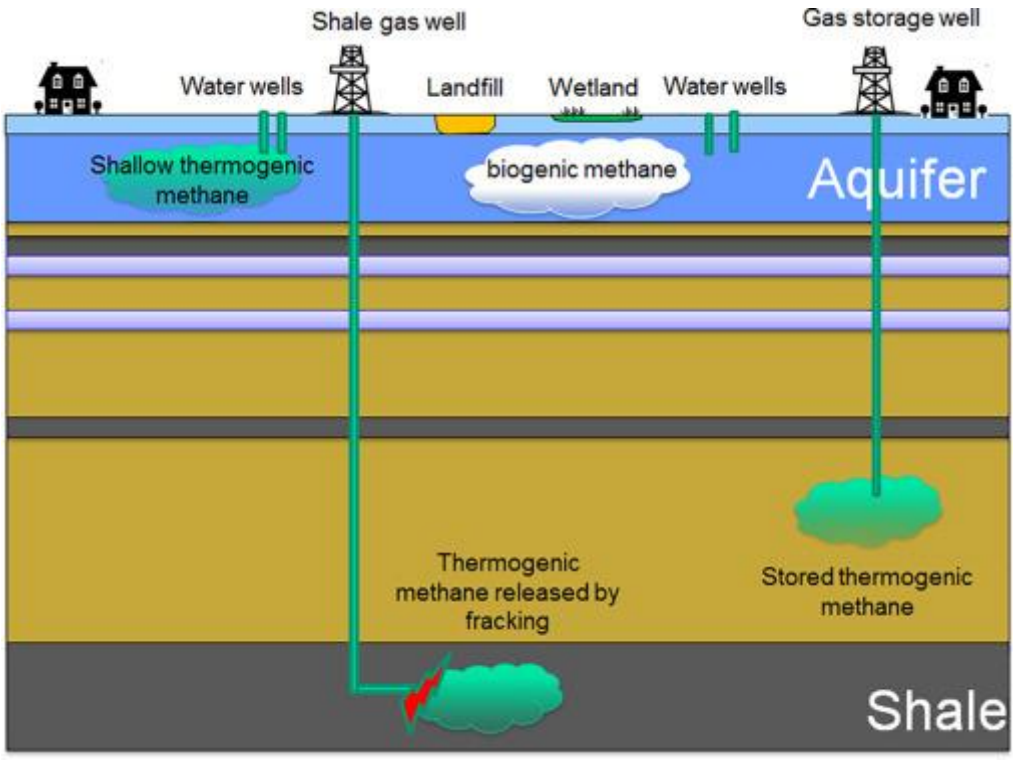

Figure 1-1: Schematic diagram illustrating the different types of methane sources within the subsurface (Bell et al., 2017).

1.4.1 Biogenic methane

Biogenic methane forms at shallow depths due to bacterial activity diagenetically transforming organic matter to gain energy (Whiticar, 1999). This bacterial activity involves methanogens chemically breaking down organic matter contained in shallow sediments to methane (Whiticar, 1999). There are two routes to produce biogenic methane, both of which require an absence of oxygen (Darling and Gooddy, 2006). The first route is via the fermentation of acetate which produces methane and CO_2, and the second route is through the reduction of carbon dioxide which solely produces methane (Whiticar et al., 1986). Both processes can occur simultaneously (Conrad and Klose, 1999). The fermentation of acetate primarily occurs in lake sediments and for most groundwaters, is the most likely route for biogenic methane production (Darling and Gooddy, 2006). The net reaction pathway for the fermentation of acetate is as follows:

$$CH_3COOH \longrightarrow CH_4+CO_2$$

CO_2 reduction only occurs in sufficiently reduced conditions, where the production of H_2 is also taking place (Darling and Gooddy, 2006). Environments typical of such conditions include peat bogs and landfills and the process is also dominant within marine sediments (Darling and Gooddy, 2006). The general reaction for CO_2 reduction is as follows:

$$CO_2+8H^++8e^- \longrightarrow CH_4+ 2H_2O$$

Natural gas formed as a result of bacterial activity has a very high (potentially greater than 99%) methane content (USGS, 2018). This is due to bacterial processes producing methane at the early stages of the diagenesis process (Schoell, 1980). Generation of biogenic methane is more commonly associated with finer grain sediments due to their higher initial organic carbon content (USGS, 2018).

Groundwaters associated with methane derived from biogenic sources generally have a low salinity with less than 2 to 4 Moles of Chlorine (Cl) (EPA, 2011), high alkalinity with less than $10m_{eq}/K$ and a low concentration of alternative electron acceptors (SO_4 > 1mM) (EPA, 2011). As bacterially derived methane is produced rapidly during the diagenesis process, it exhibits high methane (C_1) to ethane (C_2) ratios (Darling and Gooddy, 2006) with average C_1/C_2 and C_3

(propane) ratios of 1,000 to 10,000 (Stuart, 2012). Heavier isotopes, such as $d^{13}C$ and $d^{2}H$ are also depleted in comparison to other subsurface methane sources, typically resulting in $d^{13}C_{CH4} < -55‰$ and $d^{2}H_{CH4} < -150‰$ (Schoell, 1980). Deuterium isotope ratios of methane can also be used to establish a biogenic source, as biogenic methane's deuterium concentrations commonly range from -180‰ to -208‰ (Schoell, 1980).

1.4.2 Thermogenic methane

Thermogenic methane is formed at depths commonly exceeding 1000m (Floodgate and Judd, 1992) and involves the thermal alteration of larger organic molecules under high pressures and temperatures (Petropedia, 2018). Thermogenic methane forms from fine grained sedimentary rocks (with high organic matter content) decomposing, and subsequently producing methane due to the heat and pressure experienced at depth (Petropedia, 2018). The thermal alteration of organic matter is a gradual process, and whereas bacterial processes produce methane early in diagenesis, thermal production of methane as thermogenic gas is the final (metagenesis) stage of hydrocarbon production (Stolper et al., 2015). As such, natural gas produced from thermogenic processes consists of methane and increased amounts of higher chain hydrocarbons (Schoell, 1980).

In the process of producing thermogenic methane (natural gas), firstly diagenesis of organic sediments occurs under mild temperatures (less than 60°C) and pressures, (Stolper et al., 2015), to form kerogen and bitumen. As the material is further buried under higher temperatures and pressures, thermal 'cracking' (catagenesis) of the kerogen occurs, thermally degrading kerogen into natural gas and petroleum (Stolper et al., 2015). Significant oil generation occurs between 60°C to 160°C whilst gas generation occurs between 160°C to 225°C. The higher the temperatures and pressures associated with the catagenesis process, the more abundant the lighter and smaller hydrocarbons as the product (Stolper et al., 2015).

Thermogenic methane has increased concentrations of higher chain hydrocarbons compared to biogenic methane, such as ethane, propane, and butane (EPA, 2011) with C_1/ C_2 and C_3

ratios <100 (Schoell, 1980). Heavier isotopes such as $\delta^{13}C$ and $\delta^{2}H$ are also enriched in thermogenically sourced methane with $\delta^{13}C_{CH4}$ in the range of -45‰ to -110‰ (Stuart, 2012; LeDoux et al., 2016) and $\delta^{2}H_{CH4}$ > -255‰ (LeDoux et al., 2016).

1.4.3 Abiogenic methane

There is also evidence suggesting that methane can be formed in the subsurface abiogenically; through inorganic reactions (Schoell, 1988). Such abiogenic methane has been documented in sites in Canada and South Africa, where gases exsolving from fractures have stable isotope signatures similar to that of abiogenic gases that are produced through water rock interactions (Lollar et al., 2006). The water rock interactions that can produce methane abiogenically include serpentinization, and surface catalysed polymerization (Lollar et al., 2006). However, abiogenic methane is difficult to identify, as often its chemical signature can be obscured by mixing with biogenic methane (Lollar et al., 2006).

1.5 Distinguishing methane sources

1.5.1 Hydrocarbon abundance and stable isotopes

Traditionally, hydrocarbon abundance $C_1/(C_2+C_3)$ and stable isotopes ($\delta^{13}C_{CH4}$, $\delta^{13}C_{CO2}$, and δD_{CH4}) are used to distinguish between thermogenic and bacterial methane sources, and differentiate sources of differing thermal maturities (Fig.1.2) (Györe et al., 2017; Jackson et al., 2013; Osborn et al., 2011; Schoell 1980; Stuart, 2012; Whiticar, 1999). This is due to both biogenic and thermogenic methane having characteristic signatures in terms of their stable isotopes and hydrocarbon ratios. Biogenic methane has a characteristic fingerprint of CH_4 to heavier hydrocarbon ratios of 1,000-10,000, and stable isotope signature $\delta^{13}C_{CH4}$ < -55‰ and $\delta^{2}H_{CH4}$ < -150‰ (Schoell, 1980). Conversely, thermogenic methane exhibits ratios of < 100, with stable isotope signatures $\delta^{13}C_{CH4}$ of -45‰ to -110‰ and $\delta^{2}H_{CH4}$ > -255‰ (Stuart, 2012; LeDoux et al., 2016).

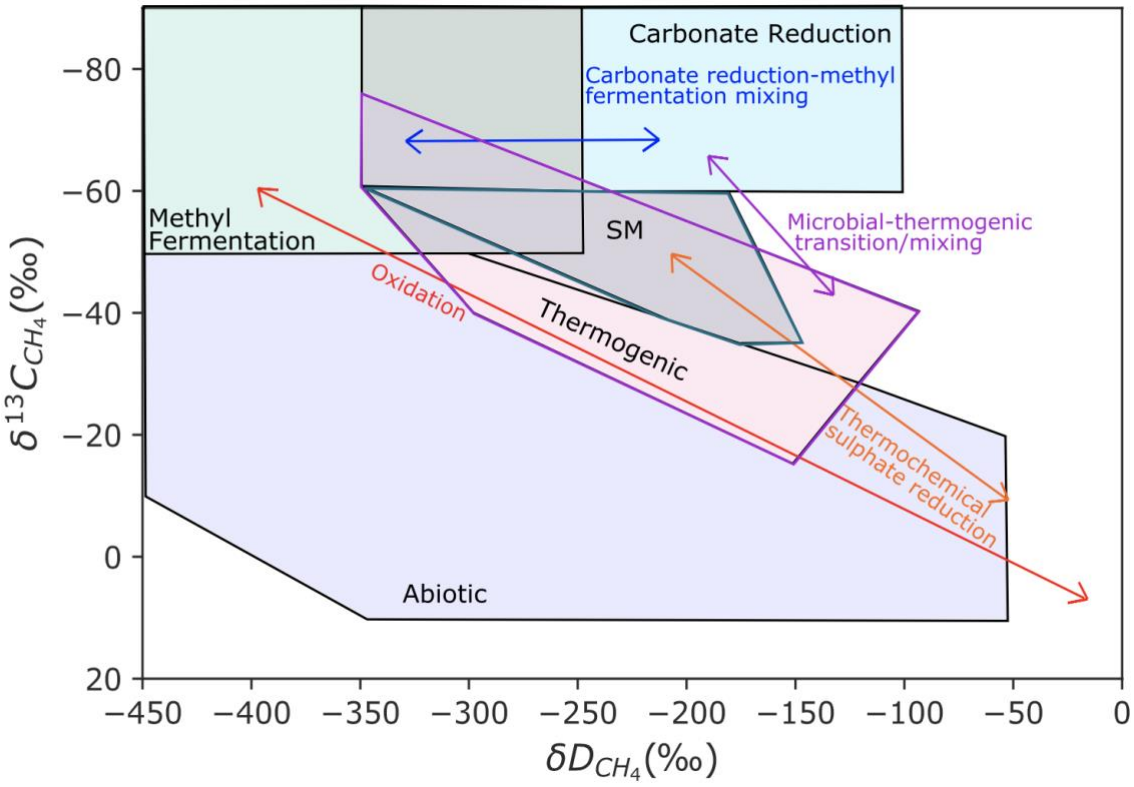

Figure 1-2: Classification of methane sources plot highlighting the different methane signatures (SM= secondary methane), as well as the influence of methane source mixing, oxidation, and sulphate reduction on isotopic signatures. Plot adapted from Whiticar, 1999 and Milkov and Etiope 2018.

However, several processes can alter the hydrocarbon abundance and stable isotope signature of CH_4 and can result in the misidentification of the gas source. Processes include the mixing of different sources of methane; microbial oxidation and sulfate reduction, which can enrich bacterial CH_4 in ^{13}C and ^{2}H to that of thermogenic sources (Barker and Fritz, 1983; LeDoux et al., 2016; Molofsky et al., 2013; Whiticar, 1999), or fractionation during transport within the subsurface (Darrah et al., 2015).

1.5.2 Noble gases

Noble gases provide a useful complement for methane source analysis (Darrah et al., 2014), as their non-reactive nature means that they remain unaffected by biological or chemical processes (Darrah et al., 2014; Darrah et al., 2015; Gyore et al., 2017). However, whilst noble gases are inert to chemical or biological processes their isotopic and relative abundances are

affected by physical processes. This means that noble gases can be used as tracers within the subsurface environment (Ballentine and Sherwood Lollar, 2002).

Noble gases have three well defined sources: the mantle, where primordial noble gases have been trapped during the Earth's formation; the crust, where radiogenic noble gases are generated from radioactive decay of U, Th and K; and the atmosphere, which contains outgassed noble gases (Fig. 1.3) (Ballentine et al., 2002). These three distinct sources are well characterised within the atmosphere and the subsurface (Darrah et al., 2014).

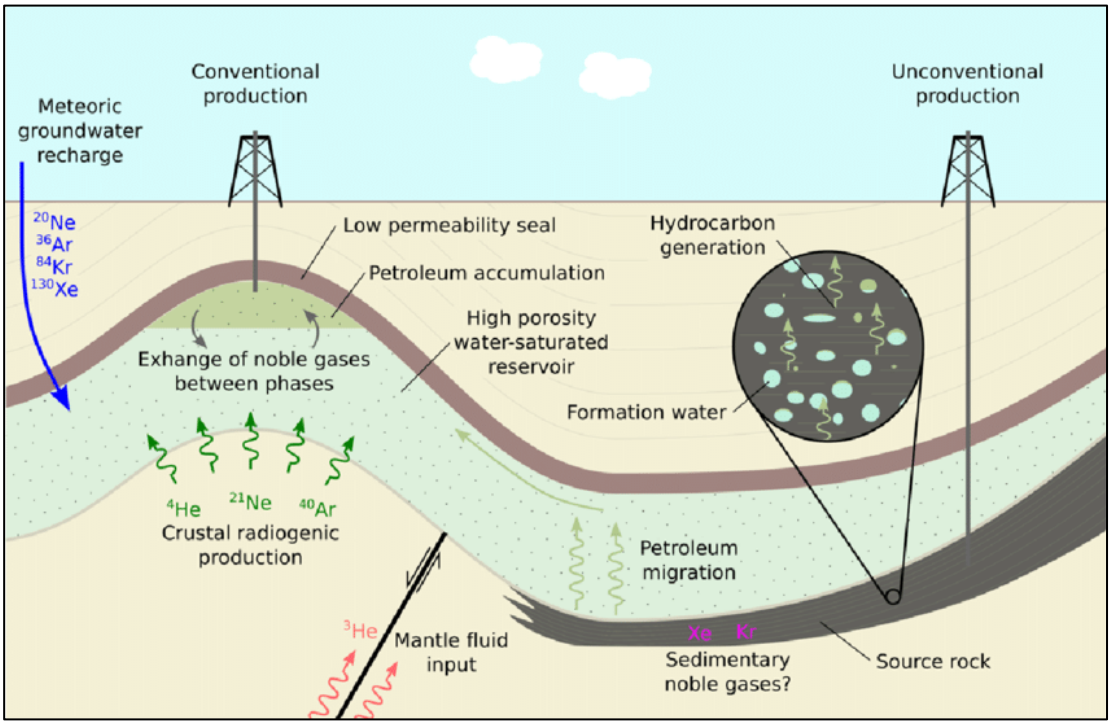

Figure 1-3: Diagram highlighting the different sources of noble gases within the subsurface: atmosphere, crustal, and mantle (Byrne et al., 2017).

Atmospheric noble gases (^{20}Ne, ^{36}Ar) are principally introduced into the subsurface environment through the infiltration of precipitation, where the difference in solubility of noble gases results in fractionated elemental ratios from the original atmospheric ratios (Lupton and Evans, 2013). As such, the composition of noble gases in recharge water is referred to as Air Saturated Water (ASW) (Ballentine et al., 2002). Atmospheric concentrations of helium are low at ~5.24ppm (Lupton and Evans, 2013), with a typical

$^{3}He/^{4}He$ ratio of $1.39x10^{-6}$ (^{3}He derived from outgassed mantle and cosmic sources and ^{4}He derived from crustal sources) (Ozima and Podosek, 2001). This atmospheric ratio (Ra) is often used as a reference to which other noble gas ratios are compared (Ozima and Podosek, 2001); where the atmospheric ratio equals 1 for helium.

Crustal noble gases (^{4}He, ^{40}Ar) are generated by radiogenic processes; with ^{4}He being produced through alpha decay of U and Th (Ozima and Podosek, 2001). Typical crustal $^{3}He/^{4}He$ ratios range from 0.02Ra to 0.1Ra (Ballentine and Burnard, 2002). Due to the crust having low concentrations of helium, this allows for the resolution of small concentrations found in samples. As such, He analysis can be used for tracing deep gas migration (Mackintosh and Ballentine, 2012). The production of noble gases within the crust is dependent upon the radioelement abundances and residence time with the release of such elements from minerals dependent upon temperature (Ozima and Podosek, 2001). Therefore, crustal noble gases are age accumulative; with different areas of the crust containing different noble gas contributions as a result of these factors (Ozima and Podosek, 2001). The mantle is enriched is primordial noble gases, such as ^{3}He and $^{40}Ar^{*}$, that have been trapped during the accretion and formation of the Earth (Ozima and Podosek, 2001).

Therefore, when used alongside stable isotope analysis and hydrocarbon composition, noble gases can provide a valuable insight into gas source, residence time, and migration history of gases within the subsurface. Furthermore, they remain unaffected by processes such as microbial alteration and oxidation, thermal maturity, and mineralogy etc that can affect the associated stable isotope signature (Darrah et al., 2014; Darrah et al., 2015; Gilfillan et al., 2017; Golding et al., 2013).

1.6 Potential hazards of subsurface gases

1.6.1 Risks of methane and CO_2 in the subsurface

Hazardous ground gases, such as CH_4 and CO_2, are found naturally in superficial deposits, coal and gas bearing strata, and abandoned mines. These gases can pose a significant potential hazard to human safety, as they are potentially explosive in critical concentrations when mixed with air or are toxic to life at elevated concentrations. Whilst such gases pose no threat provided they remain within the subsurface, gases can migrate through strata, groundwater and faults and be released at the surface. As such, ground gases can pose a threat to human safety, and there have been several instances in the UK where the ignition of methane gas has resulted in loss of life. Explosions at Loscoe and Abbeystead disaster highlight the dangers of undetected methane gas accumulating within the shallow subsurface. More recently the demolition of a public housing estate in the Scottish town of Gorebridge due to mine gas ingress (Ramsey et al., 2017) highlights the significant hazard posed by such gases.

1.6.2 Methane and groundwater

Methane is frequently present in local groundwater sources as a result of the migration of biogenic methane being created near the surface; or through the transportation of thermogenic methane, associated with natural gas or petroleum, from increased depths. Commonly, groundwater can act as a transport mechanism for methane, and allow it to migrate from its source and accumulate in distal locations (Edwards, 1991). There are no known human health impacts from the ingestion of methane in groundwater (Bell et al., 2017) hence, there is no formal environmental quality standard for CH_4 (Bell et al., 2017). Therefore, the main hazard that stems from methane in groundwater is because of its explosive properties, due to the potential of methane degassing from groundwater (Edwards, 1991; Stuart, 2012). Methane will degas out of groundwater if the equilibrium solubility is exceeded at the partial pressure of -1850 parts per billion per volume (Bell et al., 2017). Such degassing will occur until the system re-equilibrates; and as such, large concentrations of methane potentially accumulating poses the risk of explosion or suffocation (Bell et al., 2017). As a

result, a methane concentration of 10mg/l is considered to be the 'risk action level' (Bell et al., 2017).

1.7 Subsurface methane and the methane budget

In the past 200 years, global methane concentrations have more than doubled; with the current increase linked to human activities. As methane absorbs approximately 20 times as much heat as CO_2 (Dodds and Whiles, 2002), there are concerns regarding increasing methane concentrations in the atmosphere; with methane being the second biggest greenhouse gas after CO_2 (Dodds and Whiles, 2002).

As such, identifying previously unconsidered sources of methane is key in better understanding the methane budget (Kulongoski and McMahon, 2019). Inland waters are thought to contribute approximately 25% of the total methane concentrations globally (Bastviken, 2009) However, there is not a quantified contribution for methane associated with groundwater pumping and abstraction globally (Kulongoski and McMahon, 2019). Therefore, research into the contribution of methane from groundwater is key in terms of the wider context interest of methane migration.

Whilst there is no global methane budget for groundwater, studies into methane contributions associated with UK water supply groundwater was estimated as 0.05% of the total methane budget for the UK (Gooddy and Darling, 2005). This highlights the relatively small nature of the contribution compared to other sectors (agricultural with 37%, and landfill 22%) (Gooddy and Darling, 2005). However, groundwater only meets ~10% of Ireland and Scotland's, and 30% of England and Wales water budget; and as such, methane budgets globally may be more significant.

1.8 Research Aims

The aim of this PhD is to characterise the subsurface geochemical conditions of potential geoenergy technology sites using a range of geochemical fingerprinting techniques. The two sites investigated for this PhD are the former coal-workings UKGEOS site in Glasgow, proposed for shallow geothermal energy; and the Vale of Pickering in Yorkshire, which was originally a potential site for unconventional gas extraction, but is now being considered for geoenergy technology development. From the geochemical characterisation of the Vale of Pickering, this site is then used to develop a hydrogeological and mass transport model of methane and noble gas migration within the subsurface.

1.9 Thesis Outline:

The three main data chapters (Chapters 3, 4, and 5) are written as standalone manuscripts, and as a result, there may be some overlap and repetition in content. The outline of the thesis is as follows:

Chapter 1. Introduction

This chapter introduces the different types of methane sources within the subsurface, and the range of geochemical techniques, such as stable isotope and noble gases, that are used to identify methane source. The threat of hazardous ground gases if emitted to the surface is discussed, alongside the importance of establishing environmental baselines of potential geoenergy technology sites before their development.

Chapter 2. Techniques and methodology

This chapter describes the two main data sites for the thesis, and the analytical and laboratory methodologies used throughout for the collection and subsequent geochemical analysis of samples.

Chapter 3. Constraining the Geochemical Fingerprints of Gases from the UK Carboniferous Coal Measures at the Glasgow Geoenergy Observatories Field Site, Scotland

This published chapter outlines the methane and CO_2 gas fingerprints within the shallow geothermal UKGEOS site in Glasgow. From samples obtained during construction of the site, the presence, source and volume of coal and mine derived gases have been determined using gas composition and stable isotope analysis techniques.

Chapter 4. Stable isotope and noble gas characterisation of subsurface methane from the Vale of Pickering, Yorkshire

This chapter discusses the major gas, stable isotope and noble gas compositions of gas and groundwater samples collected from the Vale of Pickering at varying depths, to investigate the source of subsurface methane, and the potential of gas migration from depth to shallow groundwater sources.

Chapter 5. Hydrogeological and mass transport modelling of radiogenic ^{4}He noble gas within the Vale of Pickering subsurface

This chapter outlines the development of a coupled hydro-chemical model to investigate how ^{4}He noble gas signatures change with depth within the Vale of Pickering, and follows on from the geochemical characterisation presented in Chapter 4. This chapter outlines the conceptual basis for the coupled hydro-chemical model and the key parameters used in the model set up. The results of these models are discussed, as are the implications for the use of geochemical fingerprinting tools in the future.

Chapter 6. Summary and future work

This chapter summarises key findings of the thesis and describes the areas of potential future work.

1.10 References

Ballentine, C. J., Burgess, R. and Marty, B. (2002) 'Tracing Fluid Origin, Transport and Interaction in the Crust', Reviews in Mineralogy and Geochemistry, 47(1), pp. 539–614. doi:10.2138/rmg.2002.47.13.

Ballentine, C. J. and Burnard, P. G. (2002) 'Production, Release and Transport of Noble Gases in the Continental Crust', Reviews in Mineralogy and Geochemistry, 47(1), pp. 481–538. doi:10.2138/rmg.2002.47.12

Ballentine, C. J. and Sherwood Lollar, B. (2002) 'Regional groundwater focusing of nitrogen and noble gases into the Hugoton-Panhandle giant gas field, USA', Geochimica et Cosmochimica Acta, 66(14), pp. 2483–2497. doi:10.1016/S0016-7037(02)00850-5.

Barker, J.F. and Fritz, P., 1981. Carbon isotope fractionation during microbial methane oxidation. *Nature*, *293*(5830), pp.289-291.

Bastviken, D, 2009. Methane, *Encyclopedia of Inland Waters*. Vol. 2. N.p., 783–805

Bell, R.A., Darling, W.G., Ward, R.S., Basava-Reddi, L., Halwa, L., Manamsa, K. and Dochartaigh, B.Ó., 2017. A baseline survey of dissolved methane in aquifers of Great Britain. Science of the Total Environment, 601, pp.1803-1813.

Byrne, D.J., Barry, P.H., Lawson, M. and Ballentine, C.J., 2018. Noble gases in conventional and unconventional petroleum systems. Geological Society, London, Special Publications, 468(1), pp.127-149.

Cahill, A.G., Joukar, M., Sefat, M. and van Geloven, C., 2023. Evaluating methane emissions from decommissioned unconventional petroleum wells in British Columbia, Canada. *Geophysical Research Letters*, *50*(24), p.e2023GL106496.

Cahill, A.G. and Jakobsen, R., 2015. Geochemical modeling of a sustained shallow aquifer CO2 leakage field study and implications for leakage and site monitoring. *International Journal of Greenhouse Gas Control*, *37*, pp.127-141.

Conrad, R. and Klose, M., 1999. Anaerobic conversion of carbon dioxide to methane, acetate and propionate on washed rice roots. *FEMS Microbiology Ecology*, *30*(2), pp.147-155.

Darling, W.G. and Gooddy, D.C., 2006. The hydrogeochemistry of methane: evidence from English groundwaters. *Chemical Geology*, *229*(4), pp.293-312.

Darrah, T. H., Vengosh, a., Jackson, R. B., Warner, N. R. and Poreda, R. J. (2014) 'Noble gases identify the mechanisms of fugitive gas contamination in drinking-water wells overlying the Marcellus and Barnett Shales', Proceedings of the National Academy of Sciences, 111(39), pp. 14076–14081.

Darrah, T.H., Jackson, R.B., Vengosh, A., Warner, N.R., Whyte, C.J., Walsh, T.B., Kondash, A.J., Poreda, R.J. 2015. The evolution of Devonian hydrocarbon gases in shallow aquifers of the northern Appalachian Basin: Insights from integrating noble gas and hydrocarbon geochemistry. Geochimica et Cosmochimica Acta, 170, 321–355, https://doi.org/10.1016/j.gca.2015.09.006.

Dodds, W., 2002. Freshwater ecology: concepts and environmental applications. Elsevier.

Edwards, J.S., 1991, September. Potential hazards resulting from the presence of methane dissolved in groundwater. In 4th International Mine Water Congress (pp. 223-231). Ljubljana, Slovenia, Yugoslavia: International Mine Water Association.

EPA (2011), EPA Technical Workshop [online] Available at: https://www.epa.gov/sites/production/files/documents/distinguishingthesourceofnaturalgasaccumulationswithacombinedgas.pdf [Accessed: 08/08/23]

Floodgate, G.D. and Judd, A.G., 1992. The origins of shallow gas. Continental Shelf Research, 12(10), pp.1145-1156.

Gilfillan, S.M., Sherk, G.W., Poreda, R.J. and Haszeldine, R.S., 2017. Using noble gas fingerprints at the Kerr Farm to assess CO2 leakage allegations linked to the Weyburn-Midale CO2 monitoring and storage project. *International Journal of Greenhouse Gas Control*, *63*, pp.215-225.

Golding, S. D., Boreham, C. J. and Esterle, J. S. (2013) 'Stable isotope geochemistry of coal bed and shale gas and related production waters: A review', International Journal of Coal Geology, 120, pp. 24–40.

Gooddy, D.C. and Darling, W.G., 2005. The potential for methane emissions from groundwaters of the UK. *Science of the Total Environment*, *339*(1-3), pp.117-126.

Györe, D., Gilfillan, S.M. and Stuart, F.M., 2017. Tracking the interaction between injected CO2 and reservoir fluids using noble gas isotopes in an analogue of large-scale carbon capture and storage. Applied geochemistry, 78, pp.116-128.

Hendry, M.J., Barbour, S.L., S., Schmeling, E.E., Mundle, S.O. and Huang, M., 2016. Fate and transport of dissolved methane and ethane in cretaceous shales of the Williston Basin, Canada. *Water Resources Research*, *52*(8), pp.6440-6450.

Hendry, M.J., Schmeling, E.E., Barbour, S.L., Huang, M. and Mundle, S.O., 2017. Fate and transport of shale-derived, biogenic methane. *Scientific Reports*, *7*(1), p.4881.

Humez, P., Mayer, B., Ing, J., Nightingale, M., Becker, V., Kingston, A., Akbilgic, O. and Taylor, S., 2016. Occurrence and origin of methane in groundwater in Alberta (Canada): Gas geochemical and isotopic approaches. *Science of the Total Environment*, *541*, pp.1253-1268.

Jackson, R.E., Gorody, A.W., Mayer, B., Roy, J.W., Ryan, M.C. and Van Stempvoort, D.R., 2013. Groundwater protection and unconventional gas extraction: The critical need for field-based hydrogeological research. *Groundwater*, *51*(4), pp.488-510.

Kulongoski, J.T., McMahon, P.B., Land, M., Wright, M.T., Johnson, T.A. and Landon, M.K., 2018. Origin of methane and sources of high concentrations in Los Angeles groundwater. *Journal of Geophysical Research: Biogeosciences*, *123*(3), pp.818-831.

LeDoux S.T, Szynkiewicz, A., Faiia, A.M., Mayes, M.A., McKinney, M.L. and Dean, W.G., 2016. Chemical and isotope compositions of shallow groundwater in areas impacted by hydraulic fracturing and surface mining in the Central Appalachian Basin, Eastern United States. Applied geochemistry, 71, pp.73-85.

Lollar, B.S., Lacrampe-Couloume, G., Slater, G.F., Ward, J., Moser, D.P., Gihring, T.M., Lin, L.H. and Onstott, T.C., 2006. Unravelling abiogenic and biogenic sources of methane in the Earth's deep subsurface. Chemical Geology, 226(3-4), pp.328-339.

Lupton, J. and Evans, L. (2013) 'Changes in the atmospheric helium isotope ratio over the past 40 years', Geophysical Research Letters, 40(23), pp. 6271–6275.

Mackintosh, S. J. and Ballentine, C. J. (2012) 'Using 3He/4He isotope ratios to identify the source of deep reservoir contributions to shallow fluids and soil gas', Chemical Geology. Elsevier B.V., 304–305(0), pp. 142–150

Milkov, A.V. and Etiope, G., 2018. Revised genetic diagrams for natural gases based on a global dataset of> 20,000 samples. Organic Geochemistry, 125, pp.109-120.

Molofsky, L.J., Connor, J.A., Wylie, A.S., Wagner, T. and Farhat, S.K., 2013. Evaluation of methane sources in groundwater in northeastern Pennsylvania. *Groundwater*, *51*(3), pp.333-349.

Monaghan, A.A., Bateson, L., Boyce, A.J., Burnside, N.M., Chambers, R., De Rezende, J.R., Dunnet, E., Everett, P.A., Gilfillan, S., Jibrin, M.S. and Johnson, G., 2022. Time zero for net zero: a coal mine baseline for decarbonising heat. *Earth Science, Systems and Society*, p.9.

Osborn, Stephen G., Avner Vengosh, Nathaniel R. Warner, and Robert B. Jackson. "Methane contamination of drinking water accompanying gas-well drilling and hydraulic fracturing." *proceedings of the National Academy of Sciences* 108, no. 20 (2011): 8172-8176.

Ozima, M. and Podosek, F. A. (2001) Noble Gas Geochemistry. 2nd edn. Cambridge: Cambridge University Press

Petropedia (2018), The Significance of Biogenic and Thermogenic Gases in the Energy Space [online] Available at: https://www.petropedia.com/2/9808/oil/biogenic-and-thermogenic-gases-how-significant-they-are-in-energy-space [Accessed: 08/08/23]

Priestley (2018), Parliament, House of Commons (2018), Shale Gas and Fracking; Briefing Paper, (Number CBP 6073), London, [online] Available at: https://www.google.com/url?sa=t&rct=j&q=&esrc=s&source=web&cd=11&ved=2ahUKEwjgk97A4IreAhVITMAKHQ5wCJIQFjAKegQIBhAC&url=http%3A%2F%2Fresearchbriefings.files.parliament.uk%2Fdocuments%2FSN06073%2FSN06073.pdf&usg=AOvVaw0g7xDJDd9mfRY__e0PbTBq [Accessed: 08/08/23]

Ramsay, C., McRae, C., Ryan, E., McCallum, A., Wellington, L., Lauder, L., Millar, R., Haunch, S. and Othieno, R., 2017. Carbon dioxide ingress into residential houses at Gorebridge in Midlothian, Scotland, United Kingdom Richard Othieno. European Journal of Public Health, 27(suppl_3).

Schoell, M., 1980. The hydrogen and carbon isotopic composition of methane from natural gases of various origins. Geochimica et Cosmochimica Acta, 44(5), pp.649-661.

Schoell, M., 1988. Multiple origins of methane in the Earth. Chemical geology, 71(1-3), pp.1-10.

Stephenson, M., 2015. Shale gas and fracking: the science behind the controversy. Elsevier.

Stolper, D.A., Lawson, M., Davis, C.L., Ferreira, A.A., Neto, E.S., Ellis, G.S., Lewan, M.D., Martini, A.M., Tang, Y., Schoell, M. and Sessions, A.L., 2014. Formation temperatures of thermogenic and biogenic methane. Science, 344(6191), pp.1500-1503.

Stolper, D.A., Martini, A.M., Clog, M., Douglas, P.M., Shusta, S.S., Valentine, D.L., Sessions, A.L. and Eiler, J.M., 2015. Distinguishing and understanding thermogenic and biogenic sources of methane using multiply substituted isotopologues. Geochimica et Cosmochimica Acta, 161, pp.219-247.

Stuart M.E. 2012. Potential groundwater impact from exploitation of shale gas in the UK. British Geological Survey Open Report, OR/12/001. 33pp

U.S. EPA (U.S. Environmental Protection Agency). 2016. Hydraulic Fracturing for Oil and Gas: Impacts from the Hydraulic Fracturing Water Cycle on Drinking Water Resources in the United States. Office of Research and Development, Washington, DC. EPA/600/ R-16/236Fa.

USGS (2018), Origin: Biogenic vs. Thermogenic [online] Available at: https://pubs.usgs.gov/of/1996/of96-272/ch03s07.html [Accessed: 08/08/23]

Vengosh, A., Jackson, R.B., Warner, N., Darrah, T.H. and Kondash, A., 2014. A critical review of the risks to water resources from unconventional shale gas development and hydraulic fracturing in the United States. *Environmental science & technology*, *48*(15), pp.8334-8348.

Ward, R. S., Smedley, P. L., Allen, G., Baptie, B. J., Barkwith, A. K. A. P., Bateson, L., et al. (2019). Environmental monitoring - phase 4 final report (April 2018 - March 2019). Open Report, OR/19/044. Nottingham, UK: British Geological Survey, 225. Available at: http://nora.nerc.ac.uk/id/eprint/527726/.

Whiticar, M.J., Faber, E. and Schoell, M., 1986. Biogenic methane formation in marine and freshwater environments: CO2 reduction vs. acetate fermentation—isotope evidence. *Geochimica et Cosmochimica Acta*, *50*(5), pp.693-709.

Whiticar, M. J. (1999) 'Carbon and hydrogen isotope systematics of bacterial formation and oxidation of methane', Chemical Geology, 161(1–3), pp. 291–314.

2 Techniques and Methodology

2.1 Chapter Overview

This chapter describes the two localities where data was acquired for this thesis: The Glasgow Geoenergy observatory field site and the Vale of Pickering, in Yorkshire. Samples were collected from the Glasgow Geoenergy observatory to constrain the geochemical fingerprints of gases in the subsurface, and is discussed in Chapter 3. Gas and groundwater samples were collected from the Vale of Pickering in order to characterise methane sources and noble gas migration within the subsurface, and is discussed in Chapter 4. The data collected from the Vale of Pickering was then used to create a hydro-chemical model, of which an overview of the numerical modelling approach and code used is discussed in this chapter. The sample collection methods and analytical techniques for both the gas and groundwater samples collected from these localities are also discussed.

As Chapters 3, 4 & 5 of this thesis are written as standalone manuscripts, a more detailed methodology for the data analysis is discussed within the corresponding data chapters, and as such; there may be some repetition between chapters.

2.2 Study Locations

2.2.1 The Glasgow Geoenergy Observatory Field Site

The Glasgow Geoenergy Observatory field site is located on the west side of the Central Coalfield of the Midland Valley of Scotland, in the east of the city of Glasgow within the Cuningar Loop. The Glasgow Observatory was developed to investigate the potential energy resource available and variability of low temperature geothermal energy from shallow mine workings, and consists of 12 boreholes, which include:

- a 199m seismic monitoring borehole (BH GGC01)

- 11 shallow (max 90m depth) mine characterisation and monitoring boreholes, situated on four sub-sites within the Cuningar Loop of the River Clyde

During drilling of the seismic borehole, the strata encountered was unmined, and so a continuous 199m long core was recovered. All 11 monitoring boreholes on site encountered shallow mine workings, and rock chipping samples were obtained during drilling. More details on the Glasgow Geoenergy Observatory, and its corresponding geology and hydrogeology are discussed in Chapter 3.

2.2.2 The Vale of Pickering, Yorkshire

The Vale of Pickering, North Yorkshire, is a flat-floored valley located in the catchment of the River Derwent, and was originally a locality identified for the development of unconventional gas extraction in the UK. Whilst unconventional gas extraction in the UK seems unlikely due to the current moratorium, the Vale of Pickering site is now being considered for geoenergy technology development. More details on the Vale of Pickering's geology and hydrogeology are discussed in Chapter 4.

2.3 Sample collection

2.3.1 Sample collection for Glasgow UKGEOS site

Core and cutting samples were collected from three boreholes on site: two mine characterisation and monitoring boreholes, and a 200m deep seismic borehole. Core samples consisted of two 50mm quarter sections collected every 10m depth during drilling of the seismic borehole, with drill cuttings collected during drilling of the two shallower boreholes over 3m depth intervals. These core and cutting samples were stored in gas tight isojars (Fig.2.1) prior to gas analysis.

Duplicate sampling from the borehole allowed for two different isojar storage methods to be tested; with one set of samples stored in de-ionised water that had 1ml (20 drops) of

Benzalkonium (Zephiran) Chloride biocide added to the Isojar, with the other stored in N_2 gas. Through preliminary analysis of samples, it was evident that storage in de-ionised water resulted in higher concentrations of the exsolved gases, indicating better sample preservation (Fig.2.1).

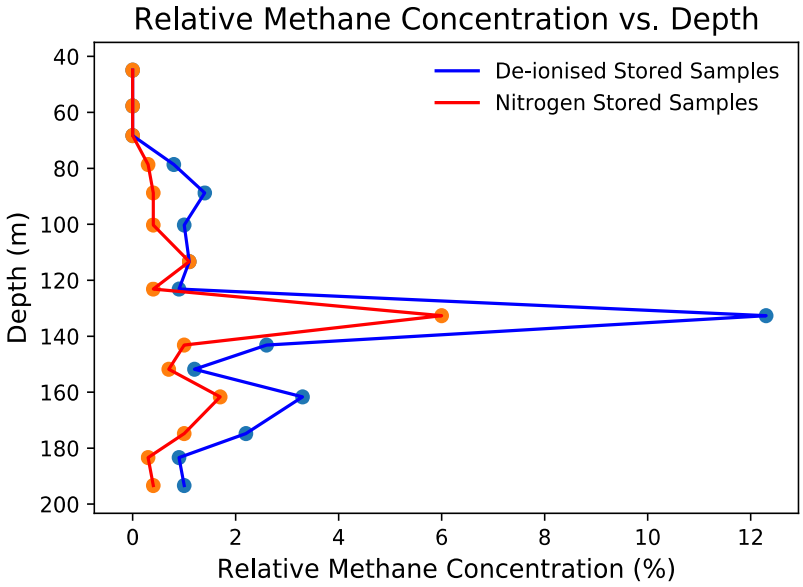

Figure 2-1: Relative methane concentrations with depth for de-ionised and N_2 stored samples, highlighting higher exsolved gas concentrations from de-ionised water storage.

As such, subsequently obtained cutting samples were solely stored in de-ionised water, with added Benzalkonium (Zephiran) Chloride biocide. All samples were then stored at standard temperature (25°C) and pressure (1atm) for a two-month period, to allow the samples to equilibrate with the headspace prior to gas analysis.

2.3.2 Sample collection for Vale of Pickering site

Duplicate samples were collected from four groundwater boreholes and two Third Energy gas wells at six locations within the Vale of Pickering. Superficial groundwater samples were collected alongside the BGS quarterly environmental baseline sampling in February 2020, with the groundwater aquifer samples and Third Energy well gas samples collected in August 2020. All samples were collected in refrigeration grade 10mm outside diameter copper tubing approximately 70cm long, connected either to the well heads by a regulator and high-

pressure hosing (Holland and Gilfillan, 2013) or to the groundwater pump outflow hose (Fig.2.2). For all samples, gas or water was flowed through the copper tubes for approximately 5 minutes prior to collection of the sample, to prevent air contamination. These tubes were then sealed by stainless steel clamps at each end to form a cold weld, helium leak tight seal (Gilfillan et al., 2017; Györe et al., 2018), with the downstream clamp sealed first followed by the upstream clamp.

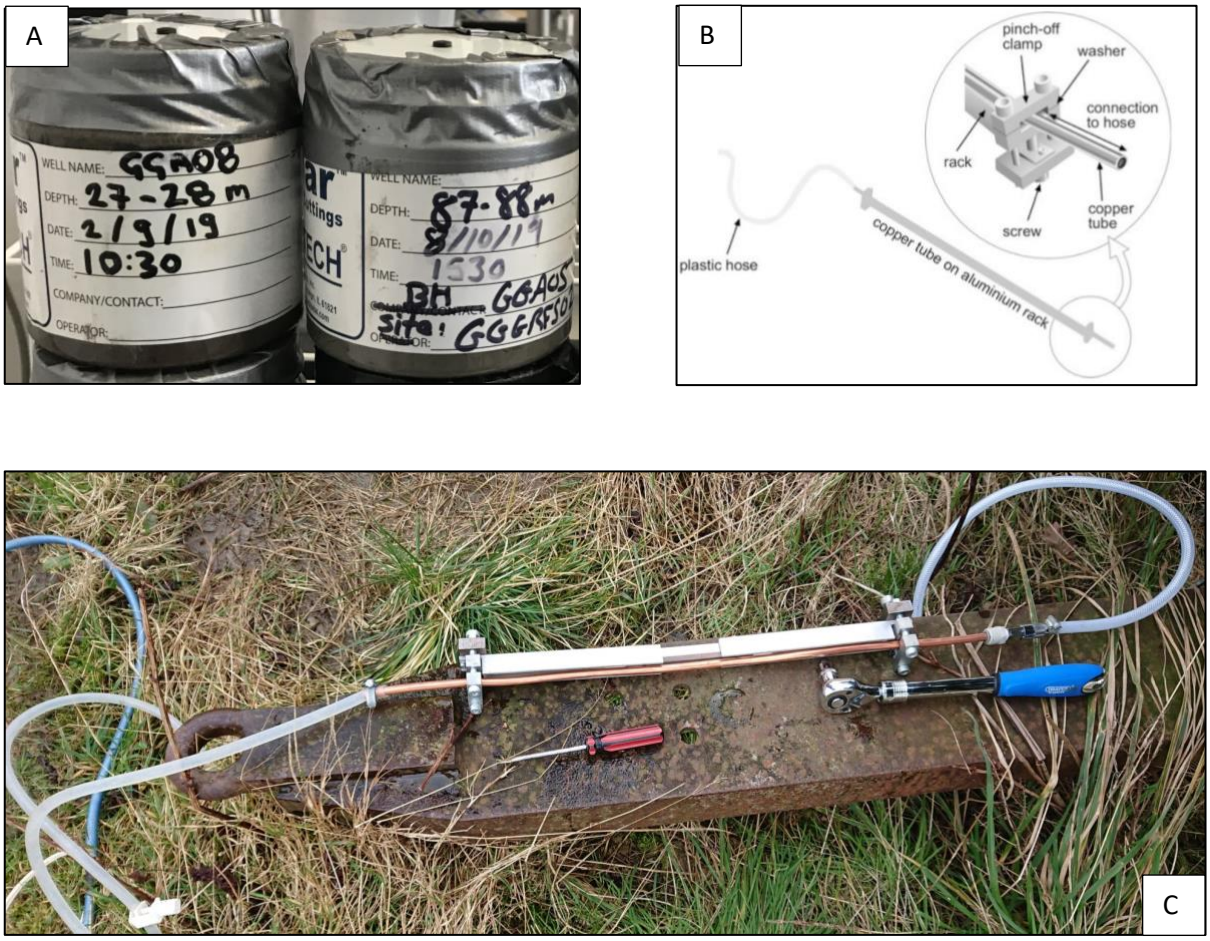

Figure 2-2: A shows the isojars used to collect the Glasgow UKGEOS core and cutting samples, which were filled either with N_2 gas or de-ionised water and sealed shut. B is a diagram of the copper tube sampling system, highlighting the steel clamps which form the cold weld seal. C shows the copper tube sampling set up in the field.

2.4 Analytical procedures

2.4.1 Major gas concentrations

For the Glasgow UKGEOS samples and for one set of the Vale of Pickering samples, major gas analysis was conducted at the Scottish Universities Environmental Research Centre (SUERC). For core and cutting samples stored within the isojar containers, 50 microlitres of gas headspace was collected in a 100 microlitre syringe and injected manually into the septa port of a Perkin-Elmer AutoSystem XL gas chromatograph (GC), via a 30m long and 0.53mm internal diameter Sigma-Aldrich Carboxen 1010 PLOT column using helium as a carrier gas. The GC was equipped with a flame ionization detector to measure light hydrocarbons and was calibrated with appropriate gas mixtures produced by CalGaz Ltd. For gas samples stored within the copper tubes, tubes were attached to an extraction line and expanded into a partial vacuum. Gas was then transferred using 100 microlitre syringe an injected manually into the GC following the same procedure as the core and cutting samples.

2.4.2 Stable isotope analysis

Stable isotope analysis for all samples from the Glasgow UKGEOS site and for one set of gas samples from the Vale of Pickering was conducted at SUERC and discussed below. A full set of groundwater and gas samples from the Vale of Pickering were analysed at the Ohio State University WHEEL laboratory by Dr Thomas Darrah, using a quadrupole mass spectrometer (SRS Residual Gas Analyzer 200) for quantification of noble gases (e.g., He, Ar, Kr, Xe), with the methodology described in detail in Hunt et. al., (2012). The final set of groundwater samples from the Vale of Pickering were analysed for $\delta^{13}C_{CH4}$ stable isotope ratios at the University of Calgary isotope lab. Both of these methods are discussed in more detail within the Chapter 4 methodology section.

2.4.2.1 Methane and Carbon Dioxide

Post gas composition analysis, samples that exhibited CO_2 and CH_4 concentrations above 1.5% by volume were then selected for CH_4 and CO_2 stable isotope analysis. Such analysis was conducted on the gas combustion line at SUERC (Fig.2.3). For the core and cutting samples of the Glasgow UKGEOS site, the extraction inlet of the gas combustion line was attached directly to the sealed isojars, with a pressure gradient applied to draw gas through the line. For the copper tubes samples, the remaining gas was expanded into a partial vacuum.

Figure 2-3: Gas combustion line at SUERC, which was used for methane and CO_2 gas stable isotope analysis. Photo shows the Glasgow UKGEOS Isojars connected directly to the extraction inlet for the line.

Following this, for all samples CO_2 was separated from volatile hydrocarbons using a procedure modified from Kusakabe (2005). A liquid N_2 cooled isopentane trap (-160°C) was applied to collect CO_2 and water before an acetone slush bath was used (~ -78°C) to retain water and vaporise CO_2. The CO_2 was then collected separately in a liquid N_2 cooled cold finger. The CH_4 samples were combusted over a CuO catalyst at 900°C into CO_2 and water,

which were collected in a liquid N_2 cooled cold finger. A pressure gradient drawing gases through the furnace was maintained by the cold finger trapping combustion products. After combustion, the cold finger was heated with an acetone slush bath (~ -78°C) to retain water and vaporise CO_2. This CO_2 was collected separately in a separate liquid N_2 cooled cold finger. Both the original and combusted CO_2 were analysed on a VG SIRA II dual-inlet IRMS, calibrated to internal standards (Dunbar et al., 2016), with measured values relative to V-PDB standards. The cold finger containing the collected water was connected to a manifold, heated to vapour, and reduced to H_2 over a nickel catalyst at 800°C. H_2 was analysed in a separate Delta Optima Plus dual-inlet IRMS, and calibrated to internal standards (Donnelly et al., 2001). $\delta^{13}C$ values are reported relative to V-PDB international standard and δD values are quoted relative to V-SMOW (Craig 1957; Gonfiantini 1984; Coplen 1995) with known uncertainties of 0.3% ($\delta^{13}C$) and 3% (δD). All ratios are reported using the delta (δ) notation, in per mill (‰), following Equation 2.1.

$$\delta X = \left[\frac{(Rsample)}{(Rstandard)} - 1\right] \times 1000$$

Equation 2.1

2.4.3 Noble gas analysis

Noble gas analysis for a full set (6 samples) of groundwater and gas samples from the Vale of Pickering was carried out at the Ohio State University WHEEL laboratory by Dr Thomas Darrah, using a quadrupole mass spectrometer for the quantification of noble gases (e.g., He, Ar, Kr, Xe), and discussed in more detail in Chapter 4 methods. The 2s analytical error for the $^{3}He/^{4}He$ ratio is approximately 0.5%, with the 1s error of $^{40}Ar/^{36}Ar$ and $^{4}He/^{20}Ne$ isotope ratios being 0.2%. A 1s error of 0.3% for $^{38}Ar/^{36}Ar$, and 1% for $^{20}Ne/^{22}Ne$, $^{21}Ne/^{22}Ne$ and $20Ne/^{36}Ar$. All noble gas abundances have an uncertainty of 1.5%.

2.5 Numerical Modelling

2.5.1 Modelling approach and code

Due to the complexity of groundwater systems within the subsurface, conceptual models are used to simplify and capture the key hydrogeological components that describe the hydrogeological environment. The development of these conceptual models can then be used to mathematically model hydrogeological processes within the environment (e.g., head distributions, transient scenarios, mass transport etc). Mathematical models can be solved both analytically and numerically. However, analytical models require a high level of simplification, with the resulting assumptions limiting their application to groundwater systems (Anderson and Woessner, 1992). As such, numerical models which can solve for a system that is heterogeneous, with complex boundaries and source terms etc is the standard approach used for modelling groundwater scenarios.

For this study, the open-source finite element code OpenGeoSys (OGS) (Kolditz et al., 2012) was used, which is specifically developed to model coupled thermal, hydraulic, mechanical, and chemical (THMC) processes within porous and fractured media. OGS has been fully benchmarked against a number of test cases as described in 'Thermo-Hydro-Mechanical-Chemical Processes in Fractured Porous Media: Modelling and Benchmarking' (Shao, 2015). The 2D mesh used for this model was constructed using GMSH, an automatic mesh generator software (Geuzaine and Remacle, 2009). Model results and data plots were undertaken in Tecplot 360 (Tecplot 2023).

2.5.2 Numerical modelling overview

Thermal, hydraulic, mechanical, or chemical processes are described by balance equations based on the conservation of either mass or energy. For this model, a coupled hydro-chemical process model was constructed to model the transport of stable isotopes and noble gases within the subsurface of the Vale of Pickering. Within this section, the general numerical modelling background and approach are described, with the site conceptual model and

specific model parameters further discussed in Chapter 5. Full derivations of the empirical calculations are provided in Appendix B.

For this coupled hydro-chemical model, the governing equations for hydraulic flow and chemical transport are applied. The three-dimensional balance equation from Darcy's Law is as follows:

$$S_s \frac{\partial h}{\partial t} = \frac{\partial}{\partial x}\left(K_x \frac{\partial h}{\partial x}\right) + \frac{\partial}{\partial y}\left(K_y \frac{\partial h}{\partial y}\right) + \frac{\partial}{\partial z}\left(K_z \frac{\partial h}{\partial z}\right) - Q$$

Equation 2.2

Where K is hydraulic conductivity (m/s), *S*s is the specific storage, t is time (s), $\mathrm{h\ is\ hydraulic\ head\ (m)}$ and Q is the volumetric flow rate (m^3/s). This equation is valid for a saturated, non-deforming porous medium with heterogeneous hydraulic conductivity. The steady-state model in this study was calculated with specific storage (S_s) equal to zero. This equation is valid for a saturated, non-deforming porous medium with heterogeneous hydraulic conductivity.

Chemical (mass) transport is controlled by advection/and or diffusion and can be described through the mass balance equation for mass transport:

$$\frac{\partial C}{\partial t} + \nabla . (vC - D\nabla C) = 0$$

Equation 2.3

Where C is the concentration (kg/m^3), t is the time (s), D is the hydrodynamic dispersion coefficient (m^2/s), v is advective velocity (m/s), with the system being modelled as having no source or sink terms (=0). For this study, the transport of noble gases within a closed system is controlled by diffusion, and is solved by Equation 2.4, after Fetter (1999).

$$\frac{\delta C}{\delta t} = D^* \frac{\delta^2 C}{\delta x^2}$$

Equation 2.4

Where concentration (C), at time (t), and distance (x). D^* is the apparent diffusion co-efficient (m^2/s), and can be calculated as:

$$D^* = \frac{D_{aq}}{R\tau}$$

Equation 2.5

Where D_{aq} is the aqueous diffusion coefficient, R is the retardation factor (1) and τ is the tortuosity factor of the porous rock matrix.

For this model, diffusion coefficients for the noble gases were calculated using the Wilke-Chang (1955) estimation method:

$$D^o_{AB} = \frac{7.4X10^{-8}(\phi M_B)^{\frac{1}{2}}T}{\eta_B V_A^{0.6}}$$

Equation 2.6

Where $D^o{}_{AB}$ is the diffusion coefficient of solute A (noble gas) at low concentrations within solvent B (water) (cm^2/s), f is the association factor of solvent B (2.6 for water), M_B is the molecular weight of solvent B (g/mol), T is temperature (K), η_B is the viscosity of solvent B (cP), and V_A the molar volume of solute A at its normal boiling temperature (cm^3/mol).

2.6 References

Anderson, M.P., Woessner, W.W. and Hunt, R.J., 1992. Applied groundwater modeling: Simulation of flow and advective transport. *Academic Press Inc., San Diego, CA. Journal of Hydrology*, *140*, pp.393-395.

Craig, H., 1957. Isotopic standards for carbon and oxygen and correction factors for mass-spectrometric analysis of carbon dioxide. *Geochimica et cosmochimica acta*, *12*(1-2), pp.133-149.

Darrah, T.H. and Poreda, R.J. 2012. Evaluating the accretion of meteoritic debris and interplanetary dust particles in the GPC-3 sediment core using noble gas and mineralogical tracers. *Geochimica et Cosmochimica Acta*, **84**, 329–352, https://doi.org/10.1016/J.GCA.2012.01.030.

Darrah, T.H., Tedesco, D., Tassi, F., Vaselli, O., Cuoco, E. and Poreda, R.J. 2013. Gas chemistry of the Dallol region of the Danakil Depression in the Afar region of the northern-most East African Rift. *Chemical Geology*, **339**, 16–29, https://doi.org/10.1016/j.chemgeo.2012.10.036.

Donnelly, T., Waldron, S., Tait, A., Dougans, J. and Bearhop, S., 2001. Hydrogen isotope analysis of natural abundance and deuterium-enriched waters by reduction over chromium on-line to a dynamic dual inlet isotope-ratio mass spectrometer. *Rapid Communications in Mass Spectrometry*, *15*(15), pp.1297-1303

Dunbar, E., Cook, G.T., Naysmith, P., Tripney, B.G. and Xu, S. 2016. AMS ^{14}C Dating at the Scottish Universities Environmental Research Centre (SUERC) Radiocarbon Dating Laboratory. *Radiocarbon*, **58**, 9–23, https://doi.org/10.1017/RDC.2015.2.

Fetter, C.W., Boving, T.B. and Kreamer, D.K., 1999. *Contaminant hydrogeology* (Vol. 1138). Upper Saddle River, NJ: Prentice hall.

Geuzaine, C., and Remacle, J. F., 2009. Gmsh: A 3-D finite element mesh generator with built-in pre-and post-processing facilities. International journal for numerical methods in engineering, 79(11), 1309-1331.

Gilfillan, S.M., Sherk, G.W., Poreda, R.J. and Haszeldine, R.S., 2017. Using noble gas fingerprints at the Kerr Farm to assess CO2 leakage allegations linked to the Weyburn-Midale

CO2 monitoring and storage project. *International Journal of Greenhouse Gas Control*, *63*, pp.215-225.

Gonfiantini, R., 1984. Stable isotope reference samples for geochemical and hydrological investigations. *Int. J. Appl. Radiat. Isot.;(United Kingdom)*, *35*(5).

Györe, D., McKavney, R., Gilfillan, S.M. and Stuart, F.M., 2018. Fingerprinting coal-derived gases from the UK. *Chemical Geology*, *480*, pp.75-85.

Holland, G. and Gilfillan, S. 2013. Application of Noble Gases to the Viability of CO_2 Storage. *In*: *Advances in Isotope Geochemistry*. 177–223., https://doi.org/10.1007/978-3-642-28836-4_8.

Hunt, A.G., Darrah, T.H. and Poreda, R.J., 2012. Determining the source and genetic fingerprint of natural gases using noble gas geochemistry: A northern Appalachian Basin case study The Noble Gas Signature of the Appalachian Basin. *AAPG bulletin*, *96*(10), pp.1785-1811.

Kolditz, O., Bauer, S., Bilke, L., Böttcher, N., Delfs, J. O., Fischer, T., ... & Park, C. H., 2012. OpenGeoSys: an open-source initiative for numerical simulation of thermo- hydro-mechanical/chemical (THM/C) processes in porous media. Environmental Earth Sciences, 67(2), 589-599.

Kusakabe, M., 2005. A closed pentane trap for separation of SO2 from CO2 for precise $\delta^{18}O$ and & $\delta^{34}S$ measurements. *Geochemical Journal*, *39*(3), pp.285-287

Moore, M.T., Vinson, D.S., Whyte, C.J., Eymold, W.K., Walsh, T.B. and Darrah, T.H. 2018. Differentiating between biogenic and thermogenic sources of natural gas in coalbed methane reservoirs from the Illinois Basin using noble gas and hydrocarbon geochemistry. *Geological Society Special Publication*, 468, 151–188, https://doi.org/10.1144/SP468.8.

Tecplot. 2023. Tecplot CFD visualisation and analysis tools https://www.tecplot.com/.

Wilke, C. R., and Chang, P., 1955. Correlation of diffusion coefficients in dilute solutions. AIChE Journal, 1(2), 264-270.

3 Constraining the geochemical fingerprints of gases from the UK Carboniferous Coal Measures at the Glasgow Geoenergy Observatories Field Site, Scotland.

3.1 Chapter Overview

This chapter aims to characterise and constrain the subsurface CH_4 and CO_2 gas fingerprints from the UK Carboniferous Coal Measures of the Glasgow UKGEOS site, through the utilisation of a range of geochemical fingerprinting techniques. This chapter presents the first CH_4 and CO_2 concentration-depth profiles and stable isotope ($\delta^{13}C_{CH4}$, $\delta^{13}C_{CO2}$, and δD_{CH4}) profiles obtained from UK mine workings, through analysis of headspace gas samples degassed from cores and chippings collected during construction of the Glasgow Geoenergy Observatory. These findings are then used to investigate the variability of gas fingerprints with depth within unmined Carboniferous coal measures and Glasgow coal mine workings, providing an important 'time-zero' record of the site. By determining the presence, magnitude, and origin of subsurface gases, and how their geochemical fingerprints evolve within the shallow subsurface, is vital to developing an understanding of how to manage the risk posed by ground gases in geoenergy technology development.

The work presented in this chapter has been previously published in Earth Systems, Science, and Society Journal as:

"*Constraining the Geochemical Fingerprints of Gases from the UK Carboniferous Coal Measures at the Glasgow Geoenergy Observatories Field Site, Scotland.*"

(Chambers, R.M., Johnson, G., Boyce, A.J. and Gilfillan, S., 2023. Constraining the geochemical fingerprints of gases from the UK carboniferous coal measures at the Glasgow geoenergy observatories field site, Scotland. *Earth Science, Systems and Society*, *3*, p.10073.)

The abstract has been removed, but the remainder of the text has been included unchanged and as a result, there is some repetition with the Chapter 2 methodology section.

3.2 Introduction

The use of thermal energy contained within groundwater in abandoned, flooded, coal mines has considerable potential to contribute to the provision of low carbon heating or cooling to assist in meeting global net-zero carbon emission targets (Adams et al., 2019; Monaghan et al., 2022; Stephenson et al. 2019). A quarter of UK homes and businesses lie above former coalfields, providing a highly permeable network of buried mine workings flooded with water at above-ambient temperatures (Adams et al., 2019; Monaghan et al., 2022). However, there are a multitude of manageable, but significant techno-societal risks associated with the utilisation of the heat from mine waters, related to both the direct site operation and the environment surrounding it, such as resource sustainability and efficiency, reservoir quality, operation maintenance, ground motion, ground gases and environmental change (Monaghan et al., 2022; NERC, University of Strathclyde, and BGS 2019).

In order to address these issues, there is a clear need for applied research on minewater heat utilisation, to provide an open evidence base to enable knowledge transfer to assist with social acceptance, constraining the economic models and reducing development, operational and post closure risk of a mine water heat site (NERC et al. 2019; Stephenson et al. 2019). In conjunction with a growing number of underground laboratories worldwide, the UK Geoenergy Observatory in Glasgow ('Glasgow Observatory') is a unique facility for investigating shallow, low-temperature mine water thermal energy resources in abandoned and flooded workings at depths of around 50–85m. This site provides a vital record of the "time-zero" baseline conditions prior to activities commencing at the site and a record of any environmental changes induced by operations to extract or reinject heat into the mine workings.

Coal derived gas is an important energy resource and a potential source of greenhouse gas, as the majority of coal and coal bearing strata contain significant quantities of gases (Hall et al., 2005, CL-AIRE, 2021). These gases pose a significant potential hazard as they are either potentially explosive in critical concentrations when mixed with air, or are toxic to life at elevated (from ambient) concentrations. Gases found in a mine are typically mixtures of atmospheric air, inert gases, water vapour and one or more of the following: O_2, CO, CO_2, CH_4, H_2S, H_2 and NO_x (Hall et al., 2005; CL:AIRE, 2021). Whilst these pose no threat provided they stay in the mine, they can migrate through voids and strata and be emitted at the surface above the mine. Release of this gas as a result of minewater heat extraction would pose both an unwelcome climate feedback of greenhouse gases, and a potential hazard to the local population, as exemplified by recent demolition of a public housing estate in the Scottish town of Gorebridge due to mine gas ingress (Ramsey et al., 2017).

Whilst CH_4 associated with coal is predominantly considered as being produced thermogenically due to the burial and thermal maturation of coals, a number of studies have shown that bacterial coal bed CH_4 can be produced from microbial activity within lower maturity coals under anoxic conditions (Gründger et al., 2015; Guo et al., 2012; Krüger et al., 2008; Strąpoć et al., 2011). Traditionally, hydrocarbon abundances ($C_1/(C_2+C_3)$ and stable isotopes ($\delta^{13}C_{CH4}$, $\delta^{13}C_{CO2}$, and δD_{CH4}) of CH_4 and other associated hydrocarbon gases are used to distinguish between thermogenic and bacterial CH_4 sources (Györe et al., 2017; Jackson et al., 2013; Osborn et al., 2011; Schoell 1980; Stuart, 2012; Whiticar, 1999). Hydrocarbon ratios of 10^3 to 10^5, $\delta^{13}C_{CH4}$ of < -55‰; and δ^2H_{CH4} < -150‰ are characteristic of bacterial CH_4 (Schoell, 1980); with thermogenic CH_4 gas typically containing ratios of < 100, with $\delta^{13}C_{CH4}$ values -45‰ to -110‰ and δ^2H_{CH4} > -255‰, respectively (Stuart, 2012; LeDoux et al., 2016). However, several processes can alter the hydrocarbon abundance and stable isotope signature of CH_4 and can result in the misidentification of the gas source. Processes include the mixing of different sources of CH_4; or microbial oxidation, which can enrich bacterial CH_4 in ^{13}C and ^2H to that of thermogenic sources (Barker and Fritz, 1983; LeDoux et al., 2016; Molofsky et al., 2013; Whiticar, 1999).

Here, we outline how sampling and analysis of gases from drilling at the Glasgow Observatory during its construction has enabled the determination of the presence, source and volume of coal and mine derived gases (CO_2 and CH_4) in the subsurface at the site. We use the geochemical tools outlined above to determine the source of the gases encountered and to provide a unique insight into the variation of gas signatures with depth and mining activities within flooded coal mines.

3.3 Setting of the UK Geoenergy Observatory in Glasgow, Scotland

The Glasgow Observatory has been developed to investigate the potential energy resource available and variability of low temperature geothermal energy from shallow mine workings (Monaghan et al., 2019). The Observatory is located on the west side of the Central Coalfield of the Midland Valley of Scotland, in the east of the city of Glasgow within the Cuningar Loop (Monaghan et al., 2019) in an area where prolific coal mining activity has occurred. Due to historic coal mining and extensive industrial activity, the site contains significant made ground of waste building material, which overlies Quaternary glacial and post glacial deposits that are up to 25m thick (Monaghan et al., 2019). These superficial deposits overlie the Scottish Coal Measures Group, a group of fluvio-deltaic Carboniferous sedimentary rocks that contain cyclical sequences of mudstone, siltstone, sandstone, and coals that were deposited during repeated marine regressions and transgressions in the Westphalian period (Cameron and Stephenson, 1985, Monaghan et al., 2019). The Glasgow Observatory's infrastructure consists of 12 boreholes: a 200m seismic monitoring borehole (GGC01), drilled and installed on site during a three-month period from November 2018 to January 2019; and 11 shallow (max 90m depth) mine characterisation and monitoring boreholes, drilled and installed from May 2019 to January 2020. Superficial deposits and the bedrock encountered by all boreholes at the Cuningar Loop site were drilled by reverse circulation rotary drilling to ensure good sample recovery (Monaghan et al., 2022). The 11 monitoring boreholes are situated in the Cuningar loop of the River Clyde, on four sub-sites (GGERFS01, GGERFS02, GGERFS03, GGERFS05); with the seismic monitoring borehole located on sub-site GGERFS10, >1.5km east in the area of Dalmarnock (Fig. 3.1). Strata at site GGERFS10 was unmined, and a continuous 199m long

core was recovered from drilling. All other 11 monitoring boreholes on site encountered shallow mine workings, and rock chipping samples were obtained during drilling.

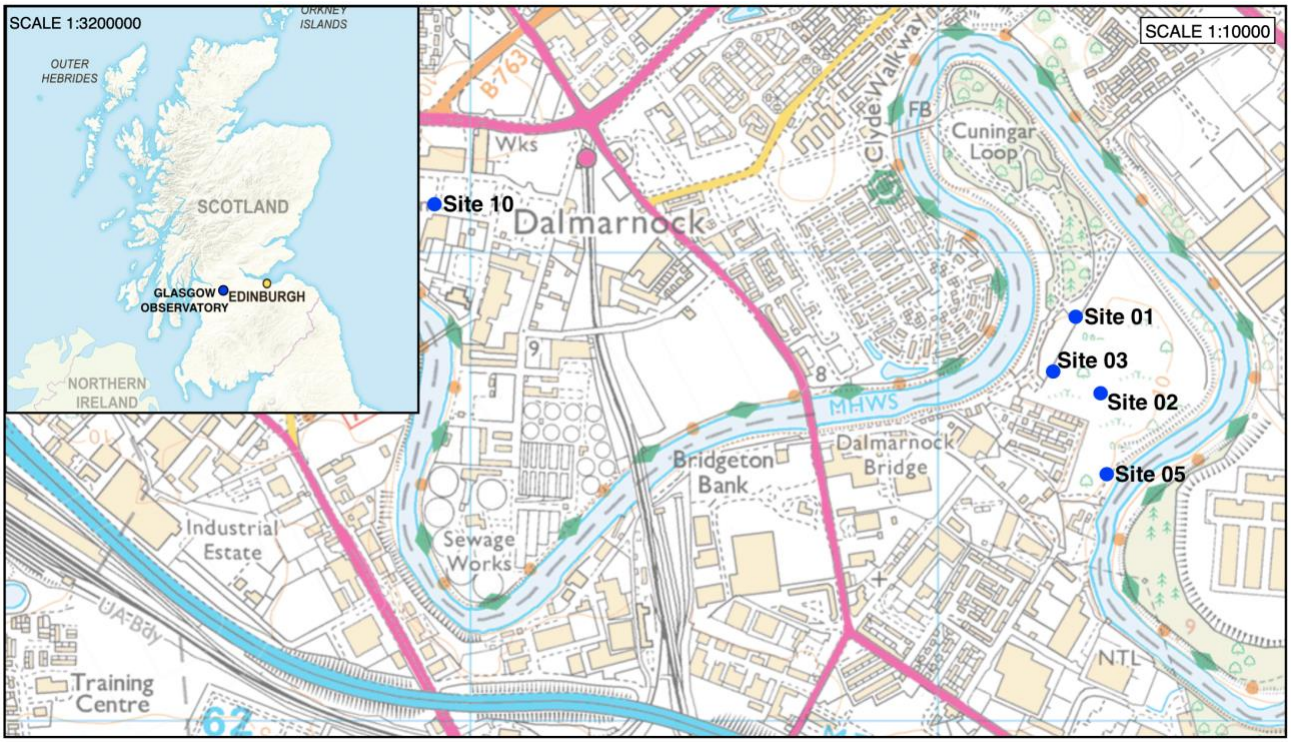

Figure 3-1:The UK Geoenergy Observatory is located in the Eastern side of Glasgow, the largest city in Scotland, located next to the River Clyde, in the Midland Valley of Scotland. The site consists of 12 boreholes, located at five sites, four of these are located within the Cuningar Loop formed by a meander of the River Clyde, with the GGC01 borehole located at site 10 in the Dalmarnock area. Contains Ordnance Survey data © Crown copyright and database rights. All rights reserved [2021] Ordnance Survey (100025252).

Hydrogeologically, the glacio-fluvial superficial deposits found on the site are thought to form part of a linear shallow aquifer system, which is up to 2 to 3km wide, located beneath Glasgow (Ó Dochartaigh et al., 2019). The superficial aquifer is thought to be highly heterogeneous and complex, due to the heterogeneity of the deposits, and the effect of urban influences (Ó Dochartaigh et al., 2019). The Carboniferous bedrock on the GGERFS site typically forms complex, layered aquifer systems that are dominated primarily by fracture flow (Ó Dochartaigh et al., 2019). Mining of such deposits has resulted in significant changes in the natural groundwater flow paths and hydrogeological conditions (Ó Dochartaigh et al., 2019).

The presence of mine voids, workings and other waste materials frequently results in significant change (often increases) in transmissivity within the aquifer, resulting in previously unconnected groundwater bodies to be linked (Ó Dochartaigh et al., 2019; Younger and Robins, 2002).

3.4 Materials and Methods

Samples were collected from three boreholes on site: GGA05, located at site GGERFS02; GGA08, located at site GGERFS03; both of which are mine characterisation and monitoring boreholes, and GGC01; the 200m deep seismic monitoring borehole located in Dalmarnock. (Full borehole data obtained from Monaghan et al., 2021; British Geological Survey (2020a, b).

Rock samples consisting of two 50mm quarter sections of core were obtained approximately every 10m depth during drilling of the GGC01 seismic monitoring borehole and drill cutting samples from GGA05 and GGA08 boreholes were collected over 3m depth intervals (Fig. 3.2). The collection of core and cutting samples at 10m and 3m intervals within the subsurface allowed for additional resolution in the complexity of the gas signatures on site, which would not have been obtained from standard borehole samples. These core and cutting samples were then stored in gas tight isojars prior to analysis of the exsolved gases. Duplicate sampling from the seismic monitoring borehole allowed two different isojar storage methods to be tested; with one set of samples stored in de-ionised water that had 1ml (20 drops) of Benzalkonium (Zephiran) Chloride biocide added to the Isojar, and the other purged with N_2 gas. Preliminary analysis of the samples from the seismic monitoring borehole clearly indicated that storage in de-ionised water resulted in higher concentrations of the exsolved gases, indicating better sample preservation, hence the subsequent obtained cutting samples were solely stored in de-ionised water, with added Benzalkonium (Zephiran) Chloride biocide. The full suite of GC data for all core and cutting samples from both preservation methods is provided in Appendix A. All samples were then stored at standard temperature (25°C) and pressure (1atm) for a two-month period, to allow the samples to equilibrate with the

headspace prior to gas analysis conducted at the Scottish Universities Environmental Research Centre (SUERC).

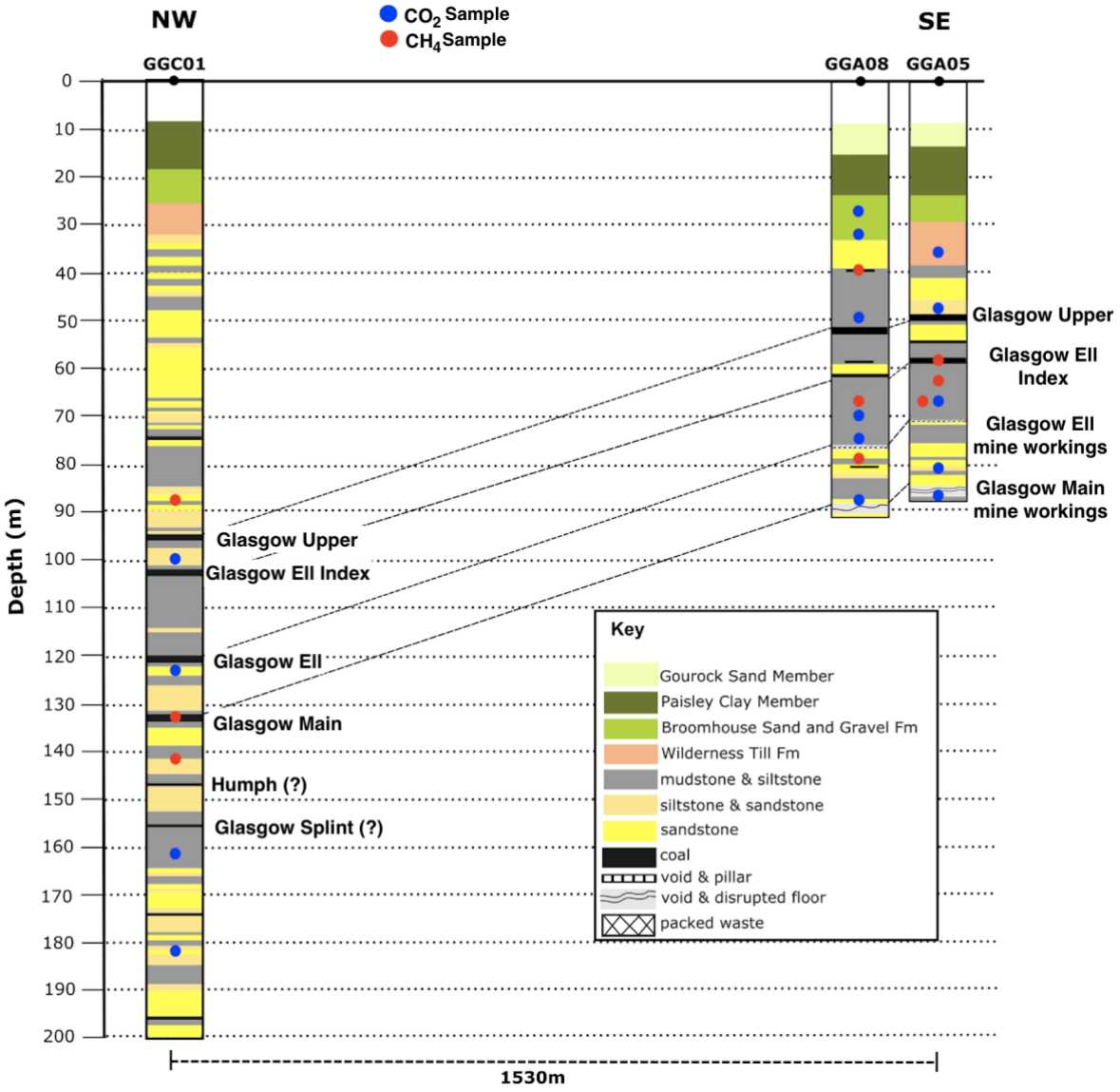

Figure 3-2: Composite logs of GGC01, GGA05, and GGA08 boreholes, and the depths of the core and cutting samples that were obtained for stable isotope analysis. The borehole logs indicate the major coal seams (Glasgow Upper, Glasgow Ell Index, Glasgow Ell, Glasgow Main), with Glasgow Ell and Glasgow Main coal seams have been mined in the shallow GGA05 and GGA08 boreholes. These seams can be correlated to unmined coal seams in GGC01.

50 microlitres of the gas headspace was collected from the isojars in a 100 microlitre syringe and injected manually into the septa port of a Perkin-Elmer AutoSystem XL gas chromatograph (GC), via a 30m long and 0.53mm internal diameter Sigma-Aldrich Carboxen

1010 PLOT column using helium carrier gas. The GC was also equipped with a flame ionization detector to measure light hydrocarbons and was calibrated with appropriate gas mixtures produced by CalGaz Ltd. Concentration data is recorded as mg/L in the gas phase, as determined from % components, with the full GC data provided in Tables A.1, A.2 and A.3 in Appendix A.

Samples that exhibited CO_2 and CH_4 concentrations above 1.5% by volume were then selected for stable isotope analysis. Stable isotope determinations were conducted on the gas combustion line at SUERC. The extraction inlet was attached directly to the sealed isojars; with a pressure gradient applied to draw gas through the line. CO_2 was separated from volatile hydrocarbons using a procedure modified from Kusakabe (2005). A liquid N_2 cooled isopentane trap (-160°C) was applied to collect CO_2 and water before an acetone slush bath was used (~ -78°C) to retain water and vaporise CO_2. The CO_2 was then collected separately in a liquid N_2 cooled cold finger. The CH_4 samples were combusted over a CuO catalyst at 900°C into CO_2 and water, which were collected in a liquid N_2 cooled cold finger. A pressure gradient drawing gases through the furnace was maintained by the cold finger trapping combustion products. After combustion, the cold finger was heated with an acetone slush bath (~ -78°C) to retain water and vaporise CO_2. This CO_2 was collected separately in a separate liquid N_2 cooled cold finger. Both the original and combusted CO_2 were analysed on a VG SIRA II dual-inlet IRMS, calibrated to internal standards (Dunbar et al., 2016), with measured values relative to V-PDB standards. The cold finger containing the collected water was connected to a manifold, heated to vapour, and reduced to H_2 over a nickel catalyst at 800°C. H_2 was analysed in a separate Delta Optima Plus dual-inlet IRMS, and calibrated to internal standards (Donnelly et al., 2001). $\delta^{13}C$ values are reported relative to V-PDB international standard and δD values are quoted relative to V-SMOW (Craig 1957; Gonfiantini 1984; Coplen 1995) with known uncertainties of 0.3% ($\delta^{13}C$) and 3% (δD).

3.5 Results

3.5.1 CH_4 and CO_2 Gas Concentrations from Core and Cutting Samples

Gas concentration data for all core and cutting samples are provided in Tables A.1, A.2 and A.3 in Appendix A. Exsolved gas headspace analysis of core samples from the unmined GGC01 borehole determined the presence of both CH_4 and CO_2 gas from depths below 77m. CH_4 gas concentrations for GGC01 range from 6 to 88mg/L (mean= 17mg/L, Std.dev= 23mg/L), with samples with increased concentrations correlating to areas immediately surrounding unmined coal seams (Glasgow Main coal, and potentially the Humph coal and Glasgow Splint coals) (Fig. 3). CO_2 concentrations in GGC01 occur in samples where CH_4 concentrations are lowest or absent, and range from 2 to 118mg/L (mean=33mg/L, Std.dev=37mg/L) (Fig. 3.3).

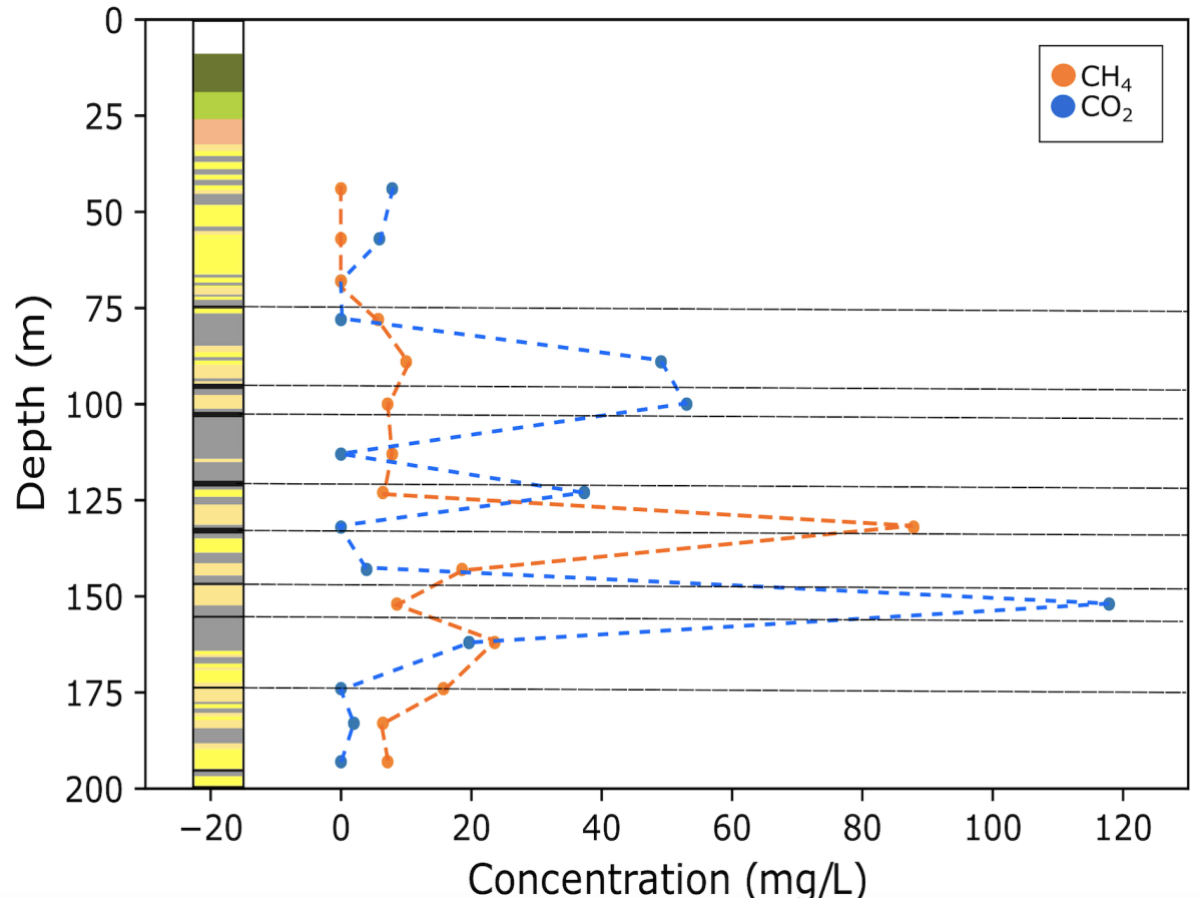

Figure 3-3: Stratigraphic log of BH GGC01 and CH_4 and CO_2 concentrations with depth (black dashed lines indicate coal seams). The figure highlights that increased concentrations of CH_4 gas correlate to areas immediately surrounding the unmined coal seams in the subsurface. The highest CO_2 concentrations occurred in samples with lowest CH_4 concentrations, or where CH_4 was absent.

For mined boreholes GGA05 and GGA08, considerably less instances of elevated CH_4 concentrations were found to be present throughout the succession. It is noted that the majority of samples have CH_4 levels below detection limits, which compliments groundwater concentration data (Palumbo-Roe et al., 2021) (Figs.3.4 & 3.5). In GGA08, CH_4 gas was identified at four stratigraphic depths, and correlates with unmined coal seams (a minor coal unit at 38-40m depth, and the Glasgow Upper coal seam at 52-53m depth), and the area directly below the Glasgow Ell coal mine workings (78-79m depth). In GGA05, CH_4 gas was solely detected at 57 to 67m depth in a cluster of samples in the area directly above the collapsed Glasgow Ell mine workings (Fig. 3.4). CH_4 concentrations for GGA05 and GGA08 boreholes ranged from 6 to 324mg/L mean= 53mg/L, Std.dev= 102mg/L), with the highest CH_4 concentration correlating to the unmined Glasgow Ell index coal seam in GGA05. These values are higher than in-situ groundwater CH_4 concentrations recorded e.g., Glasgow Main (174 µg/L-185µg/L) and Glasgow Upper (117µg/L-145µg/L) (Palumbo-Roe et al., 2021).

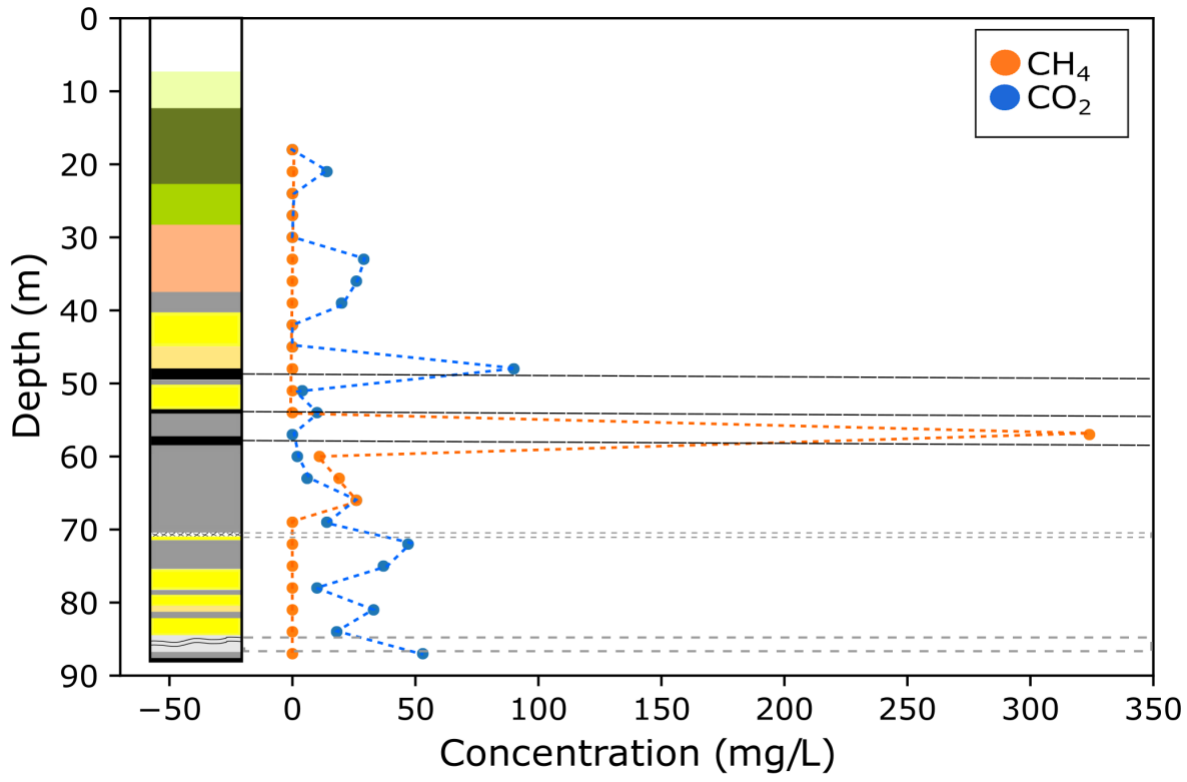

Figure 3-4: Stratigraphic log of BH GGA05 and CH_4 and CO_2 concentrations with depth (black dashed lines indicate coal seams and grey dashed boxes indicate coal mine workings). CH_4 was solely detected at 57 to 67m depth in a cluster of samples, in the succession directly above the Glasgow Ell mine workings. The CO_2 gas did not show the same trend, and was present throughout the stratigraphic succession.

However, CO_2 gas was present throughout the succession of both GGA05 and GGA08 boreholes, with concentrations ranging from 4-130mg/L (mean=31mg/L, Std.dev= 30mg/L) (Figs. 3.4 & 3.5), and corresponds well with measured groundwater concentrations of 105mg/L to 256mg/L (Palumbo-Roe et al., 2021). In both GGA05 and GGA08, the highest CO_2 gas concentrations occurred at the unmined Glasgow Upper coal seam, and at both the Glasgow Ell and Glasgow Main mine workings.

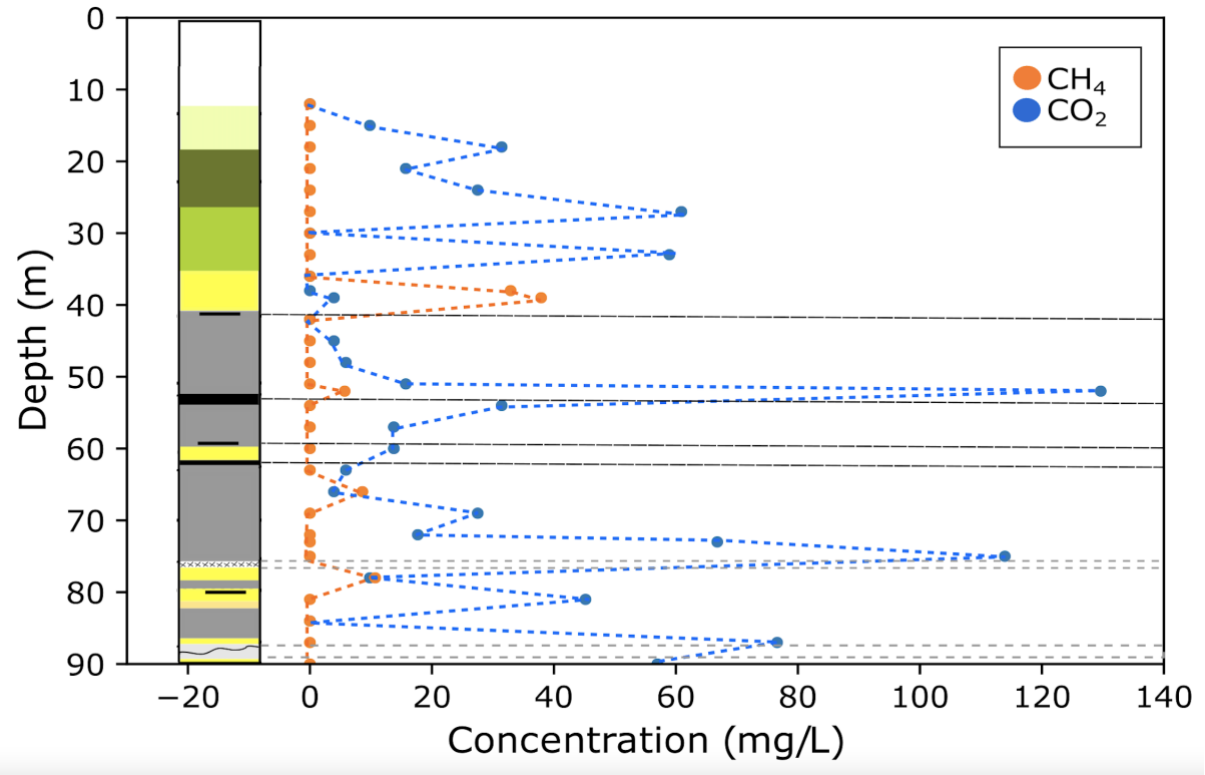

Figure 3-5: Stratigraphic log of BH GGA08 and CH_4 and CO_2 concentrations with depth black dashed lines indicate coal seams and grey dashed boxes indicate coal mine workings). CH_4 was identified at four stratigraphic depths; all of which correspond to areas of coal seams or mine workings. Conversely, CO_2 was present throughout the entire stratigraphic sequence, and generally present in higher concentrations than CH_4.

3.5.2 CH_4 and CO_2 Stable Isotope Values

Core samples from the unmined GGC01 borehole exhibit a narrow $\delta^{13}C_{CH4}$ range of -73.4‰ to -64‰, which is characteristic of a biogenic CH_4 source (Stolper et al., 2018; Osborn et al., 2011; Whiticar et al., 1999; Schoell, 1980). Associated deuterium values for GGC01 also fall

within a narrow range of δD_{CH4}, with values of -277‰ to -240‰, and compliment the biogenic origin implied by $\delta^{13}C_{CH4}$ values. The shallow mined GGA05 and GGA08 boreholes have $\delta^{13}C_{CH4}$ values that range from -70‰ to -14.3‰, and -74.1‰ to -19.7‰, respectively. GGA05 and GGA08 δD_{CH4} values also exhibit a large range; with values of -182‰ to 17.3‰, and -259‰ to -88‰. However, as evidenced in Table A.4 in Appendix A, there are four samples from GGA05 and GGA08 that are enriched in $^{13}C_{CH4}$ and $^{2}H_{CH4}$, which account for the large range in $\delta^{13}C_{CH4}$ and δD_{CH4} values. Excluding these samples, GGA05 and GGA08 have $\delta^{13}C_{CH4}$ values of -74.1‰ to -70‰ and δD_{CH4} values of -259‰ to -182‰ corresponding with the biogenic CH_4 signatures observed in GGC01.

Carbon isotope compositions for CO_2 range from -12.7‰ to -6.1‰ for GGC01; -29‰ to -10‰ for GGA05; and -25.5‰ to -11.4‰ for GGA08. Such values align with previously reported values of coal bed globally ($\delta^{13}C_{CO2}$= -27‰ to +19‰) (Rice, 1993). The carbon isotope values of Dissolved Inorganic Carbon ($\delta^{13}C_{DIC}$) of produced waters were obtained during pumping tests conducted by the BGS for the shallow mine monitoring boreholes. Analysis of these samples found that $\delta^{13}C_{DIC}$ in the groundwaters range from -12.8‰ to -7.1‰, with an average value of -10.9‰ (Palumbo-Roe et al., 2021). For the Midland Valley of Scotland, these results fall within the upper range of values previously recorded for coal measures (Palumbo-Roe et al., 2021).

3.6 Discussion

3.6.1 Subsurface CH_4 Sources at the Glasgow Observatory

Figure 3.6 shows the genetic $\delta^{13}C_{CH4}$ and δD_{CH4} diagram by Milkov and Etiope (2018) for GGC01, GGA05, and GGA08 highlighting evidence for two distinct CH_4 signatures. The majority of samples show evidence for the production of CH_4 by carbonate reduction, with the indication of the addition of minor amounts of CH_4 produced through methyl-type fermentation. Through plotting isotopic values of CH_4 and CO_2 from the same stratigraphic unit (Fig. 3.7), it is evident that the majority of samples exhibit a greater ^{13}C enrichment, with

an isotopic fractionation >55% for $^{13}C_{CH4}$ relative to $^{13}C_{CO2}$. This is indicative of CH_4 production primarily by carbonate reduction (Whiticar, 1999). The $^{13}C_{CH4}$ and $^{2}H_{CH4}$ enriched samples appear to plot in the thermogenic CH_4 origin field of Figure 3.6. However, previous studies have consistently shown that during CH_4 oxidation, ^{12}C is preferentially removed resulting in a marked decrease in isotopic fractionation between CH_4 and CO_2, and during advanced stages, this fractionation can range between 5-25% (Barker and Fritz, 1981; Whiticar, 1999). Figure 3.7 highlights the difference $\Delta 13C_{CO2\text{-}CH4}$ is close to 5‰, and follows the evolution pathway for CH_4 oxidation. Hence, this data implies that bacterial CH_4 is originally generated from high organic content sedimentary units and coals under anoxic conditions primarily via the carbonate reduction pathway (Gründger et al., 2015; Guo et al., 2012; Krüger et al., 2008). Subsequently, at 63 to 79m depth at the GGERF site, the oxidative consumption of bacterial coal bed CH_4 occurs resulting in a distinctly enriched ^{13}C and ^{2}H CH_4 signature.

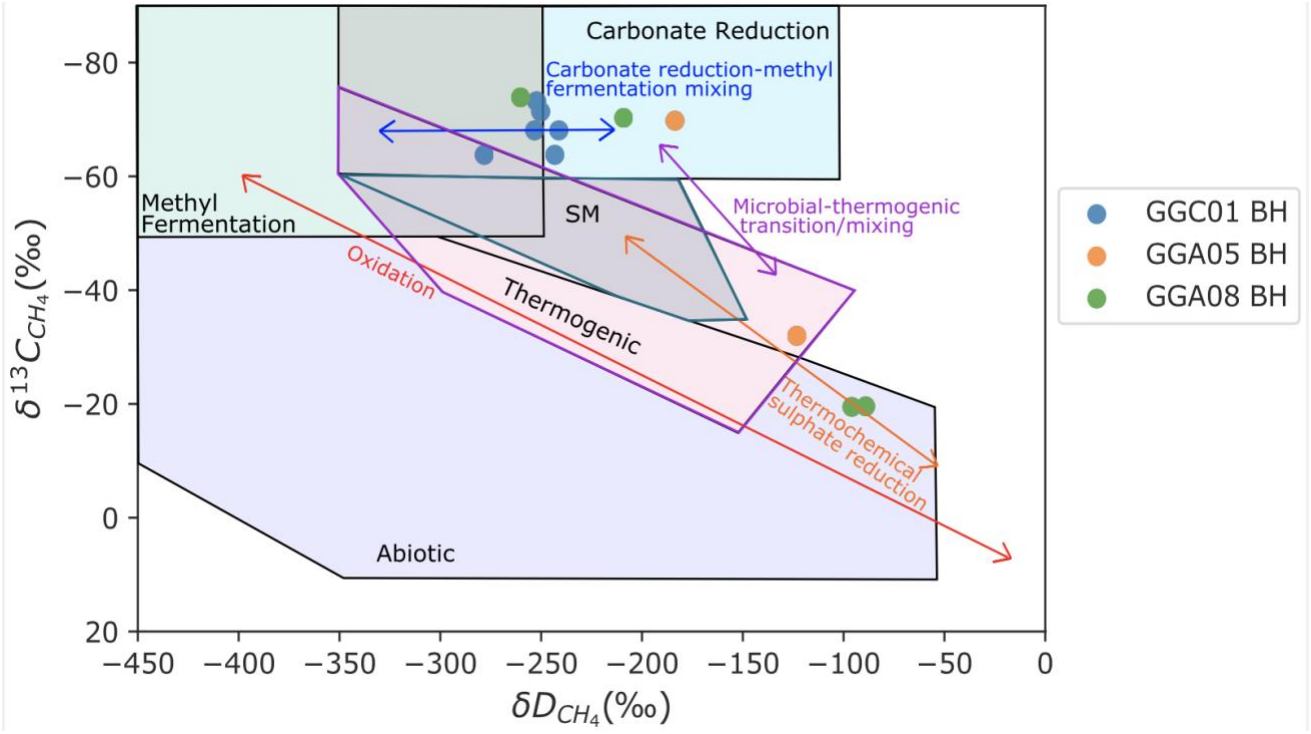

Figure 3-6: Plot of δD_{CH4} and $\delta^{13}C_{CH4}$ stable isotopic analyses of CH_4 gas exsolved from core and cutting samples from GGC01, GGA05, and GGA08 boreholes. (Secondary CH_4 (SM) boundary indicated in green and thermogenic CH_4 boundary indicated in purple). Processes that affect the isotopic and molecular composition are highlighted (oxidation and thermochemical sulphate reduction). Mixing of microbial gases produced through carbonate reduction and methyl fermentation is indicated by the blue mixing arrow, with mixing of thermogenic and microbial methane indicated by the purple mixing arrow. The majority of samples plot within the biogenic CH_4 zone, with a potential mixing of both carbonate reduction and methyl type fermentation sources.

Enriched samples plotting outside of biogenic origin fields are a result of CH_4 oxidation. The classification areas of biogenic and thermogenic CH_4 sources are adapted from Whiticar, 1999, and the plot is adapted from Milkov and Etiope, 2018.

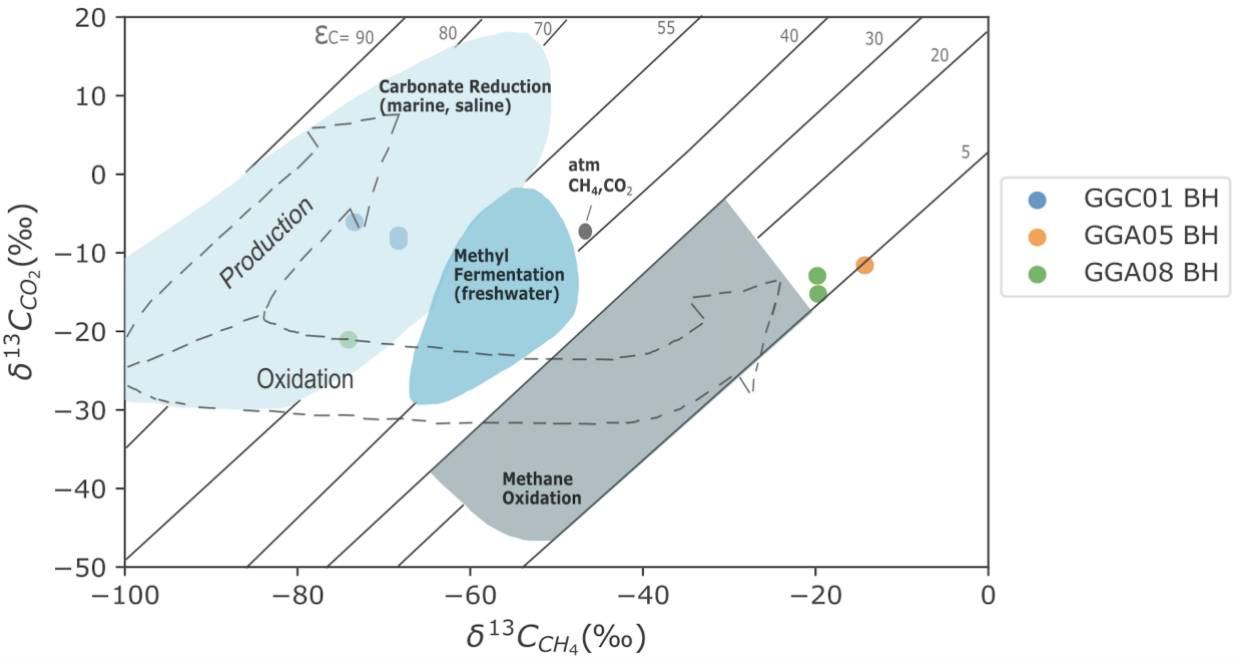

Figure 3-7: Isotope combination plot of $\delta^{13}C_{CH4}$ and $\delta^{13}C_{CO2}$ data from GGC01, GGA05, and GGA08 boreholes; with isotope fractionation lines and partitioning trajectories as a result of CH_4 formation and oxidation processes. The majority of samples exhibit greater ^{12}C enrichment with an isotopic fractionation indicative of CH_4 production by carbonate reduction. The three enriched samples that plot around 5% isotope fractionation indicate CH_4 oxidation, as ^{12}C is preferentially removed resulting in a decrease in isotopic fractionation between $^{13}C_{CH4}$ relative to $^{13}C_{CO2}$. Isotope plot adapted from Whiticar, 1999.

3.6.2 CO_2 Signatures

Sources of CO_2 gas within coal beds are dependent on the burial and uplift history of the stratigraphic units, and may also contain CO_2 contributions from other sources such as dissolved atmospheric and soil gas, magmatic or mantle degassing, microbial degradation of organic substrates, and the thermal maturation of kerogen (Dai et al., 1996; Golding et al., 2013). In relation to interpreting $\delta^{13}C_{CO2}$ and $\alpha^{13}C_{CO2\text{-}CH4}$ values, there are a number of non-methanogenic processes that can affect gas signatures and therefore shift $\alpha^{13}C_{CO2\text{-}CH4}$ from the 'true' methanogenic fractionation value (Baublys et al., 2015; Chen et al., 2023; Flores et al., 2008; Golding et al., 2013; Vinson et al., 2017). Such processes include the mixing of

biogenic and thermogenic gases, methane oxidation resulting in the conversion of CH_4 to CO_2, bacterial processes which produce CO_2 such as sulfate reduction, and interaction with formation waters resulting in gas losses (Golding et al., 2013; Vinson et al., 2017, Whiticar et al., 1986). The mixing of biogenic and thermogenic gases can lower the $\alpha^{13}C_{CO2\text{-}CH4}$ value, as thermogenic gas typically has a more enriched $\delta^{13}C_{CH4}$ and depleted $\delta^{13}C_{CO2}$ signature than biogenic gas (Vinson et al., 2017; Whiticar et al., 1986). Methane oxidation affects the $\alpha^{13}C_{CO2\text{-}CH4}$ values as the residual un-oxidated methane has a more enriched $\delta^{13}C_{CH4}$ signature and therefore lowers the apparent $\alpha^{13}C_{CO2\text{-}CH4}$ value (Chen et al.; Vinson et al., 2017; Whiticar, 1999). Bacterial processes such as sulfate reduction can consume CH_4 and produce CO_2, with little fractionation on the carbon values, resulting in the lowering of the $\alpha^{13}C_{CO2\text{-}CH4}$ value (Vinson et al., 2017). Finally, CH_4 and CO_2 can be lost through dissolution and advection as groundwater flows through the coal bed formation. Therefore, a semi-open system where CH_4 and CO_2 are not fully retained results in the $\alpha^{13}C_{CO2\text{-}CH4}$ value being affected (Golding et al., 2013; Vinson et al., 2017).

Microbial coal bed gases tend to have carbon and hydrogen fractionation factors ($\alpha^{13}C_{CO2\text{-}CH4}$= (1000 + $\delta^{13}C_{CO2}$) / (1000 + $\delta^{13}C_{CH4}$)) close to expected $\alpha^{13}C_{CO2\text{-}CH4}$ values for the carbonate reduction pathway (1.06 to 1.09) (Chen et al., 2023; Golding et al., 2013; Vinson et al., 2017).$^{13}C_{CO2}$ and $^{13}C_{CH4}$ values from close stratigraphic horizons, highlighted in Fig.3.7, indicate a consistent $\alpha^{13}C_{CO2\text{-}CH4}$ value of 1.06 for all GGC01 samples, and for some shallow samples from GGA05 and GGA08, indicating a characteristic CO_2 reduction pathway for methanogenesis. However, several GGA05 and GGA08 samples from 66 to 79m depth have much lower $\alpha^{13}C_{CO2\text{-}CH4}$ values (1.003-1.007), evidencing the potential for non-methanogenic processes altering the 'true' methanogenic fractionation factor. The dissolution of microbial CO_2 results in enriched $\delta^{13}C_{DIC}$ values of 8‰ relative to the gas phase CO_2 (Clark and Fritz, 1997). With pumping test data (Palumbo-Roe et al., 2021) establishing measured $\delta^{13}C_{DIC}$ values of -12.8‰ to -7.1‰ within groundwater contained in the mineworkings, a general enrichment of 8‰ can be observed between $\delta^{13}C_{DIC}$ and $\delta^{13}C_{CO2}$ values (For example: superficial deposits $\delta^{13}C_{DIC}$ = -12.8‰ to -10.9‰ and $\delta^{13}C_{CO2}$ = -25.5‰ to -21‰; Glasgow

Upper $\delta^{13}C_{DIC}$ = -11.2‰ to -10.9‰ and $\delta^{13}C_{CO2}$ = -18.3‰; Glasgow Main $\delta^{13}C_{DIC}$ = -10.8‰ and $\delta^{13}C_{CO2}$ = -19.8‰). The additional enrichment of $\delta^{13}C_{DIC}$ observed in the samples may be explained by interaction with carbonates via precipitation and dissolution reactions, the source of which may potentially derive from sulphuric acid produced through pyrite oxidation within the former coal mine workings (Palumbo-Roe et al., 2021). As such, the varying $\delta^{13}C_{CO2}$ signatures within the site highlight a potential for a combination of non-methanogenic processes such as methane oxidation and dissolution occurring, highlighting the complications of using isotopic identification techniques.

3.6.3 Stable Isotope Profiles with Depth

The stable isotope profiles with depth are plotted for CH_4 and CO_2 in Fig.3.8, illustrating that there is no clear correlation of the CH_4 stable isotope ratios with depth. There is a consistent biogenic $\delta^{13}C_{CH4}$ signature of -75‰ to -64‰, with a distinct zone of markedly heavier CH_4 occurring between a depth of 63 and 79m, corresponding to enriched $\delta^{13}C_{CH4}$ values of -32.2‰ and -14.3‰. At Borehole GGA05, the heavily oxidised signatures occur within 5 to 9m above the collapsed Glasgow Ell coal mine workings, in both clay and silt sedimentary units that contain thin coal seams and have high organic content. The enriched $^{13}C_{CH4}$ signatures for GGA08 are found in clay, silt, and sand sedimentary units, with moderate organic content within 3 to 9m of the same Glasgow Ell workings. In both GGA05 and GGA08 boreholes, enriched $^{13}C_{CH4}$ and $^{2}H_{CH4}$ signatures are observed at 66-67m depths, hence it is unlikely this enriched signature is the result of air ingress into isojars during sample storage.

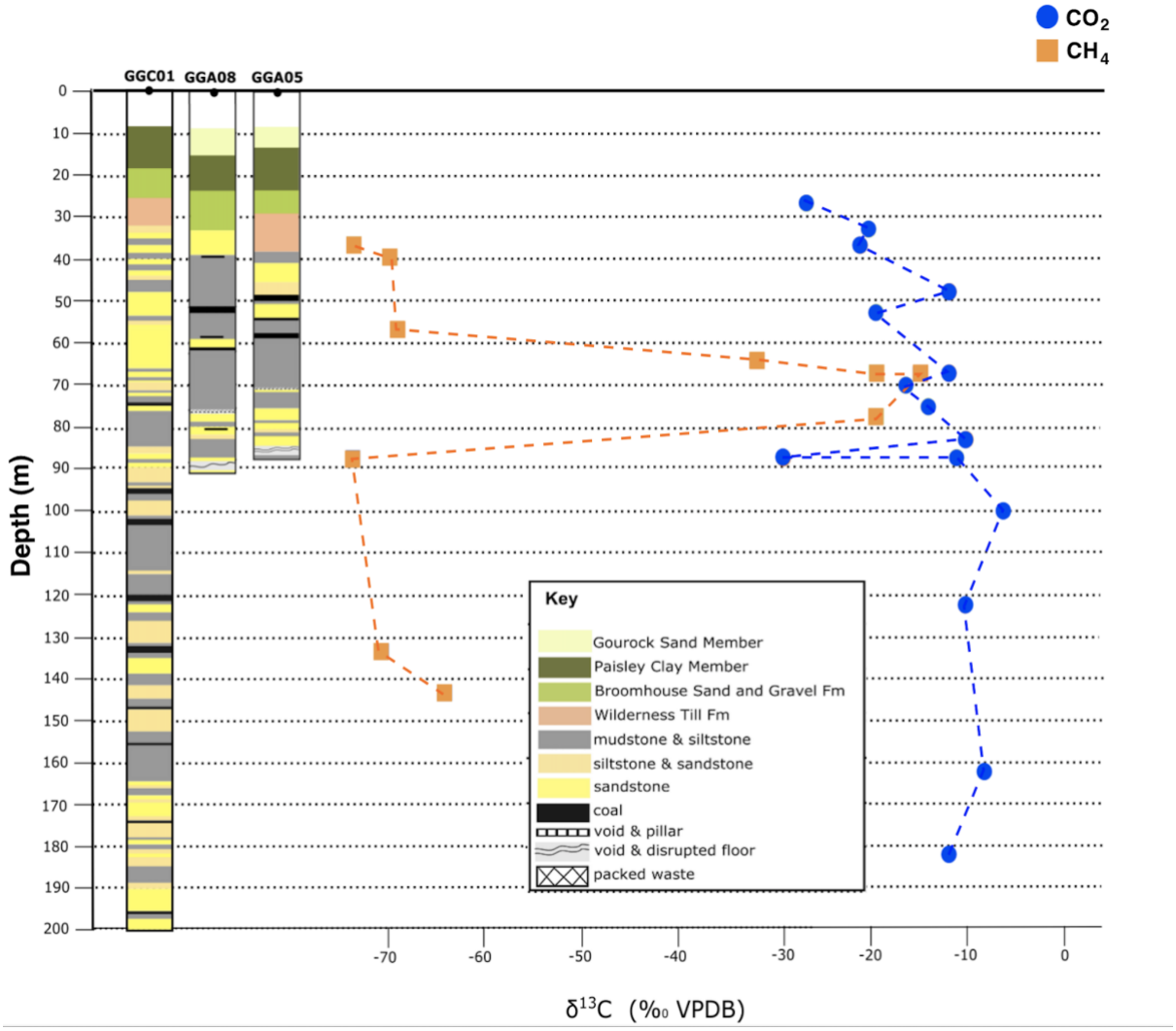

Figure 3-8: Isotopic depth plots of CH_4 and CO_2 $\delta^{13}C$ values from GGC01, GGA05, and GGA08 boreholes; with the corresponding stratigraphy. CH_4 stable isotopes have no clear correlation with depth, with a consistent biogenic signature present, and a distinct zone of enriched CH_4 in the area surrounding the Glasgow Ell mine workings. CO_2 gas exhibits a consistent depleted $^{13}C_{CO2}$ signature with shallower depth, highlighting the increasing influence of shallow groundwater within the subsurface.

A consistent signature was observed in the CO_2 from these samples, with CO_2 gas signatures showing a progressive depletion in $^{13}C_{CO2}$ at shallower depths (from ~-10‰ at 180m depth to -23‰ in the shallowest sample (36m depth)) (Fig. 3.8). Values recorded from the superficial deposits are the most depleted in $^{13}C_{CO2}$, with the unmined bedrock samples from GGC01 being the most enriched in ^{13}C, with the exception of a distinct depleted CO_2 sample (-29‰) occurring at ~90m depth, in the area of the Glasgow Main mine-workings.

3.6.4 Lessons for the monitoring of minewater geothermal sites

In establishing the environmental baseline of the site, ground gas baseline surveys were also undertaken at the Glasgow Observatory, in order to determine if potential mine gases or gas originating from overlying made ground could be detected in the near surface environment (Monaghan et al., 2022). Through these surveys, CO_2 and CH_4 flux at the soil-atmosphere interface, ground gas concentrations of CO_2, CH_4, H_2, H_2S, O_2, a proxy for N_2, and a limited number of carbon stable isotope samples were measured (see Monaghan et al., 2022 for full sampling methodology).

Ground gas CH_4 concentrations were comparable to atmospheric gas (<3ppm by volume) and CH_4 flux was typically below detection limits (Monaghan et al. 2022), which corresponds well to our measured CH_4 concentration data, with the majority of samples having CH_4 levels below detection limits, and the highest CH_4 concentration levels recorded in the areas of unmined coal seams, or the Glasgow Ell mine workings. CO_2 flux measured above the site was consistent with uncontaminated rural (Ward et al., 2019) and other UK sites previously surveyed. However, there were instances of moderate ground gas concentrations (10-20% by volume) in isolated points across surveys (Monaghan et al., 2022). From limited carbon stable isotope ratios, $\delta^{13}C$ values typically range from –23.59‰ and –26.31‰ and compare well to our shallowest GGA05 and GGA08 samples, as $\delta^{13}C_{CO2}$ values get progressively lower to a value of -23.0‰, as soil gas CO_2 has an increasing influence through shallow groundwaters. This also highlights gas concentrations and signatures are highly variable and closely linked to stratigraphic horizon in the shallow subsurface, as it is evident that mine gas signatures from the workings does not impact ground gas (Monaghan et al., 2022). From stoichiometric CO_2: O_2 relationships, ground gas appears to be a mixture of natural origin of photosynthetic production, and of microbial oxidation of CH_4 to CO_2 (Monaghan et al., 2022).

The comparison of ground gas data with core and cutting gas measurements is critical for the monitoring of geothermal and other geoenergy activities, as it allows for the sensitive measuring and tracking of key hazardous gases that may arise from subsurface use

(Monaghan et al., 2022). Our results show that the CO_2 contained in the subsurface below 100m depth is geochemically distinct from that of the shallow subsurface (0-90m depth), meaning that an increase of CO_2 levels at the near-surface originating from deeper mine workings below 100m from any potential perturbation of the system may be detectable using $\delta^{13}C$ measurements. However, further work is required to ascertain the detection limit, and if gas migration processes would significantly change the $\delta^{13}C$ signature of the migrating CO_2.

3.7 Conclusions

We identify the presence of both CH_4 and CO_2 in the gases exsolved from core and cutting samples taken from boreholes GGC01, GGA05, and GGA08 at the Glasgow Observatory site. Our results show that there is no correlation between gas concentration and depth, as both CH_4 and CO_2 gas concentration values are highly variable and are closely linked to individual stratigraphic horizons. We find evidence that CH_4 present in the site's Carboniferous coal measures is of biogenic origin, produced primarily through the carbonate reduction pathway, with a potential mixing of CH_4 from methyl-type fermentation. Enriched ^{13}C and ^{2}H CH_4 signatures are found within 63 to 79m depth in GGA05 and GGA08 boreholes, and provide evidence of CH_4 oxidation in proximity to the Glasgow Ell coal mine workings. CO_2 gas is more abundant throughout the succession in all three boreholes and has an enriched $^{13}C_{CO2}$ signature relative to the CH_4 present. The observed CO_2 gas signature becomes progressively depleted in $^{13}C_{CO2}$ at shallower depths above 90m, with the trend being attributed to the increasing influence of groundwater containing a mixture of dissolved marine carbonate minerals and soil gas CO_2 at shallower depths. Comparing our results to determined ground gas signatures, there is no evidence of ground gas currently being impacted by gas migration from the Glasgow Observatory mine workings.

The findings presented here provide an insight into the variability of mine derived gases, and highlight the presence of distinct gas signatures that are linked to stratigraphic horizon. The gas baseline signature of the shallow subsurface of the Glasgow Observatory can be integrated into larger environmental datasets (Monaghan et al., 2022) in order to generate a

“time zero” records of the site, which are key in informing fit-for-purpose monitoring operations and developing efficient geothermal infrastructures. By characterising the shallow subsurface through depth-dependent isotopic gas fingerprints in the mined succession and comparing to distinctive ground gas isotopic compositions; there is potential to use such signatures to evaluate any potential change in the shallow subsurface environment once pumping, heat abstraction, and re-injection commence.

3.8 References

Adams, C., Monaghan, A. and Gluyas, J., 2019. Mining for heat. Geoscientist, 29(4), pp.10-15.

Barker, J.F. and Fritz, P., 1981. Carbon isotope fractionation during microbial methane oxidation. *Nature*, *293*(5830), pp.289-291.

Baublys, K.A., et al., 2015. Microbial controls on the origin and evolution of coal seam gases and production waters of the Walloon Subgroup; Surat Basin, Australia. International Journal of Coal Geology 147-148, 85-104.

British Geological Survey (2020a): UKGEOS Glasgow GGA05 borehole information pack. British Geological Survey. (Dataset).

British Geological Survey (2020b): UKGEOS Glasgow GGA08 borehole information pack. British Geological Survey. (Dataset)

Burns, R., Wynn, P.M., Barker, P., McNamara, N., Oakley, S., Ostle, N., Stott, A.W., Tuffen, H., Zhou, Z., Tweed, F.S. and Chesler, A., 2018. Direct isotopic evidence of biogenic methane production and efflux from beneath a temperate glacier. Scientific reports, 8(1), pp.1-8.

Cameron, I.B. and Stephenson, D., 1985. British regional geology: The Midland Valley of Scotland (No. 5). Hmso Books.

Chen, X., Wang, Y., Tao, M., et al. (2023) Tracing the origin and formation mechanisms of coalbed gas from the Fuxin Basin in China using geochemical and isotopic signatures of the gas and coproduced water. Int. J. Coal Geol.

CL:AIRE, 2021. Good practice for risk assessment for coal mine gas emissions. CL:AIRE, Buckinghamshire. ISBN 978-1-905046-39-3

Clark, I.D. and Fritz, P., 1997. Environmental Isotopes in Hydrogeology. CRC Press.

Coplen, T.B., 1995. Reporting of stable carbon, hydrogen, and oxygen isotopic abundances. *Reference and intercomparison materials for stable isotopes of light elements*, *825*, pp.31-34.

Craig, H., 1957. Isotopic standards for carbon and oxygen and correction factors for mass-spectrometric analysis of carbon dioxide. *Geochimica et cosmochimica acta*, *12*(1-2), pp.133-149.

Dai, J.X., Song, Y., Dai, C. Sen, Wang, D.R., 1996. Geochemistry and accumulation of carbon dioxide gases in China. Am. Assoc. Pet. Geol. Bull. 80, 1615–1626.

Dochartaigh, B.Ó., Bonsor, H. and Bricker, S., 2019. Improving understanding of shallow urban groundwater: the Quaternary groundwater system in Glasgow, UK. *Earth and Environmental Science Transactions of the Royal Society of Edinburgh*, *108*(2-3), pp.155-172.

Donnelly, T., Waldron, S., Tait, A., Dougans, J. and Bearhop, S., 2001. Hydrogen isotope analysis of natural abundance and deuterium-enriched waters by reduction over chromium on-line to a dynamic dual inlet isotope-ratio mass spectrometer. *Rapid Communications in Mass Spectrometry*, *15*(15), pp.1297-1303.

Dunbar, E., Cook, G.T., Naysmith, P., Tripney, B.G. and Xu, S., 2016. AMS 14 C dating at the Scottish Universities Environmental Research Centre (SUERC) radiocarbon dating laboratory. *Radiocarbon*, *58*(1), pp.9-23.

Flores, R.M., Rice, C.A., Stricker, G.D., Warden, A. and Ellis, M.S., 2008. Methanogenic pathways of coal-bed gas in the Powder River Basin, United States: the geologic factor. *International journal of coal geology*, *76*(1-2), pp.52-75.

Golding, S.D., Boreham, C.J. and Esterle, J.S., 2013. Stable isotope geochemistry of coal bed and shale gas and related production waters: A review. *International Journal of Coal Geology*, *120*, pp.24-40.

Gonfiantini, R., 1984. Stable isotope reference samples for geochemical and hydrological investigations. *Int. J. Appl. Radiat. Isot.;(United Kingdom)*, *35*(5).

Gründger, F., Jiménez, N., Thielemann, T., Straaten, N., Lüders, T., Richnow, H.H. and Krüger, M., 2015. Microbial methane formation in deep aquifers of a coal-bearing sedimentary basin, Germany. *Frontiers in microbiology*, *6*, p.200.

Guo, H., Liu, R., Yu, Z., Zhang, H., Yun, J., Li, Y., Liu, X. and Pan, J., 2012. Pyrosequencing reveals the dominance of methylotrophic methanogenesis in a coal bed methane reservoir associated with Eastern Ordos Basin in China. *International journal of coal geology*, *93*, pp.56-61.

Györe, D., McKavney, R., Gilfillan, S.M. and Stuart, F.M., 2018. Fingerprinting coal-derived gases from the UK. *Chemical Geology*, *480*, pp.75-85.

Hall, J., Glendinning, S., and Younger, P. (2005). "*Is Mine Water a Source of Hazardous Gas*?," in 9th International Mine Water Congress, Oviedo, Asturias, Spain, 5-7 September 2005.

Jackson, R.E., Gorody, A.W., Mayer, B., Roy, J.W., Ryan, M.C. and Van Stempvoort, D.R., 2013. Groundwater protection and unconventional gas extraction: The critical need for field-based hydrogeological research. *Groundwater*, *51*(4), pp.488-510.

Kampbell, D.H. and Vandegrift, S.A., 1998. Analysis of dissolved methane, ethane, and ethylene in ground water by a standard gas chromatographic technique. *Journal of Chromatographic Science*, *36*(5), pp.253-256.

Krüger, M., Beckmann, S., Engelen, B., Thielemann, T., Cramer, B., Schippers, A. and Cypionka, H., 2008. Microbial methane formation from hard coal and timber in an abandoned coal mine. *Geomicrobiology Journal*, *25*(6), pp.315-321.

Kusakabe, M., 2005. A closed pentane trap for separation of SO2 from CO2 for precise $\delta^{18}O$ and & $\delta^{34}S$ measurements. *Geochemical Journal*, *39*(3), pp.285-287.

LeDoux S.T, Szynkiewicz, A., Faiia, A.M., Mayes, M.A., McKinney, M.L. and Dean, W.G., 2016. Chemical and isotope compositions of shallow groundwater in areas impacted by hydraulic fracturing and surface mining in the Central Appalachian Basin, Eastern United States. Applied geochemistry, 71, pp.73-85.

Milkov, A.V. and Etiope, G., 2018. Revised genetic diagrams for natural gases based on a global dataset of> 20,000 samples. Organic Geochemistry, 125, pp.109-120.

Molofsky, L.J., Connor, J.A., Wylie, A.S., Wagner, T. and Farhat, S.K., 2013. Evaluation of methane sources in groundwater in northeastern Pennsylvania. *Groundwater*, *51*(3), pp.333-349.

Monaghan, A.A., Bateson, L., Boyce, A.J., Burnside, N.M., Chambers, R., De Rezende, J.R., Dunnet, E., Everett, P.A., Gilfillan, S., Jibrin, M.S. and Johnson, G., 2022. Time zero for net zero: a coal mine baseline for decarbonising heat. *Earth Science, Systems and Society*, p.9.

Monaghan, A.A., Starcher, V., O Dochartaigh, B., Shorter, K. and Burkin, J., 2019. UK Geoenergy Observatories: Glasgow Geothermal Energy Research Field Site: Science Infrastructure Version 2.

Monaghan A A, Damaschke M, Starcher V, Fellgett M W, Kingdon A, Kearsey T, Hannis S, Gillespie M, Shorter K, Elsome J, Barnett M. (2021). UKGEOS Glasgow GGC01 Final Borehole Information Pack. NERC EDS National Geoscience Data Centre. (Dataset).

Monaghan, A.A., Starcher, V., Barron, H.F., Shorter, K., Walker-Verkuil, K., Elsome, J., Kearsey, T., Arkley, S., Hannis, S. and Callaghan, E., 2022. Drilling into mines for heat: geological synthesis of the UK Geoenergy Observatory in Glasgow and implications for mine water heat resources. Quarterly Journal of Engineering Geology and Hydrogeology, 55(1).

NERC, University of Strathclyde and BGS. 2019. Record of proceedings UK Geoenergy Observatories Glasgow Geothermal Energy Innovation Workshop, https://cms.ukgeos.ac.uk/event/assets/innovation_event_030619_ final.pdf

Osborn, Stephen G., Avner Vengosh, Nathaniel R. Warner, and Robert B. Jackson. "Methane contamination of drinking water accompanying gas-well drilling and hydraulic fracturing." *proceedings of the National Academy of Sciences* 108, no. 20 (2011): 8172-8176.

Palumbo-Roe, B., Shorter, K.M., Fordyce, F.M., Walker-Verkuil, K., O Dochartaigh, B.E., Gooddy, D.C. and Darling, W.G., 2021. UK Geoenergy Observatories: Glasgow borehole test pumping-groundwater chemistry.

Ramsay, C., McRae, C., Ryan, E., McCallum, A., Wellington, L., Lauder, L., Millar, R., Haunch, S. and Othieno, R., 2017. Carbon dioxide ingress into residential houses at Gorebridge in Midlothian, Scotland, United Kingdom Richard Othieno. European Journal of Public Health, 27(suppl_3).

Rice, D.D., 1993. Composition and origins of coalbed gas. *Hydrocarbons from coal: AAPG Studies in Geology*, *38*(1), pp.159-184.

Schoell, M., 1980. The hydrogen and carbon isotopic composition of methane from natural gases of various origins. Geochimica et Cosmochimica Acta, 44(5), pp.649-661.

Stuart M.E. 2012. Potential groundwater impact from exploitation of shale gas in the UK. British Geological Survey Open Report, OR/12/001. 33pp

Stephenson, M.H., Ringrose, P., Geiger, S., Bridden, M. and Schofield, D., 2019. Geoscience and decarbonization: current status and future directions. Petroleum Geoscience, 25(4), pp.501-508.

Strąpoć, D., Mastalerz, M., Dawson, K., Macalady, J., Callaghan, A.V., Wawrik, B., Turich, C. and Ashby, M., 2011. Biogeochemistry of microbial coal-bed methane. *Annual Review of Earth and Planetary Sciences*, *39*.

Stolper, D.A., Lawson, M., Formolo, M.J., Davis, C.L., Douglas, P.M. and Eiler, J.M., 2018. The utility of methane clumped isotopes to constrain the origins of methane in natural gas accumulations. Geological Society, London, Special Publications, 468(1), pp.23-52.

Vinson, D.S., Blair, N.E., Martini, A.M., et al. (2017) Microbial methane from in situ biodegradation of coal and shale: A review and reevaluation of hydrogen and carbon isotope signatures. Chem. Geol.

Ward, R. S., Smedley, P. L., Allen, G., Baptie, B. J., Barkwith, A. K. A. P., Bateson, L., et al. (2019). Environmental monitoring - phase 4 final report (April 2018 - March 2019). Open Report, OR/19/044. Nottingham, UK: British Geological Survey, 225. Available at: http://nora.nerc.ac.uk/id/eprint/527726/.

Whiticar, M.J., 1999. Carbon and hydrogen isotope systematics of bacterial formation and oxidation of methane. Chemical Geology, 161(1-3), pp.291-314.

Younger, P.L. and Robins, N.S., 2002. Challenges in the characterization and prediction of the hydrogeology and geochemistry of mined ground. *Geological Society, London, Special Publications*, *198*(1), pp.1-16.

4 Stable isotope and noble gas characterisation of subsurface methane from the Vale of Pickering, Yorkshire

4.1 Chapter Overview

This chapter aims to characterise the subsurface geochemical signature of the Vale of Pickering site, which was originally intended for unconventional gas extraction, but is now being considered for potential geoenergy technology development. This chapter follows on from Chapter 3 in utilising geochemical fingerprinting tools such as major gas and stable isotope compositions, but also includes the use of noble gas compositions in order to better constrain methane source, and to investigate the potential of gas migration from depth to shallow groundwater sources. As such, this study shows that the utilisation of combined geochemical fingerprinting techniques allows for the better characterisation of geochemical signatures within the subsurface at the Vale of Pickering.

The work presented in this chapter has been written as a stand-alone manuscript, with the intention to submit to a journal. As a result, there is some repetition with the Chapter 2 methodology section.

4.2 Introduction

Interest in the potential for shale gas extraction within the UK has increased over the past decade, primarily as a result of the significant economic success of hydraulic fracturing ('fracking') of shale gas for unconventional gas extraction in the US. The hydraulic fracturing technique has been widely used in conventional petroleum fields in both the UK onshore and offshore (Priestley, 2018), typically in vertical or deviated wells in order to improve the permeability of conventional reservoirs. However, as interest has shifted to the development of geoenergy technologies, including hydraulic fracturing of unconventional hydrocarbon systems onshore, concerns over contamination of groundwater aquifers and surface water

bodies have increased. Such concerns have arisen as a result of allegations of contamination of drinking water wells near shale gas extraction sites in the US (Jackson et al., 2013; Osborn et al., 2011). However, constraint of the definitive origin of alleged groundwater contamination within unconventional hydrocarbon extraction areas in the US has proven difficult, primarily due to a lack of pre-extraction environmental baseline data. Hence, establishing environmental baselines for groundwater bodies, before the implementation of any future geoenergy technology utilising the subsurface, is essential to establish a benchmark to allow the identification of any induced contamination of potable water sources.

The British Geological Survey (BGS) have undertaken extensive research to establish baselines for groundwater systems, focusing on potential shale gas extraction sites and major aquifer bodies (Bell et al., 2017; Ward et al., 2017). The Kirby Misperton site in the Vale of Pickering, Yorkshire was one of two sites in the U.K. where shale gas extraction was originally approved, before exploration ceased due to the moratorium implemented in 2019 after felt induced seismic activity occurred. Whilst unconventional gas development seems unlikely within the Vale of Pickering at present, determining the presence, magnitude, and origin of gases, and how their geochemical fingerprints evolve within the subsurface, is vital in understanding how to manage risks posed by ground gases in the development of future subsurface geoenergy technology in the area.

Traditionally, hydrocarbon abundances $C_1/(C_2+C_3)$ and stable isotopes ($\delta^{13}C_{CH4}$ and δD_{CH4}) of CH_4 and other associated hydrocarbon gases are used to distinguish between thermogenic and bacterial methane sources (Györe et al., 2018; Jackson et al., 2013; Osborn et al., 2011; Schoell 1980; Stuart, 2012; Whiticar, 1999). Bacterial methane is characterised by $C_1/ (C_2+C_3)$ hydrocarbon ratios of 10^3 to 10^5, and stable isotope signatures of $\delta^{13}C_{CH4}$ of < -55‰; and δ^2H_{CH4} < -150‰ (Schoell, 1980). Thermogenic methane typically exhibits ratios of < 100, with stable isotope signatures of $\delta^{13}C_{CH4}$ ranging from -45‰ to -110‰ and δ^2H_{CH4} > -255‰ (Stuart, 2012; LeDoux et al., 2016). However, several processes, such as the mixing of methane sources or microbial oxidation can alter the hydrocarbon abundance and stable isotope signature and may result in the misidentification of gas sources (Barker and Fritz, 1983;

LeDoux et al., 2016; Molofsky et al., 2013; Whiticar, 1999). Hence, utilisation of trace noble gases (He, Ne, Ar, Kr and Xe) contained within the gases can act as an effective fingerprinting tool. As noble gases are not affected by biological or chemical processes, when combined with hydrocarbon abundance and stable isotopes, they can be effective tracers of gas sources and gas migration within the subsurface (Ballentine and Sherwood Lollar, 2002; Darrah et al., 2014; Gilfillan et al., 2017; Györe et al., 2018; Moore et al., 2018).

Here, we outline the major gas, stable isotope and noble gas compositions of gas and groundwater samples from six sites across the Vale of Pickering, in order to determine the source of subsurface methane, and to investigate the potential of gas migration from depth to shallow groundwater sources.

4.3 Geological setting of the Vale of Pickering

The Vale of Pickering is a flat-floored valley located in North Yorkshire, in the catchment of the River Derwent (Bearcock et al., 2015). The valley extends in an east-west orientation to Scarborough and Bridlington in the east and to the Howardian and Hambleton Hills in the west, with the valley constrained by Jurassic Corallian strata in the North York Moors (Ward et al., 2018) (Fig. 4.1).

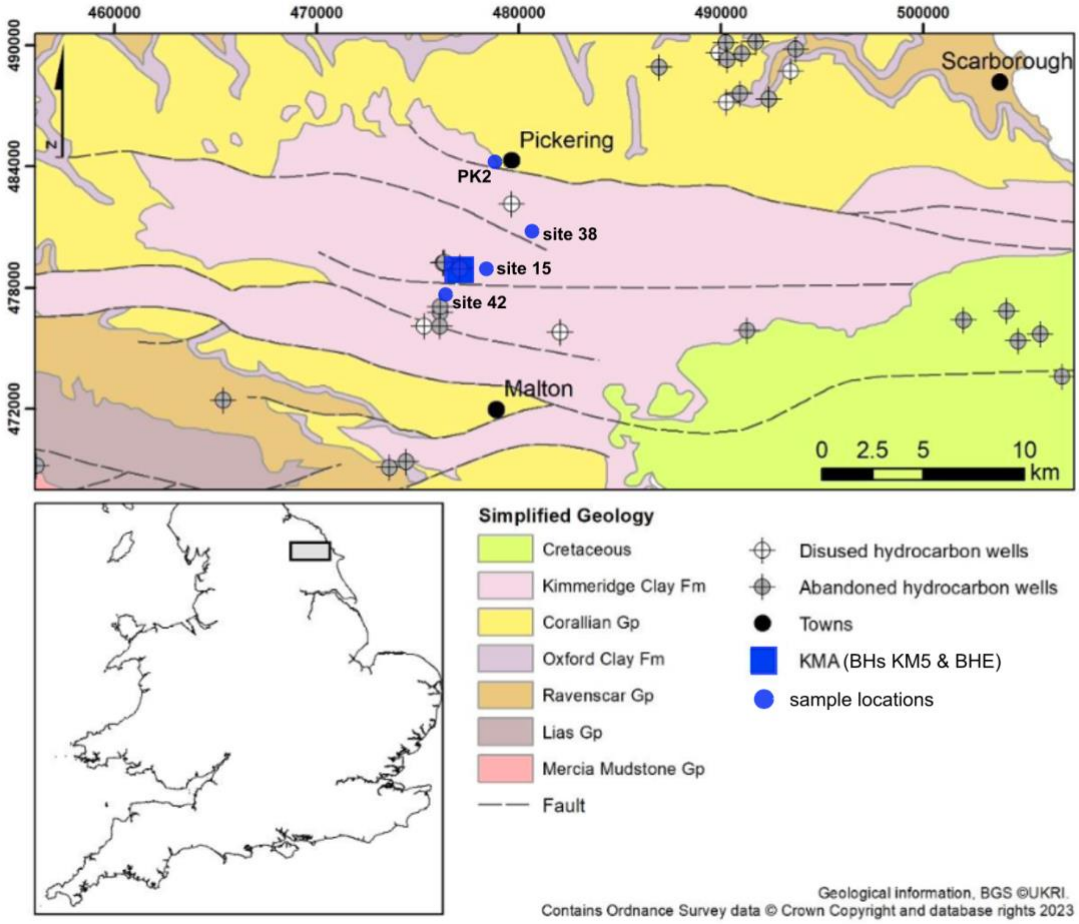

Figure 4-1: Geological map of the Vale of Pickering, highlighting the bedrock geology, faults, and the Kirby Misperton well site (blue square) (Ward et al., 2019). BGS and Third Energy sample locations are highlighted as blue circles, with the KMA well site containing both KM5 and BHE sample localities.

The Vale of Pickering is located on the southern margin of the Cleveland Basin, which was created as a result of back arc extension from the Variscan orogeny (Fraser & Gawthorpe, 1990). The basin consists of folded, faulted and eroded Carboniferous units which are over 3000m thick and was a major depositional centre comprising of 1500-2000m thick Permian, Triassic, and Jurassic deposits (Bearcock et al., 2015; Ward et al., 2018). The Zechstein Group of predominantly carbonate and evaporite sequences were deposited during the Permian, and consist of several distinct geological formations, with the Kirkham Abbey Formation being the primary reservoir of the Vale of Pickering oil and gas fields (Bearcock et al., 2015). Triassic deposits include the Sherwood Sandstone Group, consisting of fluvial sandstones and shales, and the red bed shales of the Mercia Mudstone Group (Bearcock et al., 2015). Jurassic

deposits within the Vale of Pickering include 20-50m of calcareous mudstones of the Oxford Clay units, which is overlain by the Corallian group, consisting primarily of ooidal and micritic limestones and calcareous fine-grained sandstones, but also including facies of muds, silts, and sands (Bearcock et al., 2015). These units are overlain by 400m thick Ampthill & Kimmeridge Clay deposits (termed the Kimmeridge Clay Formation), which consist primarily of fossiliferous marine mudstones, containing local thin beds of silts, clays, and limestones. The Kimmeridge Clay Formation underlies the majority of the floor of the Vale of Pickering, and is overlain locally by superficial deposits, which thickens to the east near Scarborough, but which are thin or absent in the centre of the Vale of Pickering (Bearcock et al., 2015). These superficial deposits are predominately glaciofluvial and glaciolacustrine in origin and date from the Quaternary period (Bearcock et al., 2015; Ward et al., 2018).

Hydrogeologically, the Jurassic Corallian units form the major aquifer body in the area and outcrop on the margins of the Vale of Pickering (Fig. 4.1). The Corallian aquifer is designated as a 'major resource' within the River Derwent catchment, used for both public and private supply (Ward et al., 2018). However, water is not abstracted from the aquifer within the centre of the Vale of Pickering due to its depth exceeding 200m depth as a result of faulting, and due to its high salinity (Ward et al., 2018). Within the Vale of Pickering, the Corallian aquifer is confined both by the Kimmeridge Clay and Oxford Clay Formations, and hence is believed to be hydraulically disconnected from underlying and overlying strata, with groundwater flow predominately through fractures (Allen et al., 1997; Ward et al., 2018). Local superficial deposits within the Vale of Pickering are designated as a 'secondary aquifer' within the area, as shallow (<50m depth) groundwater is used for small scale private use (Ward et al., 2018).

4.4 Sampling and analytical techniques

4.4.1 Sample collection

Duplicate samples were collected from four groundwater boreholes and two Third Energy gas wells at six locations within the Vale of Pickering (Figure 4.1 & Table 4.1). Superficial groundwater samples from sites 15, 38, and 42 were collected alongside the BGS quarterly environmental baseline sampling in February 2020, with the groundwater aquifer samples at site 51 (BHE) and Third Energy well gas samples (KM5 and Pickering 2) collected in August 2020. All samples were collected in approximately 70cm long refrigeration grade 10mm outside diameter copper tubing, connected either to the well heads by a regulator and high-pressure hosing (Holland and Gilfillan, 2013) or to the groundwater pump outflow hose. For all samples, gas or water were flowed through the copper tubes for approximately 5 minutes prior to collection of the sample, to mitigate air contamination. These tubes were then sealed by stainless steel clamps at each end to form a helium leak tight cold weld seal (Gilfillan et al., 2017; Györe et al., 2018).

4.4.2 Sample analysis

The collected samples were analysed for major gas, stable isotope, or noble gas compositions. One subset of gas samples was analysed at the Scottish Universities Environmental Research Centre (SUERC) for major gas compositions and $\delta^{13}C_{CH4}$ and δD_{CH4} stable isotopes. Bulk gases were determined with samples being manually injected into the septa port of a Perkin-Elmer AutoSystem XL gas chromatograph (GC), via a 30m long and 0.53mm internal diameter Sigma-Aldrich Carboxen 1010 PLOT column using helium carrier gas. The GC was also equipped with a flame ionization detector to measure light hydrocarbons and was calibrated with appropriate gas mixtures produced by CalGaz Ltd. $\delta^{13}C_{CH4}$ and δD_{CH4} stable isotopes were determined on the gas combustion line, where an applied pressure gradient drew gas through the line. CO_2 was separated from volatile hydrocarbons using a procedure modified from Kusakabe (2005). A liquid N_2 cooled isopentane trap (-160°C) was applied to collect CO_2 and water before an acetone slush bath was used (~ -78°C) to retain water and vaporise CO_2. The CO_2 was then collected separately in a liquid N_2 cooled cold finger. The CH_4 samples were

combusted over a CuO catalyst at 900°C into CO_2 and water, which were collected in a liquid N_2 cooled cold finger. A pressure gradient drawing gases through the furnace was maintained by the cold finger trapping combustion products. After combustion, the cold finger was heated with an acetone slush bath (~ -78°C) to retain water and vaporise CO_2. This CO_2 was collected isolated in a separate liquid N_2 cooled cold finger and analysed on a VG SIRA II dual-inlet IRMS, calibrated to internal standards (Dunbar et al., 2016), with values measured relative to V-PDB standards. The cold finger containing the collected water was connected to a manifold, heated to vapour, and reduced to H_2 over a nickel catalyst at 800°C. H_2 was analysed in a separate Delta Optima Plus dual-inlet IRMS, and calibrated to internal standards (Donnelly et al., 2001), with values denoted relative to V-SMOW. Uncertainties of $\delta^{13}C$ and δD determinations are 0.3‰ and 3‰, respectively.

A full set of water and gas samples was analysed at the Ohio State University WHEEL laboratory for major gas compositions and noble gas isotopes. Major gas concentrations were measured on a SRS Quadrupole mass spectrometer (MS) and a SRI 8610C Multi-Gas 3+ GC, which was equipped with flame ionization and thermal conductivity detectors, with uncertainties of less than ± 3% (Darrah et al., 2013; Moore et al., 2018). For noble gas analysis, samples were analysed using a quadrupole mass spectrometer (SRS Residual Gas Analyzer 200) for quantification of noble gases (e.g., He, Ar, Kr, Xe), with the methodology described in detail in Hunt et. al., (2012). The 2s analytical error for the $^{3}He/^{4}He$ ratio is approximately 0.5%, with the 1s error of $^{40}Ar/^{36}Ar$ and $^{4}He/^{20}Ne$ isotope ratios being 0.2%. A 1s error of 0.3% for $^{38}Ar/^{36}Ar$, and 1% for $^{20}Ne/^{22}Ne$, $^{21}Ne/^{22}Ne$ and $^{20}Ne/^{36}Ar$. All noble gas abundances have an uncertainty of 1.5%.

The final duplicate groundwater samples were analysed for $\delta^{13}C_{CH4}$ stable isotope ratios at the University of Calgary isotope lab. Samples were injected manually using gas-tight syringes into the helium carrier stream of a Thermo Trace GC Ultra – IsoLink system interfaced to a Thermo 253 MS via a Thermo Conflo IV. The methane gas was converted to CO_2 by passing it through a combustion furnace, with separate CO_2 gas pulses then swept sequentially by the carrier gas through a water trap, and subsequently into an open split interface, which 'leaks'

the gas into the MS. The $\delta^{13}C$ values of the unknown species are then calculated by the instrument software (ISODAT 3.0 SP 0.83).

4.5 Results

The measured bulk gas, stable isotope, and noble gas geochemistry data are presented in Tables 4.1, 4.2, and 4.3.

4.5.1 Major gas compositions

CH_4 was the dominant gas present in all samples, with concentrations ranging from 78.5 to 93.9%. Trace quantities of ethane and propane were found in both gas and water samples, with the gas samples also exhibiting measurable concentrations of higher chained hydrocarbons. CO_2 contents for the gas samples ranged from 0.3 to 2.9%, though CO_2 was not measured for the groundwater samples. N_2 concentrations ranged from 2.9 to 5.1%, with a noted high value of 19% for the Pickering 2.1 sample, which may have been the result of air contamination during manual injection into the GC.

4.5.2 Stable isotope ratios

The Vale of Pickering deep gas samples exhibit a narrow range in $\delta^{13}C$ and δD values, with $\delta^{13}C_{CH4}$ ranging from -34.3 to -33.5‰ and δD_{CH4} values of -180‰ to -164‰, which are, as expected, indicative of a thermogenic gas signature. Water samples collected from the shallow superficial aquifers and the Corallian aquifer (TE BHE) are distinctly biogenic, with the shallow groundwater $\delta^{13}C_{CH4}$ values ranging from -82.9‰ to -77.9‰ and the Corallian groundwater having a $\delta^{13}C_{CH4}$ value of -79.9‰ (Fig. 4.3). Data collected by the BGS for environmental baseline monitoring also exhibit a biogenic signature for both the shallow Kimmeridge Clay and the Corallian groundwaters, with shallow groundwater (sites 15,38, & 42) $\delta^{13}C_{CH4}$ values ranging from -81.8‰ to -58.1‰ and δD_{CH4} values of -210.9‰ to -122‰, and Corallian groundwater (BHE) samples having $\delta^{13}C_{CH4}$ values of -71.8‰ to -63.1‰ and δD_{CH4} of -199.7‰ to -163‰ (Smedley et al., *in review*) (Fig. 4.2).

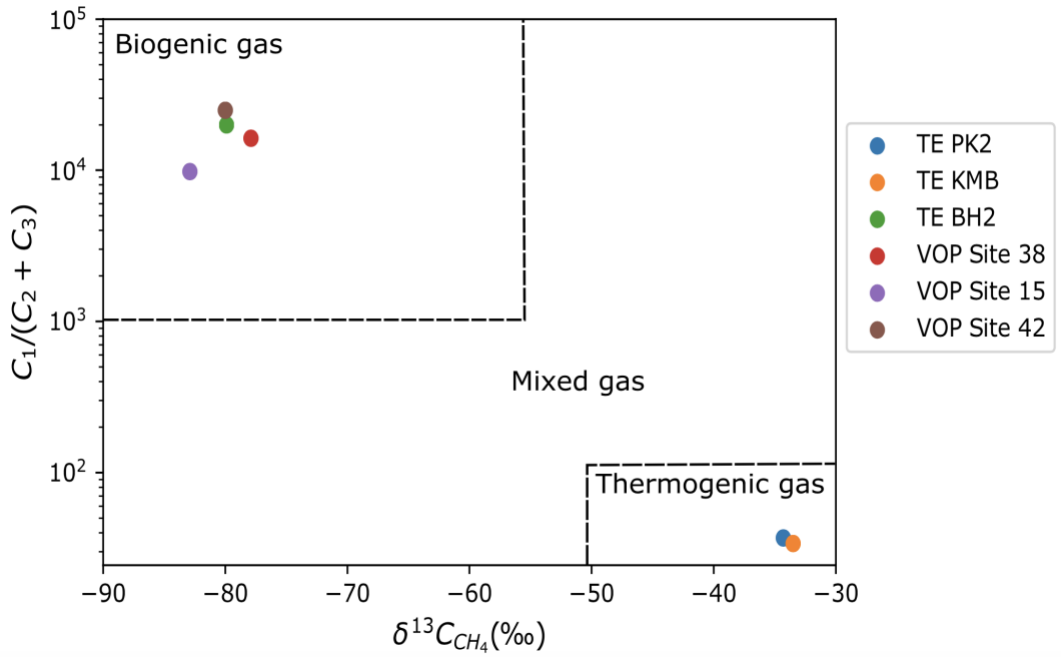

Figure 4-2: Bernard plot of gas dryness (C_1/C_2+C_3) versus $\delta^{13}C_{CH4}$ (Bernard et al., 1976). All groundwater samples plot distinctly within the biogenic methane field, with the deep gas samples plotting within the thermogenic gas range.

4.5.3 Noble gas compositions- Gas samples

4.5.3.1 Helium

Measured ^{4}He concentrations range from 3.45x10^{-4} to 4.91x10^{-4} ccSTP/cm^3 (where STP is standard temperature and pressure) in the two deep gas samples, with both gas samples exhibiting ^{4}He concentrations significantly higher than the air concentration of 5.23x10^{-6} ccSTP/cm^3. ^{3}He concentrations range from 12.35x10^{-12} to 20.81x10^{-12} ccSTP/cm^3, with the Pickering gas well having the highest ^{3}He contents. ^{3}He/^{4}He ratios are normalised to the atmospheric ratio (R_a = 1.4 x 10^{-6}) and range from 0.026 to 0.031R_a, slightly elevated from crustal radiogenic production ratios of 0.02R_a. ^{4}He/^{20}Ne ratios range from 329.6 to 869.9, which are significantly higher than the atmospheric ratio of 0.288. As ^{20}Ne is mainly derived from meteoric groundwater recharge, high ^{4}He/^{20}Ne ratios indicate negligible atmospheric contributions.

4.5.3.2 Neon

^{20}Ne concentrations range from 56.4 $x10^{-8}$ to 10.45$x10^{-7}$ ccSTP/cm^3, which are considerably lower than atmospheric concentrations of 1.64 $x10^{-5}$ ccSTP/cm^3. ^{21}Ne concentrations range from 0.16 $x10^{-8}$ to 0.3 $x10^{-8}$ ccSTP/cm^3 and ^{22}Ne concentrations range from 5.38 $x10^{-8}$ to 10.4 $x10^{-8}$ ccSTP/cm^3. $^{20}Ne/^{22}Ne$ ratios range from 10.06 to 10.48 and are higher than the air ratio of 9.81. $^{21}Ne/^{22}Ne$ ratios are consistent at 0.0289 to 0.029 for the gas samples and match the atmospheric ratio of 0.029. Ne isotopes are accounted for by 2 processes: either the crustal addition of radiogenic ^{21}Ne to air Ne, or through a mass fractionating process (Kennedy et al., 1990, Zhou et al., 2005). Comparing these values to the atmospheric $^{20}Ne/^{22}Ne$ and $^{21}Ne/^{22}Ne$ values of 9.8 and 0.0289 respectively, it is evident that these samples can be accounted for through a mass fractionation process (Fig.4.3).

4.5.3.3 Argon

^{40}Ar concentrations range from 11.84 $x10^{-5}$ to 25.04 $x10^{-5}$ ccSTP/cm^3, with $^{40}Ar/^{36}Ar$ ratios ranging from 298.74 to 314.62. With an atmospheric $^{40}Ar/^{36}Ar$ ratio of 298.6, the KM5 well matches the air value, with the Pickering well exhibiting a slightly elevated value. $^{40}Ar^*$ values range from 2.72 $x10^{-6}$ to 7.20 $x10^{-6}$ ccSTP/cm^3, with $^{4}He/^{40}Ar^*$ ratios of 68.21 to 126.72. ^{36}Ar concentrations range from 3.76 $x10^{-7}$ to 8.38 $x10^{-7}$ ccSTP/cm^3 with ^{38}Ar concentrations varying from 0.71 $x10^{-7}$ to 1.57 $x10^{-7}$ ccSTP/cm^3. $^{38}Ar/^{36}Ar$ ratios vary from 0.187 to 0.189 and correspond well to the atmospheric ratio (0.188).

4.5.3.4 Krypton and Xenon

^{84}Kr concentrations range from 0.31 $x10^{-8}$ to 1.71 $x10^{-8}$ ccSTP/cm^3 while ^{132}Xe concentrations range from 0.35 $x10^{-9}$ to 0.46 $x10^{-9}$ ccSTP/cm^3. $^{84}Kr/^{36}Ar$ ratios vary from 0.0081 to 0.020, with the KM5 well corresponding to the air ratio (0.02). $^{132}Xe/^{84}Kr$ ratios vary from 0.114 to 0.027 and are significantly higher than the air ratio of 0.00074.

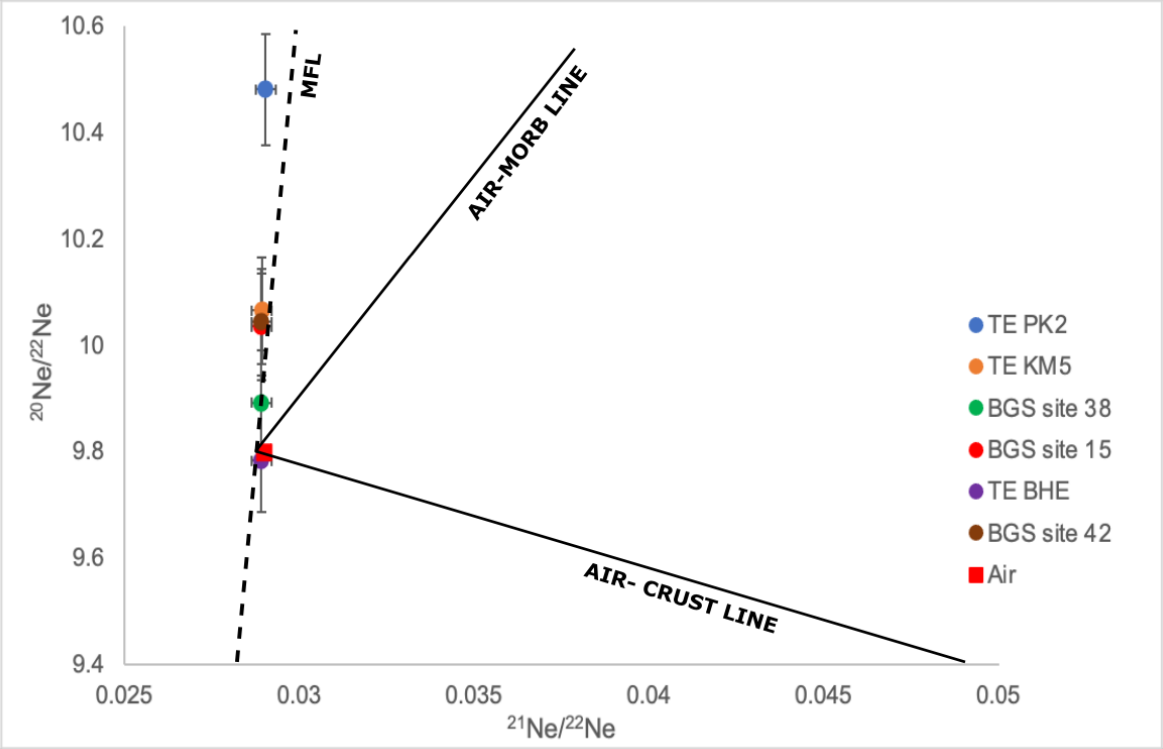

Figure 4-3: $^{20}Ne/^{22}Ne$ vs $^{21}Ne/^{22}Ne$ plot with air, with solid black lines showing air-MORB and air-crust mixing. Dashed black line shows mass fractionation processes, with all Vale of Pickering samples falling on or near the mass fractionation line. Errors are 1s.

Table 4.1: Bulk gas geochemistry and stable isotope data for the Vale of Pickering gas and water samples.

Sample name	**Date Collected**	**Analysis Location**	**Bulk gas Compositions (%)**					**Hydrocarbon Ratio ((C1/(C2+C3))**	**Stable isotopes (‰)**	
			CH_4	**C_2H_6**	**C_3H_8**	**CO_2**	**N_2**		**$\delta^{13}C_{CH4}$**	**δD_{CH4}**
Gas samples										
TE Pickering 2.1	Aug 2020	SUERC	78.5*	1.8*	0.3*	0.3*	19.0*	37	-34.3 ± 0.5	-180 ± 3
TE Pickering 2.2	Aug 2020	Ohio	93	0.026	$4.05x10^{-3}$	2.3	4.2	3110		
TE KM5 15.1	Aug 2020	SUERC	93.9	2.3	0.5	0.6	2.7	34	-33.5 ± 0.5	-164 ± 3
TE KM5 15.2	Aug 2020	Ohio	91.5	0.037	0.01	2.9	5.1	1947		
Water samples										
TE BHE 2	Aug 2020	Ohio	87.2	b.d.l	b.d.l	n.m	12.2	>10,000		
TE BHE 1	Aug 2020	Calgary							-79.9 ± 0.5	
Site 38.2	Feb 2020	Ohio	91.4	$5.6x10^{-3}$	b.d.l	n.m	8.2	16,321		
Site 38.1	Feb 2020	Calgary							-77.9 ± 0.5	
Site 15.2	Feb 2020	Ohio	78.3	$8x10^{-3}$	b.d.l	n.m	2.1	9788		

Site 15.1	Feb 2020	Calgary							-82.9 ± 0.5
Site 42.2	Feb 2020	Ohio	78.4	b.d.l	b.d.l	n.m	2.1	>10,000	
Site 42.1	Feb 2020	Calgary							-80.0 ± 0.5

Table 4.2: Noble gas concentrations for the Vale of Pickering samples expressed as cm^3 (STP)/cm^3. 1s errors quoted in brackets.

Sample name	**^{4}He (x10^{-4})**		**^{20}Ne (x10^{-8})**		**^{40}Ar (x10^{-5})**		**^{84}Kr (x10^{-8})**		**^{132}Xe (x10^{-9})**	
TE Pickering 2.2	4.91	(0.07)	56.40	(0.85)	11.84	(0.178)	0.306	(0.005)	0.349	(0.005)
TE KM5 15.2	3.45	(0.05)	104.54	(1.57)	25.04	(0.376)	1.706	(0.026)	0.457	(0.007)
TE BHE 2	3.60	(0.05)	339.89	(5.10)	433.73	(6.506)	49.18	(0.738)	27.64	(0.415)
Site 38.2	0.60	(0.009)	159.70	(2.40)	269.91	(4.454)	47.82	(0.717)	44.87	(0.673)
Site 15.2	0.27	(0.004)	416.35	(6.25)	623.55	(9.353)	69.69	(1.045)	13.18	(0.198)
Site 42.2	0.19	(0.003)	265.14	(3.98)	375.06	(5.626)	43.73	(0.656)	35.55	(0.533)

Table 4.3: Noble gas isotopic ratios for the Vale of Pickering samples.

Sample name	$^{3}He/^{4}He$ (R/R_a)	2σ	$^{4}He/^{20}Ne$	1σ	$^{20}Ne/^{22}Ne$	1σ	$^{21}Ne/^{22}Ne$	1σ	$^{40}Ar/^{36}Ar$	1σ	$^{38}Ar/^{36}Ar$	1σ
TE Pickering 2.2	0.0306	0.0002	869.9	1.74	10.48	0.105	0.0290	0.00029	314.62	0.629	0.189	0.00057
TE KM5 15.2	0.0259	0.0001	329.6	0.66	10.06	0.101	0.0289	0.00029	298.74	0.597	0.187	0.00056
TE BHE 2	0.0182	0.0001	105.9	0.21	9.78	0.098	0.0289	0.00029	297.74	0.595	0.192	0.00058
Site 38.2	0.0302	0.0002	37.3	0.07	9.89	0.099	0.0289	0.00029	295.47	0.591	0.186	0.00056
Site 15.2	0.0404	0.0002	6.4	0.01	10.04	0.100	0.0289	0.00029	295.48	0.591	0.187	0.00056
Site 42.2	0.0456	0.0002	7.2	0.01	10.04	0.100	0.0289	0.00029	295.80	0.592	0.187	0.00056

4.5.4 Noble gas compositions- Groundwater samples

In order to compare between gas and groundwater samples at the Vale of Pickering, concentrations of noble gases dissolved within the groundwaters are reported. Expected theoretical concentrations and isotope ratios of atmospheric derived noble gases dissolved within groundwater are referred to as air-saturated water (ASW). Through solubility equilibration methods (Kipfer et al., 2002) and using the regional recharge conditions of 10°C, an average altitude of 25m, and an assumed excess air Ne component of 10% (Kipfer et al., 2002), ASW values were calculated for groundwater samples.

4.5.4.1 Helium

Measured ^{4}He concentrations range from $0.19x10^{-4}$ to $3.6x10^{-4}$ ccSTP/cm^3, with all groundwater samples exhibiting ^{4}He concentrations higher than the ASW value of $5.24x10^{-8}$ ccSTP/cm^3. Groundwater ^{3}He concentrations range from $1.21x10^{-12}$ to $9.1x10^{-12}$ ccSTP/cm^3. $^{3}He/^{4}He$ ratios range from 0.0182 in the Corallian groundwater sample (BHE) to $0.0456R_a$ at Site 42. It is noted that the Corallian groundwater sample matches closely to crustal radiogenic production values of $0.02R_a$, with the shallow groundwater samples having elevated $^{3}He/^{4}He$ ratios approaching the air value (1). $^{4}He/^{20}Ne$ ratios range from 6.4 at Site 15 to 105.9 at BHE, with all groundwater samples still significantly higher than the air value of 0.288. As low $^{4}He/^{20}Ne$ ratios indicate increased contributions of atmospheric input, the shallow groundwater sites have the highest observed atmospheric input, with higher ratios with increasing depths in the Corallian groundwater and deep gas samples.

4.5.4.2 Neon

^{20}Ne concentrations in water samples vary from $1.6\ x10^{-6}$ to $4.16x10^{-6}$ ccSTP/cm^3, which are lower than atmospheric concentrations ($1.64\ x10^{-5}$ ccSTP/cm^3). ^{21}Ne concentrations range from $0.47\ x10^{-8}$ to $1.2\ x10^{-8}$ ccSTP/cm^3 and ^{22}Ne concentrations range from $16.1\ x10^{-8}$ to $41.5\ x10^{-8}$ ccSTP/cm^3. $^{20}Ne/^{22}Ne$ ratios vary from 9.78 at BHE to 10.04 at Sites 15 and 42, with the

Corallian groundwater sample being lower than the air ratio and shallow groundwater samples being comparative or slightly elevated to the air ratio of 9.81. All samples exhibit $^{21}Ne/^{22}Ne$ ratios of 0.0289, closely matching the atmospheric ratio of 0.029 and the mass fractionation trend observed in the gas samples.

4.5.4.3 Argon

^{40}Ar concentrations range from $2.70x10^{-3}$ to $6.24x10^{-5}$ ccSTP/cm^3, with $^{40}Ar/^{36}Ar$ ratios ranging from 295.47 at Site 15 to 297.74 at BHE. All groundwater samples are slightly lower than the atmospheric $^{40}Ar/^{36}Ar$ ratio of 298.6. $^{40}Ar^*$ was not identified in samples from Sites 15 and 38, with $^{40}Ar^*$ for the remaining groundwater samples ranging from $3.78x10^{-6}$ to $3.26x10^{-5}$ ccSTP/cm^3. $^{4}He/^{40}Ar^*$ ratios range from 5.05 at Site 42 to 11.04 at BHE. ^{36}Ar concentrations range from 1.0 $x10^{-5}$ to 2.11 $x10^{-5}$ ccSTP/cm^3 with ^{38}Ar concentrations from $1.87x10^{-6}$ to $3.96x10^{-6}$ ccSTP/cm^3. Groundwater $^{38}Ar/^{36}Ar$ ratios range from 0.186 at Site 38 to 0.192 at BHE, corresponding to an air value of 0.188.

4.5.4.4 Krypton and Xenon

Measured ^{84}Kr concentrations range from $4.37x10^{-7}$ to $7.0x10^{-7}$ ccSTP/cm^3 with ^{132}Xe concentrations varying from $1.32x10^{-8}$ to $4.49x10^{-8}$ ccSTP/cm^3. $^{84}Kr/^{36}Ar$ ratios vary from 0.033 at Site 15 to 0.0476 at Site 38 and are all slightly elevated from the air ratio (0.02). $^{132}Xe/^{84}Kr$ ratios vary from 0.019 at Site 15 to 0.094 at Site 38 and, as observed with the gas samples, are significantly higher than the air ratio of 0.00074.

4.6 Discussion

4.6.1 Subsurface CH_4 sources at the Vale of Pickering

Figure 4.4 shows the genetic $\delta^{13}C_{CH4}$ and δD_{CH4} diagram by Milkov and Etiope (2018) for groundwater sample data (Smedley et al., *in review*) and gas data. It is evident that there are

two distinct sources of methane for groundwater and gas samples within the Vale of Pickering, with no apparent evidence of mixing between biogenic and thermogenic sources. Groundwater samples from both shallow and Corallian aquifers show evidence for the production of methane by CO_2 reduction. From limited CH_4 and CO_2 isotope data obtained by the BGS for groundwater sites 15 and 42 (Smedley et al., *in review*) (Fig. 4.5), it is evident that the majority of samples exhibit an isotopic fractionation >55% for $^{13}C_{CH4}$ relative to $^{13}C_{CO2}$, which is indicative of CH_4 production primarily by carbonate reduction (Whiticar, 1999). For both groundwater sites, it is noted that there are samples which display a more enriched $^{13}C_{CH4}$ signature, with an isotopic fractionation less than 55% for $^{13}C_{CH4}$ relative to $^{13}C_{CO2}$. These samples exhibit evidence of potential methane oxidation (Fig. 4.5). Gas samples from the Third Energy wells display, as expected, a distinct thermogenic methane signature.

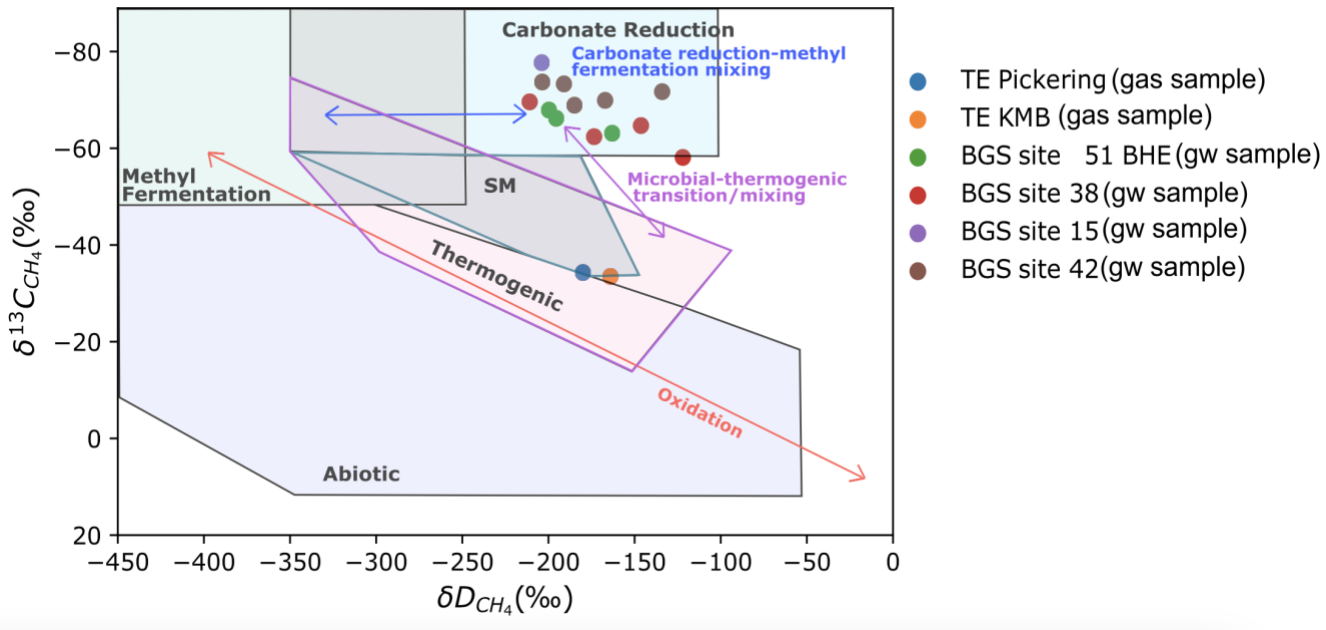

Figure 4-4: Plot of δD_{CH4} and $\delta^{13}C_{CH4}$ stable isotopic analyses of CH_4 gas from Vale of Pickering samples. (Secondary CH_4 (SM) boundary indicated in green and thermogenic CH_4 boundary indicated in purple). Processes that affect the isotopic and molecular composition are highlighted (oxidation). Mixing of microbial gases produced through carbonate reduction and methyl fermentation is indicated by the blue mixing arrow, with mixing of thermogenic and microbial methane indicated by the purple mixing arrow. All groundwater samples plot within the biogenic CH_4 zone, within the carbonate reduction pathway, with the deep gas samples plotting firmly within the thermogenic methane zone. The classification areas of biogenic and thermogenic CH_4 sources are adapted from Whiticar, 1999, and the plot is adapted from Milkov and Etiope, 2018.

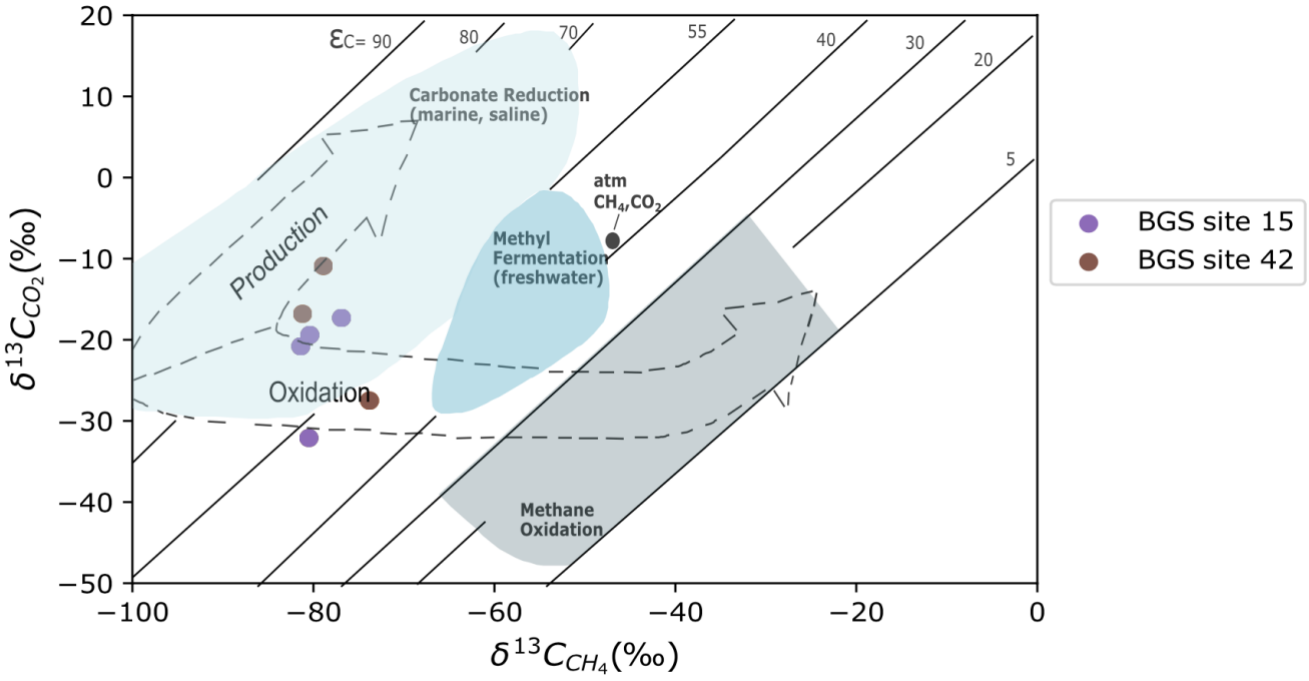

Figure 4-5: Isotope combination plot of $\delta^{13}C_{CH4}$ and $\delta^{13}C_{CO2}$ data from BGS groundwater samples from sites 15 and 42 (Smedley et al., in review); with isotope fractionation lines and partitioning trajectories as a result of CH_4 formation and oxidation processes. The majority of samples exhibit greater ^{12}C enrichment with an isotopic fractionation indicative of CH_4 production by carbonate reduction. There are two slightly enriched samples that may potentially indicate methane oxidation. Isotope plot adapted from Whiticar, 1999.

4.6.2 Origin of noble gases

Noble gases, unlike methane stable isotopes, are not altered by chemical processes, oxidation reactions, or microbial activities due to their unreactive and inert nature (Ballentine et al., 2002, Sherwood Lollar and Ballentine 2009), and therefore exhibit their original composition in groundwaters, independent of microbial processes (Darrah et al., 2014). As such, noble gases are a useful tool in distinguishing subsurface gas sources and identifying potential transport mechanisms.

4.6.2.1 Radiogenic helium

The radiogenic noble gas ^4He is a useful tool in determining groundwater ages and radiogenic sources within basin systems (Byrne et al., 2018; Cheng et al., 2021; Zhou and Ballentine,

2006). The ^{4}He present in groundwater can be derived from atmospheric sources in air-saturated water, the radioactive decay of U of Th, or from external fluxes (e.g., mantle sources). The $^{3}He/^{4}He$ ratio for gas and groundwater samples from the Vale of Pickering ranges from 0.018 to 0.046R_a, with all samples exhibiting a value around that of the crustal production ratio (0.02Ra), with higher ratios at shallow groundwater sites evidencing an increased influence of atmosphere (1). All samples have $^{4}He/^{20}Ne$ values in excess of the atmospheric ratio, ranging from 6.4 to 870. The $^{4}He/^{20}Ne$ values increase with depth in the Vale of Pickering samples and provide evidence of increased mixing with a radiogenic helium source (Fig.4.6).

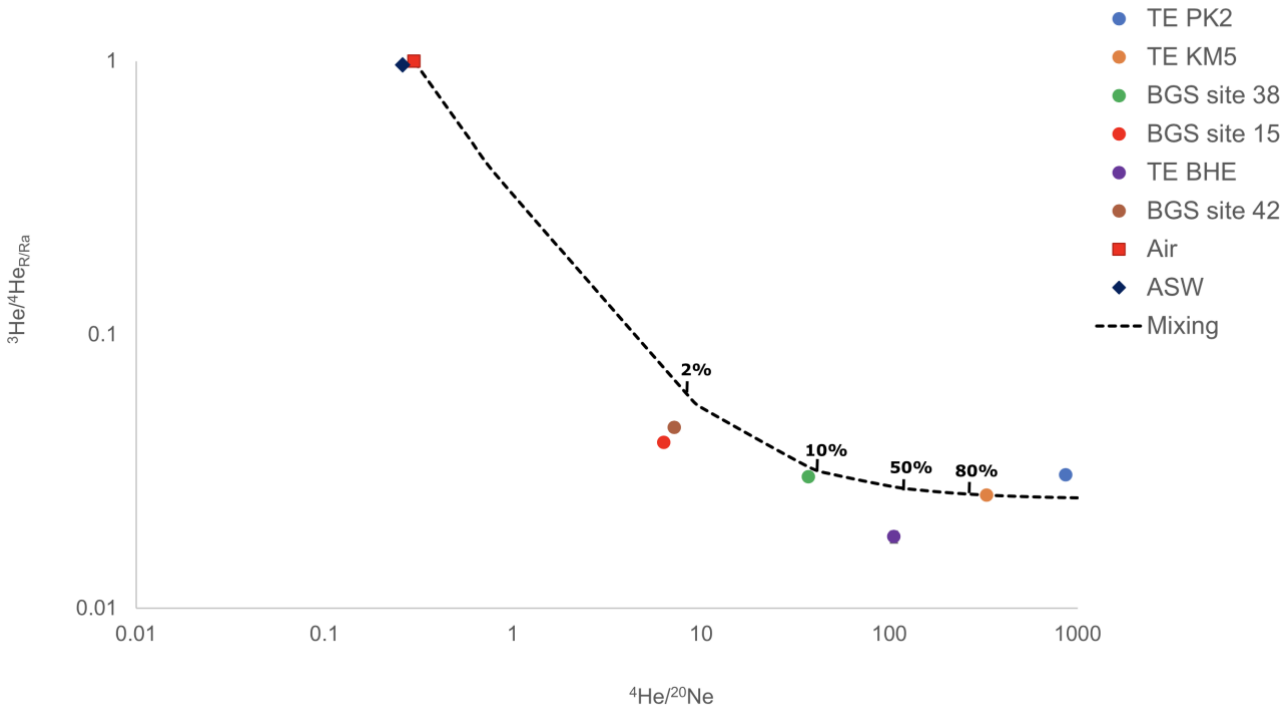

Figure 4-6: $^{3}He/^{4}He$ vs $^{4}He/^{20}Ne$ plot for Vale of Pickering samples. The mixing trajectory between the deep gas Pickering sample and ASW is shown (dashed black line). It is evident that samples fall along a trend of mixing between shallow ASW like groundwater and a deep, radiogenic ^{4}He signature, highlighting the potential for the migration of radiogenic ^{4}He from depth. From the mixing line, it can be estimated that approximately 2 to 50 % of ^{4}He is sourced from depth. 1s error bars are smaller than symbols.

Using a simple mixing model (Fig. 4.6), the relationship arising from the mixing of air ($^{3}He/^{4}He=1_{Ra}$, $^{4}He/^{20}Ne= 0.3$) and the KM5 gas sample ($^{3}He/^{4}He=0.026_{Ra}$, $^{4}He/^{20}Ne= 330$) can be predicted (Gilfillan et al., 2017; Utley et al., 2023). KM5 was chosen to be the end member for this mixing model as the Corallian groundwater sample (BHE) is located on the same site. Figure 4.6 highlights that most samples have lower $^{3}He/^{4}He$ ratios than the predicted mixing relationship. However, $^{4}He/^{20}Ne$ ratios appear to follow a trajectory similar to the predicted mixing line, highlighting there may be a deeper sourced gas end-member mixing with air within the subsurface to create these ^{4}He signatures. As such, it appears shallow groundwater samples have a resolvable radiogenic sourced ^{4}He component, with groundwater from BGS sites 42 and 15 containing approximately 2% of ^{4}He present in the KM5 sample, groundwater from BGS site 38 having 10%, and groundwater sourced from Corallian aquifer at BHE potentially having approx. 50% radiogenically sourced ^{4}He.

As previously discussed, ^{4}He concentrations are elevated, and $^{4}He/^{20}Ne$ ratios for all samples are higher than the atmospheric ratio (0.288). The high ^{4}He values may be derived from the in-situ generation and diffusive loss of U and Th, or from an external flux (Ballentine and Burnard, 2002; Utley et. al., 2023). If diffusive and radiogenic equilibrium have been established within the basin system, ^{4}He is released at a constant rate dependent upon several rock parameters, such as porosity and U and Th concentrations in the rock (Torgersen and Ivey 1985). As such, ^{4}He concentrations within a groundwater system should increase with increasing residence time (Andrews et al., 1991). From Andrews et al., 1991, for any sedimentary unit with a uniform contents of radioelements, the He concentration $c(z,T)$ at depth z(m) of age T (years) and diffusion coefficient, D can be expressed as:

$$c_{(z,T)}\ GT\ 1-\exp(-2z\ \pi DT) \quad [4.1]$$

where the rate of ^{4}He generation (G) from the decay of U and Th can be calculated from:

$$G\rho\ 1.17\times10^{-13}[U]+2.88\times10^{-14}[Th]\ cm^{3}\ STPcm^{-3}\ a^{-1} \quad [4.2]$$

Where ρ is the rock density, and [U] and [Th] is the uranium and thorium contents of the sedimentary unit. From these equations, the theoretical ^{4}He concentration profiles with

depth for four lithological units (Kirkham Abbey Fm. Sherwood Sandstone, Corallian, and Kimmeridge Clay Fm) were calculated in order to investigate the potential source of elevated ^{4}He within the Vale of Pickering samples. These four sedimentary units were chosen due to being identified as key units within the stratigraphy: with the Kirkham Abbey Fm as a natural gas source rock, the Corallian as an aquifer body, and the Kimmeridge Clay as a cap rock. For these calculations, there are several uncertainties due to a lack of information regarding unit specific parameters such as U and Th contents and specific rock densities. As such, some assumptions have been made based on pre-existing data obtained from analogous sedimentary units. For the diffusion co-efficient, it was assumed that the units were fully water saturated (D= 0.032m^2/a), with U and Th concentration values chosen as representative values indicative of the lithological unit modelled. Average rock densities of 2.4 to 2.6 g/cm^3 and the earliest deposition ages of the lithological units were used. All parameters used to calculate the ^{4}He profiles are shown in Table 4.4.

Table 4.4: Parameters used in equations 4.1 and 4.2 for calculation of generated and stored ^{4}He in the lithological units. Parameters for the Kimmeridge Clay estimated from Ivanovich and Alexander, 1985; Carbonate units estimated from Graf,1960 and Eisenbud and Gesell, 1997; and Sherwood sandstone parameters estimated from Andrews and Lee, 1979.

	[U] (ppmm)	**[Th] (ppmm)**	**Density (g/cm^3)**	**Time (Ma)**
Kimmeridge Clay	2.2	6.5	2.6	157
Corallian	2.2	5	2.5	163
Sherwood Sandstone	1	3	2.4	260
Kirkham Abbey	2.1	2.4	2.5	272

The theoretical profiles of generated and stored ^{4}He for the four lithological units with depth are shown in Figure 4.7, alongside groundwater and gas ^{4}He concentration data plotted at their corresponding depths. From the measured ^{4}He concentrations in both the shallow (30-40m depth) and deeper Corallian (222m depth) groundwater samples, it is evident that all groundwater samples do not fit with the modelled theoretical ^{4}He diffusion profiles. ^{4}He groundwater concentrations are higher than modelled profiles and indicate a potential

additional source of ^{4}He input. This indicates the system to be open to the flow of radiogenic noble gases to these shallower units and follows the prediction of the gas mixing model. Deep gas samples from the Pickering and KMB wells do not fall on the modelled ^{4}He generation profile, exhibiting higher ^{4}He concentrations also. As such, this indicates that ^{4}He concentrations cannot be accounted for through the in-situ production of ^{4}He in the surrounding stratigraphy alone, with additional ^{4}He from a deeper sourced gas end member from the underling basement a potential external flux.

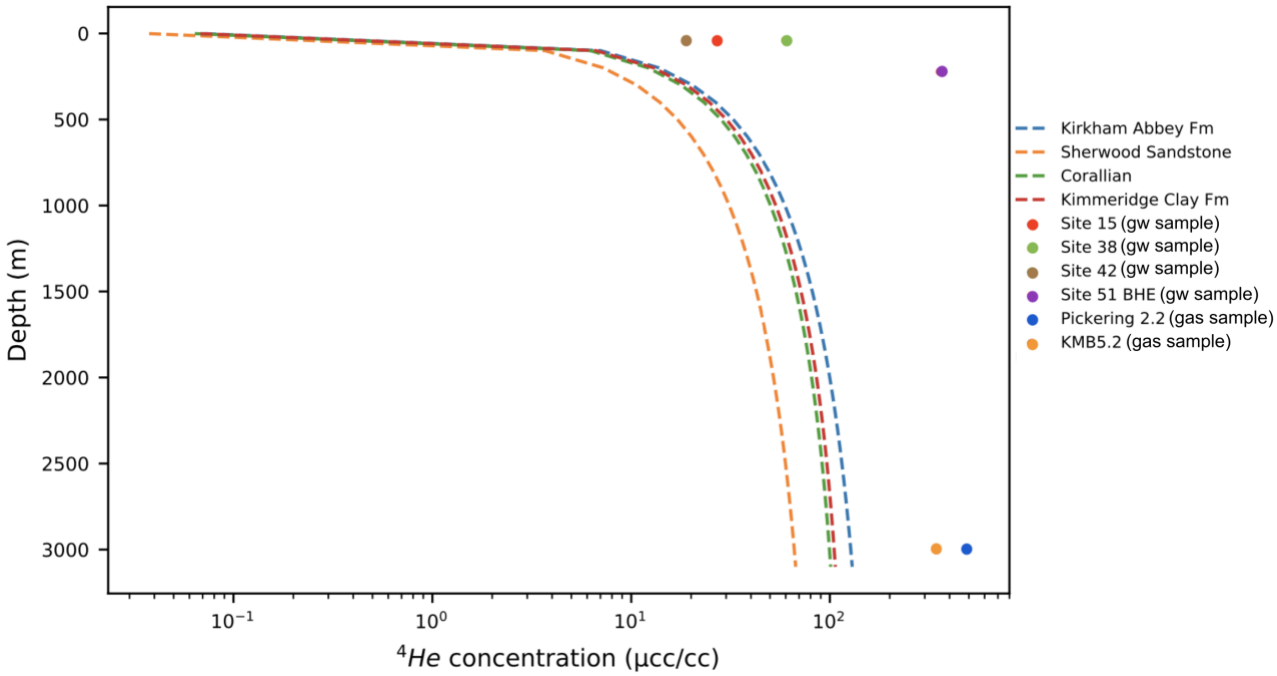

Figure 4-7: Theoretical concentration profiles of ^{4}He against depth for the Kirkham Abbey Fm, Sherwood Sandstone, Corallian, and Kimmeridge Clay units, modelled after Andrews et al., 1991 for the diffusion coefficient of water (D=0.0315m^2/a). ^{4}He concentration data for groundwater and gas samples are also plotted with depth and highlight samples do not fit any of the modelled stored ^{4}He profiles, with all groundwater and gas samples having an additional ^{4}He contribution.

4.6.3 Geochemical integration for subsurface characterisation

As the isotopic ratio of atmospheric components are consistent within shallow groundwater, with only minor variations as a result of temperature, elevation, and salinity (Ballentine et al., 2002), the ratios of ASW gases can allow for the investigation of gas-water interactions and potential gas migration (Gilfillan et al., 2008; Darrah et al., 2014: Darrah et al., 2015). As both diffusion and gas-phase partitioning result in the enrichment of lighter noble gases (He and

Ne) in fluids that migrate away from the gas source, $^{4}He/CH_4$ and $^{20}Ne/^{36}Ar$ can be used as effective fingerprinting tools to evaluate gas migration and potential gas sources (Darrah et al., 2015). $^{20}Ne/^{36}Ar$ ratios for the Vale of Pickering samples fall into two distinct groups, with all groundwater samples having a signature consistent with ASW, and the Third Energy gas samples having an enriched $^{20}Ne/^{36}Ar$ signature (Fig.4.8). With regards to $^{132}Xe/^{36}Ar$, the gas samples have a signature similar to that of ASW, with the groundwater samples having an enriched $^{132}Xe/^{36}Ar$ ratio relative to ASW. For $^{84}Kr/^{36}Ar$ ratios, the gas and groundwater samples of the Vale of Pickering are again distinct from each other, with groundwater samples exhibiting signatures that is characteristic of mixing between air and ASW values (Fig.4.8).

As ^{4}He values within the Vale Pickering cannot be accounted for through in-situ production or atmospheric sources, it is evident that ^{4}He comes from an external, exogeneous source (Zhou and Ballentine, 2006). Thermogenic gases are dominated by CH_4, C_2H_6, and radiogenic ^{4}He, whereas ^{20}Ne and ^{36}Ar are primarily sourced from the atmosphere, entering the subsurface through interactions with formation waters (Gilfillan et al., 2008; Darrah et al., 2015). As both $CH_4/^{36}Ar$ and $^{4}He/^{20}Ne$ have similar solubility constants in water (β_{CH4}/β_{Ar}= 1 and β_{He}/β_{Ne}= 1.2 at 10°C, STP) (Darrah et al., 2015), $CH_4/^{36}Ar$ and $^{4}He/^{20}Ne$ ratios can be used to directly compare the proportions of thermogenic and air-saturated-water (ASW) components (Darrah et al., 2015) within groundwater samples. $CH_4/^{36}Ar$ ratios can therefore be used as a tracer of the gas-water ratio (the percentage components of CH_4 and air in the samples), despite any gas-fluid partitioning that may have occurred (Darrah et al., 2015). In the Vale of Pickering groundwater samples, $CH_4/^{36}Ar$ values range from 37,115 to 91,000, with all samples except BGS site 15 exceeding the $CH_4/^{36}Ar$ saturation (40,000) (Fig. 4.9). This indicates groundwater equilibration with a methane rich source at greater depths (Darrah et al., 2015). It is also noted that during biogenic methanogenesis, there is no mechanism for the production of He, Ar, and Ne. As such, groundwaters containing shallow microbial gas are expected to have $CH_4/^{36}Ar < CH_4$ solubility and $^{4}He/^{20}Ne$ ratios near ASW values (Darrah et al., 2015). All samples have $^{4}He/^{20}Ne$ ratios in excess of ASW (0.26), and coupled with high $CH_4/^{36}Ar$ ratios, confirm an exogeneous and non-biogenic source.

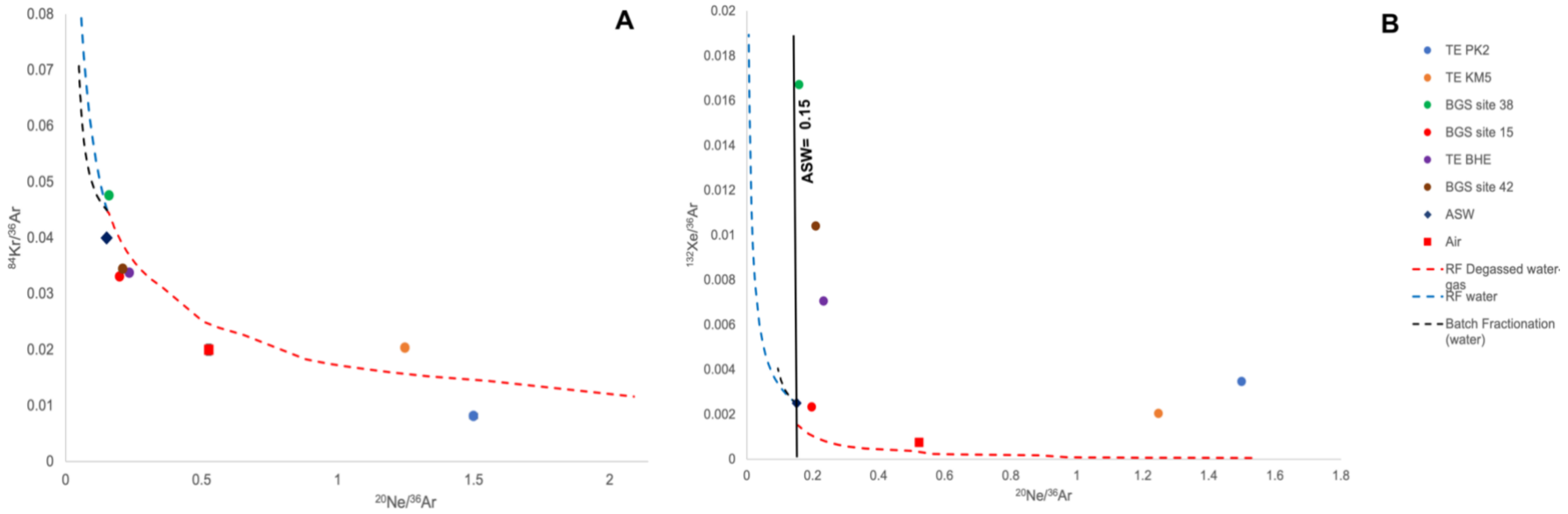

Figure 4-8: *$^{84}Kr/^{36}Ar$ vs $^{20}Ne/^{36}Ar$ (**A**) and $^{132}Xe/^{36}Ar$ vs $^{20}Ne/^{36}Ar$ (**A**) plots for the Vale of Pickering samples. The $^{84}Kr/^{36}Ar$ vs $^{20}Ne/^{36}Ar$ (**A**) plot highlights that groundwater samples exhibit a signature characteristic of mixing between Air and ASW, with the exception of BGS site 38 which is enriched in $^{84}Kr/^{36}Ar$ relative to ASW. Again, the Third Energy samples plot distinctly separate from groundwater samples. Batch and Rayleigh fractionation lines (batch mixing= black, Rayleigh fractionation of degassed water-gas= red, and Rayleigh fractionation (water)=blue) plotted highlight that high $^{20}Ne/^{36}Ar$ ratios can be accounted for through the re-dissolution of noble gases into a degassed groundwater.*

*The $^{132}Xe/^{36}Ar$ vs $^{20}Ne/^{36}Ar$ (**B**) plot highlights all groundwater samples having a consistent $^{20}Ne/^{36}Ar$ ratio around ASW, with groundwater samples exhibiting varying amounts of ^{132}Xe. Conversely, the Third Energy samples have similar $^{132}Xe/^{36}Ar$ ratios to ASW, with enriched $^{20}Ne/^{36}Ar$ ratios than Air. Batch and Rayleigh fractionation lines (batch mixing= black, Rayleigh fractionation of degassed water-gas= red, and Rayleigh fractionation (water)=blue) plotted highlight that $^{132}Xe/^{36}Ar$ vs $^{20}Ne/^{36}Ar$ trends cannot be explained by any singular fractionation process. All 1s error bars are smaller than symbols.*

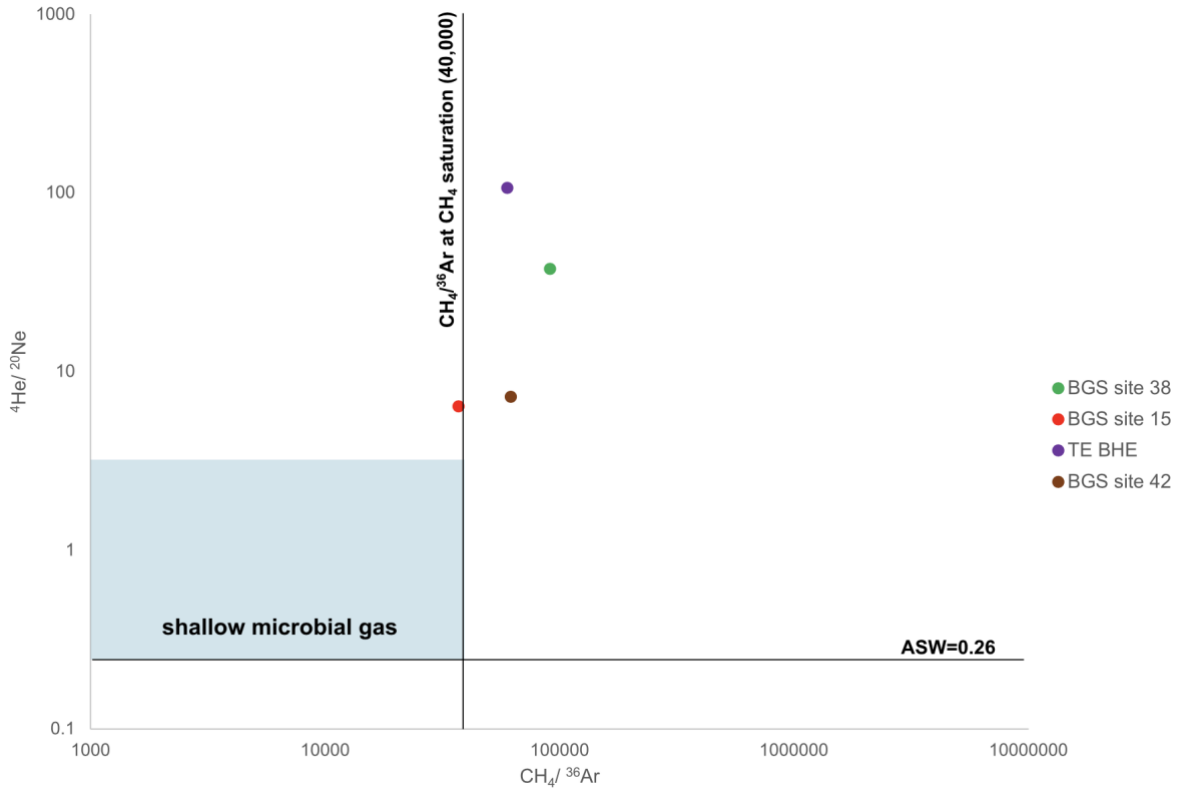

Figure 4-9: $^4He/^{20}Ne$ vs. $CH_4/^{36}Ar$ plot for the Vale of Pickering groundwater samples. The trend of increasing $^4He/^{20}Ne$ and $CH_4/^{36}Ar$ shows groundwater equilibration with a methane rich source at greater depths, with all groundwater samples exceeding ASW values. During biogenic methanogenesis, there is no mechanism for He, Ne, or Ar production, and so values expected are $CH_4/^{36}Ar$ < CH_4 solubility and $^4He/^{20}Ne$=ASW (blue square) (Darrah et al., 2015). All samples exceed these values, with all samples except the groundwater sample collected from BGS site 15 plotting above CH_4 saturation. As such, elevated ^4He values must be from an exogeneous and non-biogenic source (Darrah et al., 2015). 1s error bars are smaller than symbols.

4.7 Conclusions

We find that methane is present within the fluids contained in the subsurface of the Vale of Pickering throughout the stratigraphy and is the dominant gas in all samples. From C_1/C_2+C_3 ratios, $\delta^{13}C_{CH4}$ and δD_{CH4} signatures, we identify that there are two distinct methane sources present within the Vale of Pickering samples, with methane in both the shallow superficial and Corallian groundwater samples being produced biogenically by CO_2 reduction. This is substantiated by groundwater samples evidencing a $\delta_{13}C$ fractionation signature of >55% for $^{13}C_{CH4}$ relative to $^{13}C_{CO2}$. We also evidence that there are some groundwater samples which display a more enriched $^{13}C_{CH4}$ signature, with a fractionation of <55% for $^{13}C_{CH4}$ relative to

$^{13}CCO_2$, potentially evidencing methane oxidation. The Third Energy gas samples exhibited a distinct thermogenic gas signature.

Both $^{3}He/^{4}He$ and $^{4}He/^{20}Ne$ ratios are elevated in comparison to atmospheric values, and plot near or on the mixing line between the KM5 gas end member and the atmosphere. This highlights the potential mixing of deep thermogenic gas with atmospheric noble gases in the shallow subsurface, with an approximate 2 to 50% of radiogenic ^{4}He present in groundwater samples. From ^{4}He generation calculations, it is apparent that measured ^{4}He concentrations cannot be generated from the in-situ decay of U and Th within the Vale of Pickering stratigraphy alone. As such, ^{4}He values must be sourced from an external radiogenic flux. $CH_4/^{36}Ar$ ratios were used as a tracer for the gas-water ratio, with $CH_4/^{36}Ar$ values exceeding the $CH_4/^{36}Ar$ saturation values, indicating groundwater equilibrium with a methane rich source at greater depths. This is supported by all samples having $^{4}He/^{20}Ne$ ratios in excess of ASW (0.26), and coupled with high $CH_4/^{36}Ar$ ratios, confirm an exogeneous and non-biogenic source.

$^{20}Ne/^{36}Ar$, $^{132}Xe/^{36}Ar$, and $^{84}Kr/^{36}Ar$ ratios for gas and groundwater samples are both geochemically distinct from each other. The Vale of Pickering groundwater samples have $^{20}Ne/^{36}Ar$ ratios consistent with ASW, $^{84}Kr/^{36}Ar$ ratios characteristic of mixing between air and ASW, and $^{132}Xe/^{36}Ar$ values being enriched relative to ASW. This is distinct from the Third Energy gas samples, which display enriched $^{20}Ne/^{36}Ar$ signatures, and $^{132}Xe/^{36}Ar$ values similar to that of ASW.

This study shows that the use of noble gas geochemistry alongside gas composition and stable isotope ratio allows for the better characterisation of geochemical signatures within the subsurface at the Vale of Pickering, and the identification of different methane sources within the subsurface. This study highlights the need for an understanding of fluid migration pathways and their associated geochemical signature and establishes a useful baseline in the event of future geoenergy technology development of the site.

4.8 References

Allen, D.J., Brewerton, L.J., Coleby, L.M., Gibbs, B.R., Lewis, M.A., MacDonald, A.M., Wagstaff, S.J. and Williams, A.T., 1997. The physical properties of major aquifers in England and Wales.

Andrews, J.N. and Lee, D.J., 1979. Inert gases in groundwater from the Bunter Sandstone of England as indicators of age and palaeoclimatic trends. *Journal of Hydrology*, *41*(3-4), pp.233-252.

Ballentine, C. J. and Sherwood Lollar, B. (2002) 'Regional groundwater focusing of nitrogen and noble gases into the Hugoton-Panhandle giant gas field, USA', Geochimica et Cosmochimica Acta, 66(14), pp. 2483–2497. doi:10.1016/S0016-7037(02)00850-5.

Ballentine, C.J., Burgess, R. and Marty, B. 2002. Tracing fluid origin, transport and interaction in the crust. *In*: *Reviews in Mineralogy and Geochemistry*. 539–614., https://doi.org/10.2138/rmg.2002.47.13.

Beaton, A. (2003) Coal-Bearing Formations and Coalbed-Methane Potential in the Alberta Plains and Foothills. *CSEG RECORDER, Recorder* 28, Vol.28 No.09.

Barker, J.F. and Fritz, P., 1981. Carbon isotope fractionation during microbial methane oxidation. *Nature*, *293*(5830), pp.289-291.

Bearcock, J.M., Smedley, P.L. and Milne, C.J., 2015. Baseline groundwater chemistry: the Corallian of the Vale of Pickering, Yorkshire.

Bell, R.A., Darling, W.G., Ward, R.S., Basava-Reddi, L., Halwa, L., Manamsa, K. and Dochartaigh, B.Ó., 2017. A baseline survey of dissolved methane in aquifers of Great Britain. Science of the Total Environment, 601, pp.1803-1813.

Bernard, B.B., Brooks, J.M. and Sackett, W.M., 1976. Natural gas seepage in the Gulf of Mexico. *Earth and Planetary Science Letters*, *31*(1), pp.48-54.

Burns, R., Wynn, P.M., Barker, P., McNamara, N., Oakley, S., Ostle, N., Stott, A.W., Tuffen, H., Zhou, Z., Tweed, F.S. and Chesler, A., 2018. Direct isotopic evidence of biogenic methane production and efflux from beneath a temperate glacier. Scientific reports, 8(1), pp.1-8.

Clark, I.D. and Fritz, P., 1997. Environmental Isotopes in Hydrogeology. CRC Press.

Darrah, T. H., Vengosh, a., Jackson, R. B., Warner, N. R. and Poreda, R. J. (2014) 'Noble gases identify the mechanisms of fugitive gas contamination in drinking-water wells overlying the Marcellus and Barnett Shales', Proceedings of the National Academy of Sciences, 111(39), pp. 14076–14081

Darrah, T.H., Jackson, R.B., Vengosh, A., Warner, N.R., Whyte, C.J., Walsh, T.B., Kondash, A.J., Poreda, R.J. 2015. The evolution of Devonian hydrocarbon gases in shallow aquifers of the northern Appalachian Basin: Insights from integrating noble gas and hydrocarbon geochemistry. Geochimica et Cosmochimica Acta, 170, 321–355, https://doi.org/10.1016/j.gca.2015.09.006.

Donnelly, T., Waldron, S., Tait, A., Dougans, J. and Bearhop, S., 2001. Hydrogen isotope analysis of natural abundance and deuterium-enriched waters by reduction over chromium on-line to a dynamic dual inlet isotope-ratio mass spectrometer. *Rapid Communications in Mass Spectrometry*, *15*(15), pp.1297-1303.

Dunbar, E., Cook, G.T., Naysmith, P., Tripney, B.G. and Xu, S., 2016. AMS 14 C dating at the Scottish Universities Environmental Research Centre (SUERC) radiocarbon dating laboratory. *Radiocarbon*, *58*(1), pp.9-23.

Eisenbud, M. and Gesell, T.F., 1997. *Environmental radioactivity from natural, industrial and military sources: from natural, industrial and military sources*. Elsevier.

Fraser, A.J. & Gawthorpe, R.L. 1990. Tectono-stratigraphic development and hydrocarbon habitat of the Carboniferous in northern England. In: HARDMAN, R.F.P. & BROOKS, J. (eds) Tectonic Events Responsible for Britain's Oil and Gas Reserves. Geological Society, London, Special Publi- cations, 55, 49–86,

Gilfillan, S.M., Sherk, G.W., Poreda, R.J. and Haszeldine, R.S., 2017. Using noble gas fingerprints at the Kerr Farm to assess CO2 leakage allegations linked to the Weyburn-Midale CO2 monitoring and storage project. *International Journal of Greenhouse Gas Control*, *63*, pp.215-225.

Graf, D.L. 1960. Geochemistry of carbonate sediments and sedimentary carbonate rocks, part 3, minor element distribution. Division of the Illinois State Geological Survey, Circular 301.

Gründger, F., Jiménez, N., Thielemann, T., Straaten, N., Lüders, T., Richnow, H.H. and Krüger, M., 2015. Microbial methane formation in deep aquifers of a coal-bearing sedimentary basin, Germany. *Frontiers in microbiology*, *6*, p.200.

Guo, H., Liu, R., Yu, Z., Zhang, H., Yun, J., Li, Y., Liu, X. and Pan, J., 2012. Pyrosequencing reveals the dominance of methylotrophic methanogenesis in a coal bed methane reservoir associated with Eastern Ordos Basin in China. *International journal of coal geology*, *93*, pp.56-61.

Györe, D., McKavney, R., Gilfillan, S.M. and Stuart, F.M., 2018. Fingerprinting coal-derived gases from the UK. *Chemical Geology*, *480*, pp.75-85.

Holland, G. & Gilfillan, S. 2013. Application of noble gases to the viability of CO2 storage. In: The noble gases as geochemical tracers. Advances in Isotope Geochemistry, Burnard, P (ed.). Springer Berlin/Heidelburg, Berlin, pp. 177-223.

Hunt, A.G., Darrah, T.H. and Poreda, R.J., 2012. Determining the source and genetic fingerprint of natural gases using noble gas geochemistry: A northern Appalachian Basin case study The Noble Gas Signature of the Appalachian Basin. *AAPG bulletin*, *96*(10), pp.1785-1811.

Ivanovich, M. and Alexander, J., 1985. *Uranium series disequilibrium: application to studies of the groundwater regime of the Harwell region* (No. AERE-R--11688). UKAEA Atomic Energy Research Establishment.

Jackson, R.E., Gorody, A.W., Mayer, B., Roy, J.W., Ryan, M.C. and Van Stempvoort, D.R., 2013. Groundwater protection and unconventional gas extraction: The critical need for field-based hydrogeological research. *Groundwater*, *51*(4), pp.488-510.

Kampbell, D.H. and Vandegrift, S.A., 1998. Analysis of dissolved methane, ethane, and ethylene in ground water by a standard gas chromatographic technique. *Journal of Chromatographic Science*, *36*(5), pp.253-256.

Krüger, M., Beckmann, S., Engelen, B., Thielemann, T., Cramer, B., Schippers, A. and Cypionka, H., 2008. Microbial methane formation from hard coal and timber in an abandoned coal mine. *Geomicrobiology Journal*, *25*(6), pp.315-321.

Kusakabe, M., 2005. A closed pentane trap for separation of SO2 from CO2 for precise $\delta^{18}O$ and & $\delta^{34}S$ measurements. *Geochemical Journal*, *39*(3), pp.285-287.

LeDoux S.T, Szynkiewicz, A., Faiia, A.M., Mayes, M.A., McKinney, M.L. and Dean, W.G., 2016. Chemical and isotope compositions of shallow groundwater in areas impacted by hydraulic fracturing and surface mining in the Central Appalachian Basin, Eastern United States. Applied geochemistry, 71, pp.73-85.

Milkov, A.V. and Etiope, G., 2018. Revised genetic diagrams for natural gases based on a global dataset of> 20,000 samples. Organic Geochemistry, 125, pp.109-120.

Molofsky, L.J., Connor, J.A., Wylie, A.S., Wagner, T. and Farhat, S.K., 2013. Evaluation of methane sources in groundwater in northeastern Pennsylvania. *Groundwater*, *51*(3), pp.333-349.

Moore, M.T., Vinson, D.S., Whyte, C.J., Eymold, W.K., Walsh, T.B. and Darrah, T.H., 2018. Differentiating between biogenic and thermogenic sources of natural gas in coalbed methane reservoirs from the Illinois Basin using noble gas and hydrocarbon geochemistry. *Geological Society, London, Special Publications*, *468*(1), pp.151-188.

Osborn, Stephen G., Avner Vengosh, Nathaniel R. Warner, and Robert B. Jackson. "Methane contamination of drinking water accompanying gas-well drilling and hydraulic fracturing." *proceedings of the National Academy of Sciences* 108, no. 20 (2011): 8172-8176.

Priestley (2018), Parliament, House of Commons (2018), Shale Gas and Fracking; Briefing Paper, (Number CBP 6073), London, [online] Available at: https://www.google.com/url?sa=t&rct=j&q=&esrc=s&source=web&cd=11&ved=2ahUKEwjgk97A4IreAhVITMAKHQ5wCJIQFjAKegQIBhAC&url=http%3A%2F%2Fresearchbriefings.files.parliament.uk%2Fdocuments%2FSN06073%2FSN06073.pdf&usg=AOvVaw0g7xDJDd9mfRY__e0PbTBq

Schoell, M., 1980. The hydrogen and carbon isotopic composition of methane from natural gases of various origins. Geochimica et Cosmochimica Acta, 44(5), pp.649-661.

Stuart M.E. 2012. Potential groundwater impact from exploitation of shale gas in the UK. British Geological Survey Open Report, OR/12/001. 33pp

Stephenson, M.H., Ringrose, P., Geiger, S., Bridden, M. and Schofield, D., 2019. Geoscience and decarbonization: current status and future directions. Petroleum Geoscience, 25(4), pp.501-508.

Stolper, D.A., Lawson, M., Formolo, M.J., Davis, C.L., Douglas, P.M. and Eiler, J.M., 2018. The utility of methane clumped isotopes to constrain the origins of methane in natural gas accumulations. Geological Society, London, Special Publications, 468(1), pp.23-52.

Strąpoć, D., Mastalerz, M., Dawson, K., Macalady, J., Callaghan, A.V., Wawrik, B., Turich, C. and Ashby, M., 2011. Biogeochemistry of microbial coal-bed methane. *Annual Review of Earth and Planetary Sciences*, *39*.

Stuart M.E. 2012. Potential groundwater impact from exploitation of shale gas in the UK. British Geological Survey Open Report, OR/12/001. 33pp

Utley, R.E., Martin-Roberts, E., Utting, N., Johnson, G., Györe, D., Zurakowska, M., Stuart, F.M., Boyce, A.J., Darrah, T.H., Gulliver, P. and Haszeldine, R.S., 2023. Multi-Isotope Geochemical Baseline Study of the Carbon Management Canada Research Institutes CCS Field Research Station (Alberta, Canada), Prior to CO2 Injection. *Earth Science, Systems and Society*, *3*, p.10069.

Ward, R S, Smedley, P. L., Allen, G., Baptie, B. J., Daraktchieva, Z., Horleston, A., Jones, D. G., Jordan, C. J., Lewis, A., Lowry, D., Purvis, R. M., Rivett, M. O. 2017. Environmental Baseline Monitoring Project: Phase II - Final Report. British Geological Survey Open Report, OR/17/049. 171pp.

Ward, R.S., Smedley, P.L., Allen, G., Baptie, B.J., Cave, M.R., Daraktchieva, Z., Fisher, R., Hawthorn, D., Jones, D.G., Lewis, A. and Lowry, D., 2018. Environmental baseline monitoring: Phase III final report (2017-2018).

Ward, R. S., Smedley, P. L., Allen, G., Baptie, B. J., Barkwith, A. K. A. P., Bateson, L., et al. (2019). Environmental monitoring - phase 4 final report (April 2018 - March 2019). Open Report, OR/19/044. Nottingham, UK: British Geological Survey, 225. Available at: http://nora.nerc.ac.uk/id/eprint/527726/.

Whiticar, M.J., 1999. Carbon and hydrogen isotope systematics of bacterial formation and oxidation of methane. Chemical Geology, 161(1-3), pp.291-314.

Zhou, Z. and Ballentine, C.J. 2006. 4He dating of groundwater associated with hydrocarbon reservoirs. *Chemical Geology*, **226**, 309–327,

5 Hydrogeological and mass transport modelling of radiogenic ^{4}He noble gas within the Vale of Pickering subsurface

5.1 Chapter Overview

This chapter outlines the development of a coupled hydro-chemical model to investigate how ^{4}He noble gas signatures change with depth within the Vale of Pickering, and follows on from the geochemical characterisation presented in Chapter 4. The modelling approach and equations used are summarised in Chapter 2 and Appendix B.

This chapter outlines the conceptual basis for a coupled hydro-chemical model and the key parameters used in the model set up. Three scenarios are modelled in order to investigate the ^{4}He signature with depth:

1. A diffusion/dispersion model simulating the ^{4}He signature of thermogenic gas from depth to the surface
2. A diffusion/dispersion model with groundwater flushing of ASW (Air Saturated Water) simulated in the Sherwood Sandstone units
3. A diffusion/dispersion model with groundwater flushing of ASW simulated in the shallow superficial deposits.

The results of these models are presented followed by a discussion of future work and the implications for the use of geochemical fingerprinting tools.

5.2 Introduction

As the need for subsurface geoenergy technologies increases, the need to address environmental concerns over the potential for shallow aquifer contamination has increased (Darrah et al., 2014; Darrah et al., 2015; Gyore et al., 2017). In order to address these concerns, and evaluate the environmental impact of geoenergy technologies (e.g.

geothermal, unconventional gas, carbon capture and storage, etc.), increased knowledge is required in the following areas:

- establishing environmental baselines of sites pre-geoenergy development,
- addressing the uncertainty in hydrogeological factors that control the presence of CH_4 in shallow aquifers, and
- the development of geochemical fingerprinting techniques to quantify the origin and migration of crustal fluids at various timescales (Darrah et al., 2015).

Traditionally, hydrocarbon abundances $C_1/(C_2+C_3)$ and stable isotopes ($\delta^{13}C_{CH4}$, $\delta^{13}C_{CO2}$, and δD_{CH4}) are used to distinguish between thermogenic and bacterial methane sources and differentiate sources of differing thermal maturities (Györe et al., 2017; Osborn et al., 2011; Schoell 1980; Stuart, 2012; Whiticar, 1999). This is due to both biogenic and thermogenic methane having characteristic signatures in terms of their stable isotopes and hydrocarbon ratios. However, hydrocarbon abundance and stable isotope signatures of CH_4 can be altered by several processes, resulting in the misidentification of the gas source. Such processes include the mixing of different sources of gases; microbial oxidation and sulfate reduction, which can enrich bacterial CH_4 in ^{13}C and ^{2}H to that of thermogenic sources (Barker and Fritz, 1983; LeDoux et al., 2016; Molofsky et al., 2013; Whiticar, 1999), or fractionation during transport within the subsurface (Darrah et al., 2015).

Gas in the subsurface is highly mobile and, as a result, the mixing of gases from multiple sources or maturities is likely. Therefore, any unique geochemical fingerprints within the gas can be easily lost (Dembicki, 2016). Noble gases, unlike methane stable isotopes, are not altered by chemical processes, oxidation reactions, or microbial activities due to their unreactive and inert nature (Ballentine et al., 2002, Sherwood Lollar and Ballentine 2009), and therefore exhibit their original composition in groundwaters, independent of microbial processes (Darrah et al., 2014). As such, noble gases are a useful tool in distinguishing subsurface gas sources and identifying potential transport mechanisms.

The noble gases (He, Ne, Ar, Kr, and Xe) occur naturally in trace quantities within all crustal fluids, with their inert nature making them an ideal geochemical fingerprinting tool in subsurface gas migration (Ballentine et al., 2002, Sherwood Lollar and Ballentine 2009). They fractionate either by elemental mass and isotopic mass, the processes of which are well constrained within geological systems (Ozima and Podosek, 2002; Ballentine et al., 2002; Burnard, 2013). As discussed previously in Chapter 4, groundwater has a distinct noble gas signature called air saturated water (ASW). Noble gases that are derived from the atmosphere are transported into the subsurface by water, as a result of aquifer recharge or through the burying of water saturated sediment (Kipfer et al., 2002) (Figure 5.1). Concentrations of noble gases within groundwater are reasonably well constrained (Ballentine and Hall, 1999; Ballentine et al., 2002).

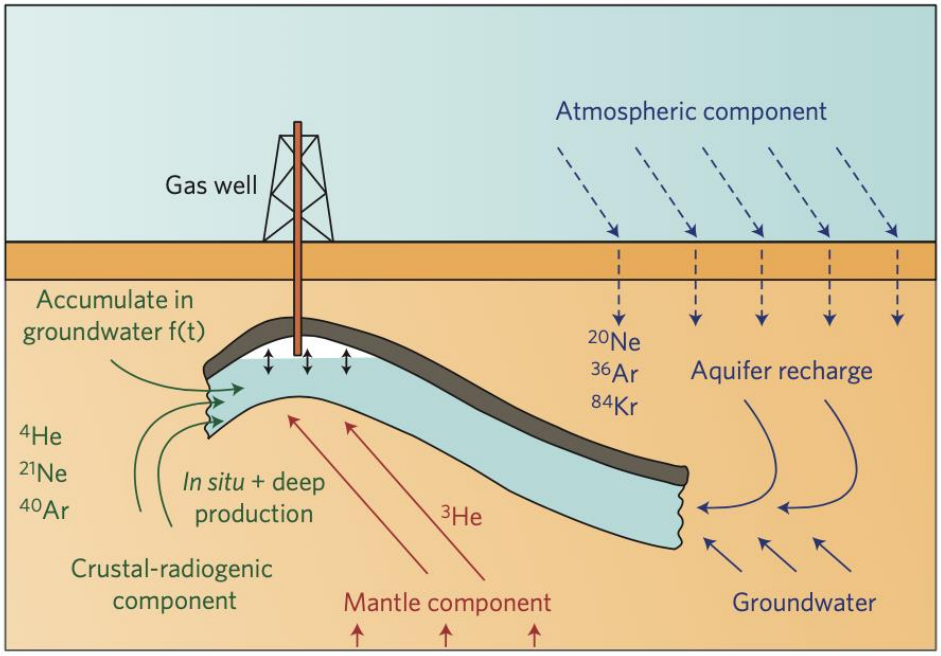

Figure 5-1: Conceptual diagram highlighting noble gas sources within the subsurface and groundwater systems (Lollar and Ballentine, 2009).

Contained within the source rock, hydrocarbons are normally devoid of such atmosphere derived noble gases (Pujol et al., 2008). As these hydrocarbons are transported out of the source rock and come into contact with groundwater, their associated noble gases will

partition into the hydrocarbon phase, transferring the atmosphere-derived noble gases into the migrating hydrocarbons (Byrne et al., 2017).

Therefore, noble gas signatures within subsurface fluids can provide a better insight and understanding into gas migration within the subsurface, and when used alongside stable isotope analysis and hydrocarbon composition, can provide a valuable insight into gas source, residence time, and migration history of gases within pathways through the subsurface. In this chapter, noble gas data obtained for the Vale of Pickering site (Chapter 4) is used to construct a coupled hydro-chemical model to investigate how the ^{4}He gas signature changes with depth, and what factors may influence noble gas ^{4}He concentrations.

5.3 Gas signatures of the Vale of Pickering

From research presented in Chapter 4, it is evident that geochemical fingerprints of gas and water samples from the Vale of Pickering allows for the identification of gas sources within the subsurface. A summary of the key conclusions from this research are highlighted in Figure 5.2, and are as follows:

- From hydrocarbon abundances (C_1/C_2+C_3) and $\delta^{13}C_{CH4}$ and δD_{CH4} stable isotopes, we identify that there are two distinct methane sources. Methane in the shallow and Corallian aquifers being of biogenic origin, and methane from gas samples collected from the Kirkham Abbey Formation displaying a thermogenic origin.
- $^{3}He/^{4}He$ and $^{4}He/^{20}Ne$ ratios are elevated in comparison to atmospheric values, and plot near or on the mixing line between the KM5 gas end member and the atmosphere. From this mixing model, the potential for mixing between deep thermogenic gas with atmospheric noble gases in the shallow subsurface is highlighted, with models showing an approximate 2 to 50% of radiogenic ^{4}He present in groundwater samples.
- Through calculating theoretical ^{4}He generation profiles for key units within the Vale of Pickering stratigraphy, it is evident that measured ^{4}He concentrations cannot be

generated from the in-situ decay of U and Th alone. Therefore, ^{4}He must be sourced from an external radiogenic flux from depth.

- $CH_4/^{36}Ar$ groundwater values exceed the $CH_4/^{36}Ar$ saturation values, indicating groundwater equilibrium with a methane rich source at greater depths.

From this research, it is clear that there is a ^{4}He flux within the Vale of Pickering subsurface, as ^{4}He concentrations are elevated compared to ASW values, and cannot be accounted from the in-situ decay of U and Th alone.

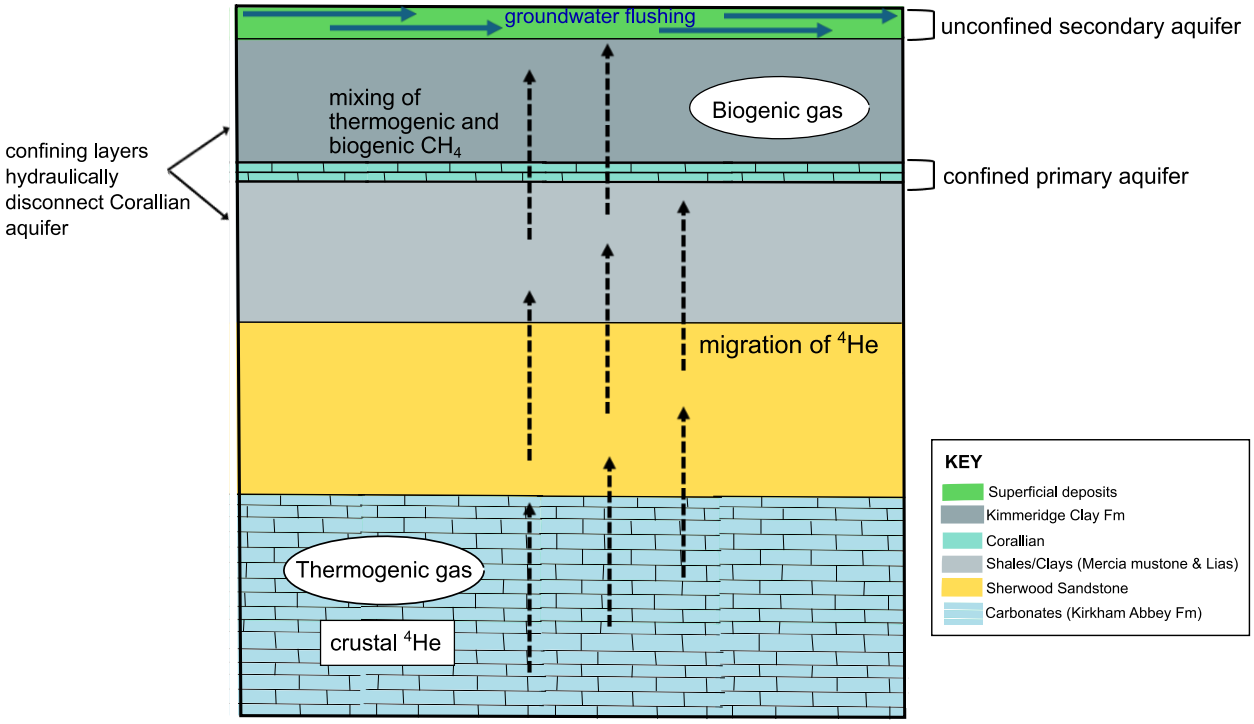

Figure 5-2: Conceptual diagram of Vale of Pickering subsurface, highlighting the hydraulically disconnected Corallian aquifer and unconfined, shallow superficial aquifer. The two identified methane sources are highlighted, with methane produced biogenically in shallower depths, and thermogenic methane within the primary reservoir of the Kirkham Abbey Formation. The migration of a crustal radiogenic ^{4}He signature from depth is shown, which is lost in the superficial aquifer due to shallow groundwater flushing.

5.4 Conceptual model

Due to the inherent complexity associated with groundwater systems within the subsurface, simplification is necessary to capture the key controlling mechanisms of a system (Kruse and Younger, 2009). A conceptual model can be defined as:

"An evolving hypothesis identifying the important features, processes and events controlling fluid flow and contaminant transport of consequence at a specific field site in the context of a recognized problem."

NRC, 2001

The development of a conceptual model (Figure 5.2) can then be used to mathematically model hydrogeological environments and processes within the subsurface (e.g. head distributions, mass transport etc.). Whilst conceptual models can be used in both analytical and numerical modelling of systems, numerical modelling has the ability to model a system that is heterogeneous, with complex boundaries, source terms etc. As such, it is the standard approach used for modelling coupled groundwater and mass transport scenarios.

Developed groundwater models never truly represent the complexity of the natural world, and as such, have an associated level of uncertainty that must be evaluated (Anderson and Woessner, 2015). As a simplification, the model that has been developed assumes that the subsurface is fully saturated. The material groups modelled are assumed to be homogeneous and isotopic, and storage has not been considered (i.e. the model is at steady state).

In order to investigate ^{4}He signatures at the Vale of Pickering three scenarios are modelled:

1. A diffusion/dispersion model simulating the ^{4}He signature of thermogenic gas from depth to the surface
2. A diffusion/dispersion model with groundwater flushing of ASW simulated in the Sherwood Sandstone units
3. A diffusion/dispersion model with groundwater flushing of ASW simulated in the shallow superficial deposits.

5.5 Modelling approach

As discussed in Chapter 2, thermal, hydraulic, mechanical, or chemical processes are described by balance equations based on the conservation of either mass or energy. For this model, a coupled hydro-chemical process model was constructed to investigate the transport of He noble gas within the subsurface of the Vale of Pickering site. The open-source finite element code OpenGeoSys (OGS) (Kolditz et al., 2012) was used, which is specifically developed to model coupled thermal, hydraulic, mechanical, and chemical (THMC) processes within porous and fractured media. OGS has been fully benchmarked against a number of test cases as described in 'Thermo-Hydro-Mechanical-Chemical Processes in Fractured Porous Media: Modelling and Benchmarking' (Shao, 2015). The 2D mesh used for this model was constructed using GMSH, an automatic mesh generator software (Geuzaine and Remacle, 2009). Full derivations of the groundwater and mass transport equations are provided in Appendix B.

As previously discussed within Chapter 2, for this hydro-chemical model, the governing equations for hydraulic flow and chemical transport are applied. The three-dimensional balance equation from Darcy's Law is:

$$S_s \frac{\partial h}{\partial t} = \frac{\partial}{\partial x}\left(K_x \frac{\partial h}{\partial x}\right) + \frac{\partial}{\partial y}\left(K_y \frac{\partial h}{\partial y}\right) + \frac{\partial}{\partial z}\left(K_z \frac{\partial h}{\partial z}\right) - Q$$

Equation 5.1

Where K is hydraulic conductivity (m/s), *S*s is the specific storage, t is time (s), h is $\mathrm{hydraulic\ head\ (m)}$ and Q is the volumetric flow rate (m^3/s). This equation is valid for a saturated, non-deforming porous medium with heterogeneous hydraulic conductivity. The steady-state model in this study was calculated with specific storage (S_s) equal to zero.

Chemical (mass) transport is controlled by advection/and or diffusion and can be described through the mass balance equation:

$$\frac{\partial C}{\partial t} + \nabla . (vC - D\nabla C) = 0$$

Equation 5.2

Where C is the concentration (kg/m^3), t is the time (s), D is the hydrodynamic dispersion coefficient (m^2/s), v is advective velocity (m/s), with the system being modelled as having no source or sink terms (=0). For transport of noble gases within a closed system controlled by diffusion, this is solved by Equation 5.3:

$$\frac{\delta C}{\delta t} = D^* \frac{\delta^2 C}{\delta x^2}$$

Equation 5.3

Where concentration (C), at time (t), and distance (x). D^* is the apparent diffusion co-efficient (m^2/s), and can be calculated using the Wilke-Chang (1955) estimation method:

$$D^o_{AB} = \frac{7.4X10^{-8}(\phi M_B)^{\frac{1}{2}}T}{\eta_B V_A^{0.6}}$$

Equation 5.4

Where $D^o{}_{AB}$ is the diffusion coefficient of solute A (noble gas) at low concentrations within solvent B (water) (cm^2/s), f is the association factor of solvent B (2.6 for water), M_B is the molecular weight of solvent B (g/mol), T is temperature (K), η_B is the viscosity of solvent B (cP), and V_A the molar volume of solute A at its normal boiling temperature (cm^3/mol).

5.5.1 Model parameterisation

5.5.1.1 Geometry and Material Properties

The Vale of Pickering is situated on the southern margin of the Cleveland Basin, which comprises of folded, faulted and eroded Carboniferous units over 3000m thick (Fraser & Gawthorpe, 1990; Ward et al., 2018). The basin itself was a major depositional centre, and

consisted of 1500-2000m thick Permian, Triassic, and Jurassic deposits (Bearcock et al., 2015; Ward et al., 2018) (Figure 5.3). The Kirkham Abbey Formation, deposited during the Permian, consists of carbonate and evaporite deposits and makes up one of several distinct geological formations of the Zechstein Group. For the Vale of Pickering gas fields, the Kirkham Abbey Formation is the primary reservoir (Bearcock et al., 2015). Overlying the Permian deposits is the Sherwood Sandstone Group, consisting of fluvial sandstones and shale of the Triassic period. These are then overlain by the Triassic Mercia Mudstone Group and the Jurassic calcareous mudstones of the Oxford Clay Formation (Bearcock et al., 2015; Ward et al., 2018). These deposits are then overlain by the Corallian group, consisting primarily of ooidal and micritic limestones and calcareous fine-grained sandstones, but also include facies of muds, silts, and sands.

The Corallian group forms the major aquifer body in the area and is designated as a 'major resource' within the River Derwent catchment, used for both public and private supply (Ward et al., 2018). Within the Vale of Pickering area, the Corallian aquifer is confined both by the Kimmeridge Clay and Oxford Clay Formations, and hence is believed to be hydraulically disconnected from underlying and overlying strata. As such, it is thought that groundwater flow is predominately through fractures (Allen et al., 1997; Ward et al., 2018). Although the Corallian aquifer is regarded as a 'major resource', groundwater is not abstracted within the centre of the Vale of Pickering due to its depth exceeding 200m depth as a result of faulting, and due to its high salinity (Ward et al., 2018).

The Corallian Group is overlain by 400m thick Ampthill & Kimmeridge Clay deposits ('Kimmeridge Clay Formation') and comprise of fossiliferous marine mudstones. The Kimmeridge Clay Formation underlies the majority of the floor of the Vale of Pickering and is locally overlain by glaciofluvial and glaciolacustrine Quaternary superficial deposits (Ward et al., 2018). These local superficial deposits are designated as a 'secondary aquifer' within the Vale of Pickering area, as shallow (<50m depth) groundwater is used for small scale private use (Ward et al., 2018).

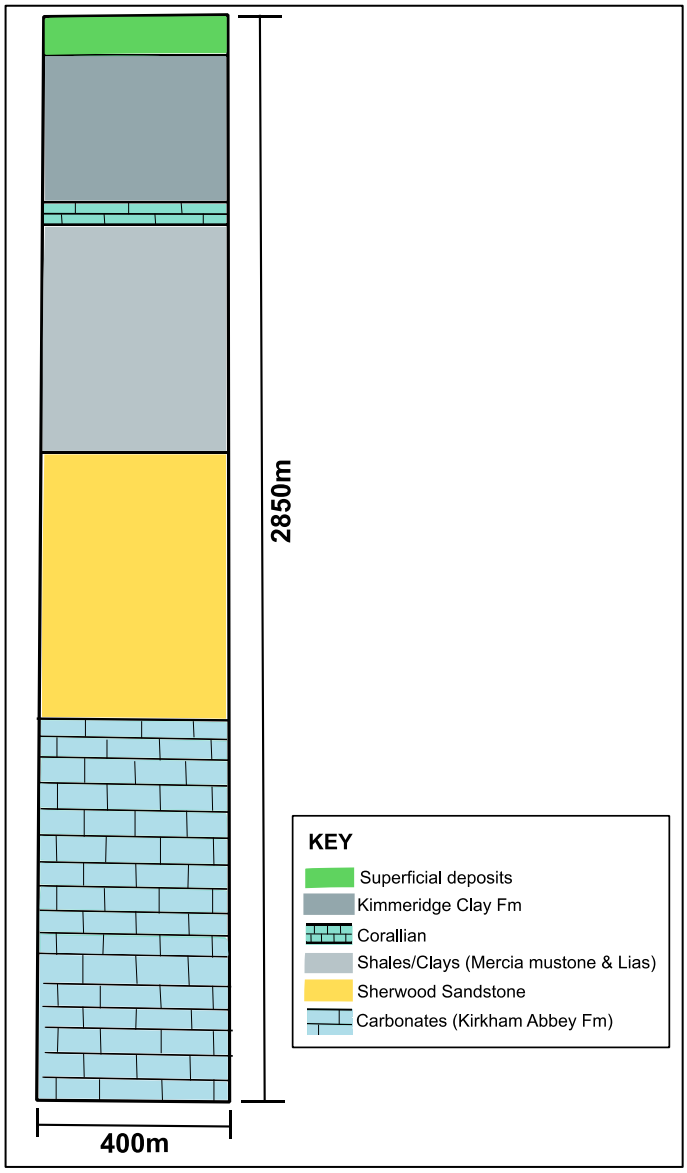

Figure 5-3: Representative 400m wide geological section of the Vale of Pickering stratigraphic units.

The model developed is a simplified vertical column section based on the Vale of Pickering subsurface, with six representative geological units:

- A carbonate unit (representative of the reservoir Kirkham Abbey Formation - KAF).
- Fine to medium grained sandstone (Sherwood Sandstone)
- A sequence of low permeability clays and shales (Mercia Mudstone and Lias Shales)
- A carbonate unit (Corallian aquifer)
- A sequence of low permeability clays (Kimmeridge Clays)
- Superficial glacio-fluvial and lacustrine unit

The six modelled geological units are assumed to be homogeneous, with the material properties used in the model highlighted in Table 5.1.

Table 5.1: Material properties used in models. Parameters for the Kimmeridge Clay estimated from Ivanovich and Alexander, 1985; Carbonate units estimated from Graf,1960 and Eisenbud and Gesell, 1997; and Sherwood sandstone parameters estimated from Andrews and Lee, 1979. Unit thicknesses are after Fraser & Gawthorpe, 1990 and Ward et al., 2018.

Material Properties	Porosity	Hydraulic conductivity (m/s)	Thickness (m)
Superficial deposits	30%	$1x10^{-5}$	100
Kimmeridge clay	40%	$1x10^{-9}$	400
Corallian	40%	$2x10^{-6}$	50
Shales	20%	$1x10^{-8}$	600
Sandstone	35%	$5x10^{-7}$	700
Carbonates (KAF)	20%	$2x10^{-6}$	1000

The depth and thickness of each unit within the model has been inferred from lithological data from borehole cutting samples and literature values from existing research (Fraser & Gawthorpe, 1990: Ward et al., 2018). As such, the depth of 2850m to the base of the carbonates is used in the model, with a width of 400m chosen to create a subsurface profile (Figure 5.4).

5.5.1.2 Boundary conditions

As He concentrations cannot be accounted for through ASW signatures or through the in-situ decay of U and Th, several models investigating the effect of diffusion and dispersion of a deeper sourced ^{4}He signature associated with thermogenic gases have been constructed.

Hydraulic head boundary conditions of 60m and 30m have been established at the base and surface of the model, in order to generate a hydraulic gradient. For the initial diffusion/dispersion model, a constant concentration boundary condition of 100% He concentration has been set at the base, reflective of measured sample concentrations. This concentration (C) models the deep gas KMB ^{4}He signature $4.91x10^{-4}$ cc (STP)/cc, with the concentration gradients modelled relative to C_0. In order to simulate the effect of groundwater flushing, polylines in the chosen stratigraphic unit (i.e. Sherwood Sandstone or shallow superficial deposits) were set up with a He concentration boundary condition representative of ASW, and a hydraulic head of 58m, to simulate groundwater flushing through the unit. These two representative units were chosen due to their aquifer properties and ability to have groundwater flushing, compared to the aquitard units above and below.

5.5.1.3 Component properties

For this model, noble gas depth dependent diffusion coefficients for ^{4}He were calculated using the Wilke-Chang (1955) estimation method:

$$D^{o}_{AB} = \frac{7.4X10^{-8}(\phi M_B)^{\frac{1}{2}}T}{\eta_B V_A^{0.6}}$$

Equation 5.5

Where D^{o}_{AB} is the diffusion coefficient of solute A (noble gas) at low concentrations within solvent B (water) (cm^2/s), f is the association factor of solvent B (2.6 for water), M_B is the molecular weight of solvent B (g/mol), T is temperature (K), η_B is the viscosity of solvent B (cP), and V_A the molar volume of solute A at its normal boiling temperature (cm^3/mol). From this, depth dependent diffusion coefficients for He is calculated (Table 5.2).

Table 5.2: Diffusion coefficients for He gas, based on the fluid composition, viscosity, and depth of the reservoir unit.

D_{AB}	m^2/s
He	4.32687E-07

5.5.2 Model assumptions and simplifications

As discussed in Section 5.4, a conceptual model is a simplification of reality. Therefore, there are associated assumptions, simplifications, and justifications (Kruse and Younger, 2009). As a simplification, all models developed as part of this research have assumed that groundwater is in steady state conditions, with the units being fully saturated. As with all flow models, there are uncertainties associated with the use of single scaled up parameter values to represent geological units, which is important to note when considering a diffusive model.

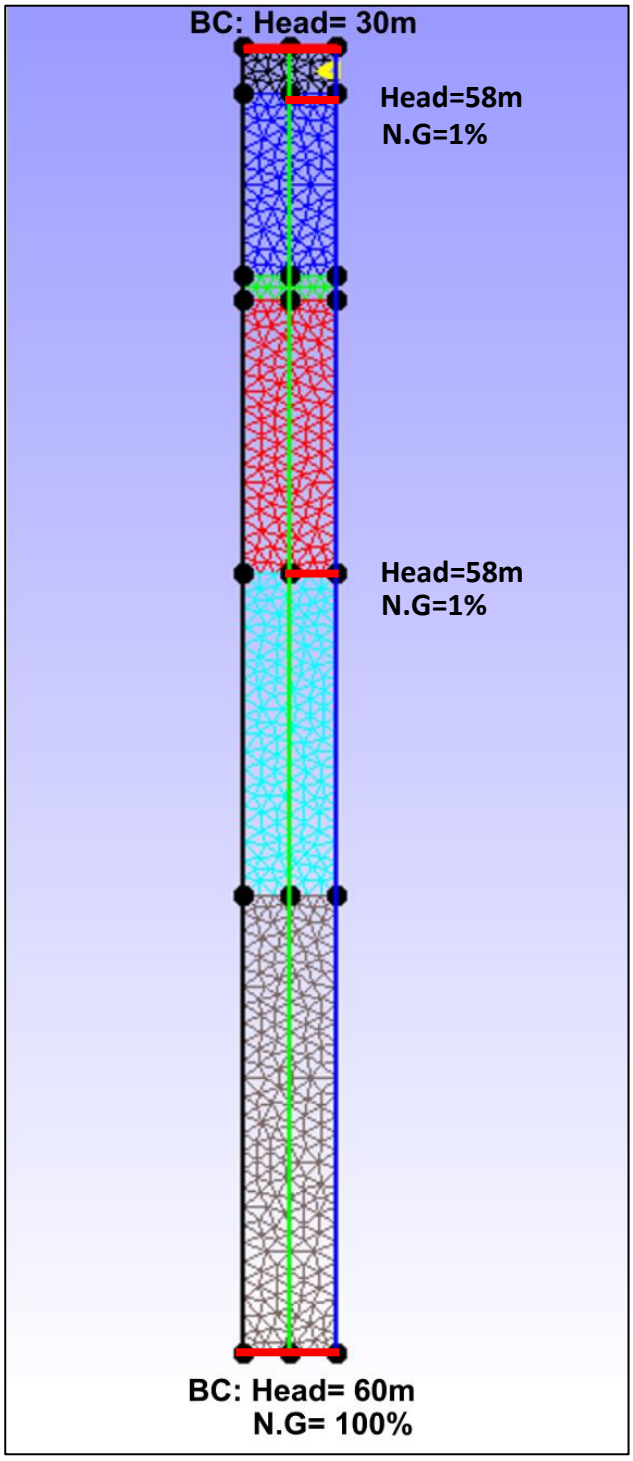

Figure 5-4: *Mesh (with a density of 40m) of the modelled section of the Vale of Pickering subsurface, with boundary conditions highlighted in red. At the base of the model, a boundary condition of 60m hydraulic head and He noble gas concentration (N.G.) of 100% is set. At the surface, a 30m hydraulic head is set up, to simulate an upward hydraulic gradient. The two locations of the groundwater flushing scenarios are highlighted (Sherwood Sandstone and superficial deposits), with their associated ASW He concentrations and heads set as boundary conditions. Model results are obtained from the green centre polyline.*

5.6 Modelling Results

5.6.1 He migration via diffusion and dispersion of thermogenic gas

The results of the diffusion and dispersion model of He from depth are presented in Figures 5.5 and 5.6. Figure 5.5 highlights the induced flow direction is from the base of the model to the top, which is as expected when no regional groundwater gradient is considered. Modelled He % concentrations through time are shown in Figure 5.5, and highlight the diffusion and dispersion of He from depth to the surface.

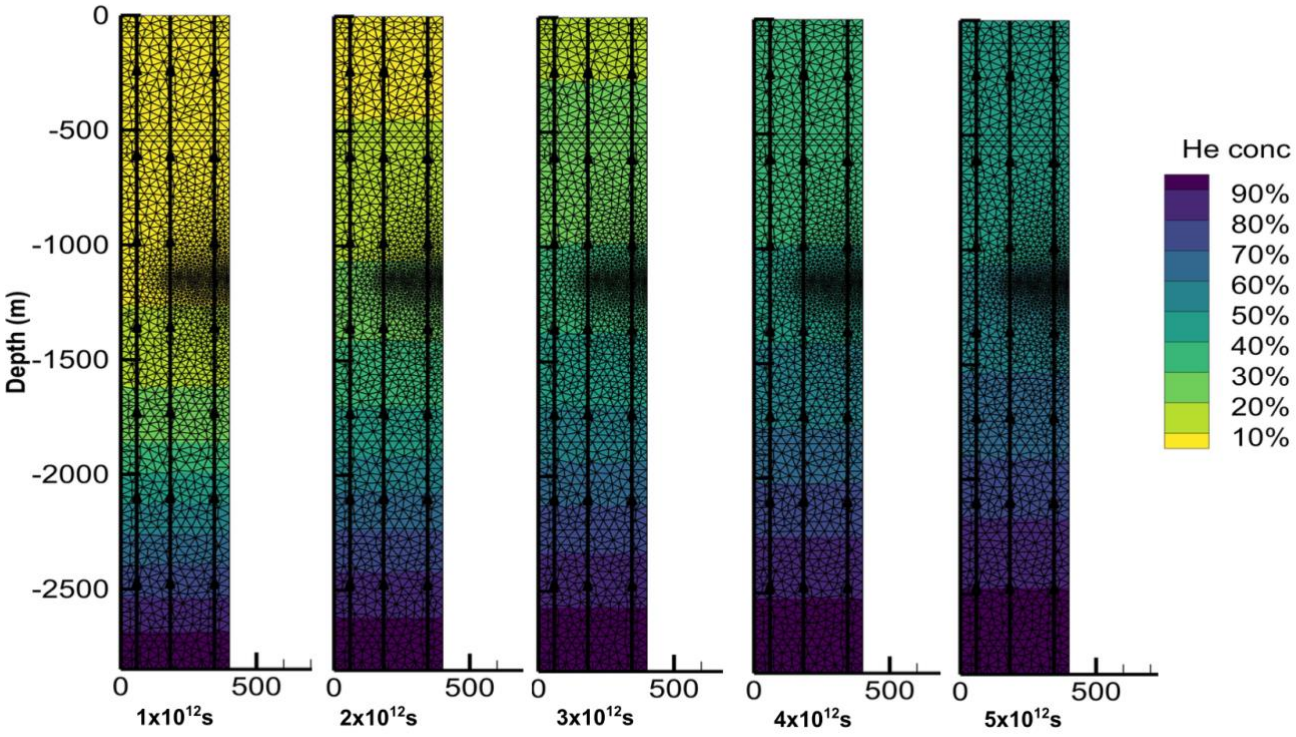

Figure 5-5: Modelled He concentration profiles in the subsurface over five time-steps as a result of diffusion and dispersion, with fluid velocity vectors highlighted.

The modelled % concentrations were converted to actual ^{4}He concentrations (cm^3 (STP)/cm^3) for the modelled diffusive ^{4}He profile through the subsurface (Figure 5.6). Figure 5.6 highlights the diffusive He trend from the base of the model at 2850m depth (Kirkham Abbey Formation) to the surface. Measured ^{4}He values from the Vale of Pickering subsurface are plotted alongside for reference.

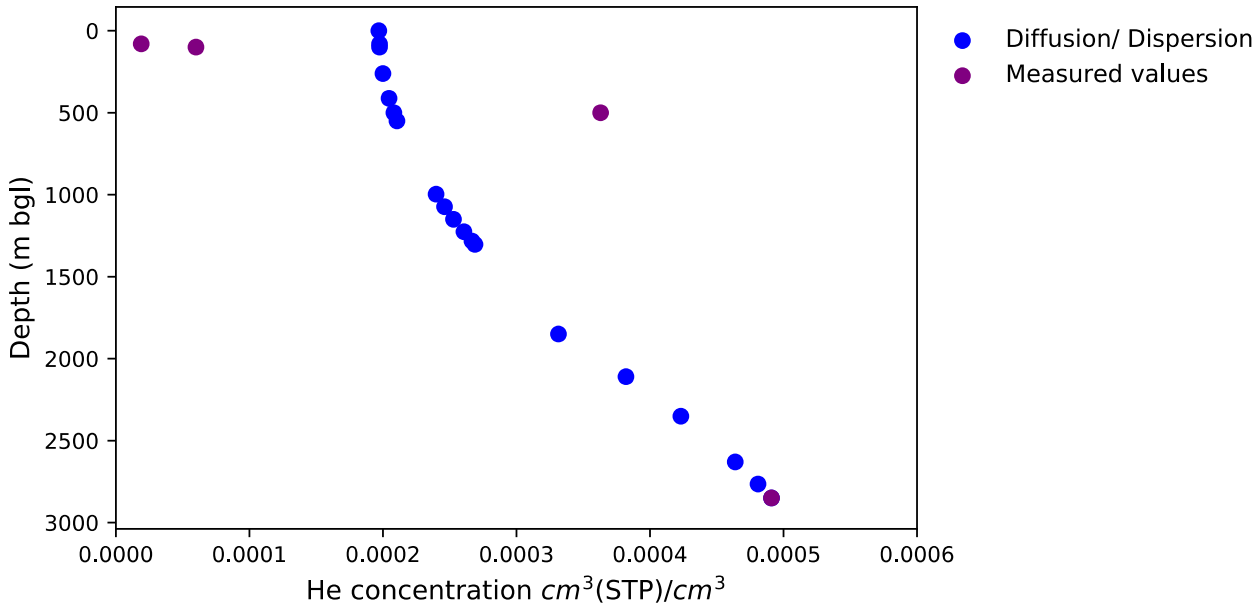

Figure 5-6: Modelled result of ^{4}He concentration profile with depth via diffusion/dispersion. Measured ^{4}He concentrations collected from the Vale of Pickering (purple) are plotted for comparison. It is evident that the modelled ^{4}He results do not correlate to measured ^{4}He values.

From the model, it is evident that diffusion and dispersion of the ^{4}He signature of the KMB thermogenic gas does not correlate to the measured values. The ^{4}He value measured in the confined Corallian aquifer is substantially larger than the modelled value, highlighting the possibility for a deeper sourced end member, with the superficial deposits having a lower ^{4}He concentration than is modelled. As such, it is clear that ^{4}He signatures with depth cannot be accounted for by the migration of ^{4}He through diffusion and dispersion alone.

5.6.2 Effect of groundwater flushing

The effect of groundwater flushing on the He signature within the subsurface is investigated at two modelled depths: within the Sherwood Sandstone units at 1150m, and within the Superficial aquifer deposits at 100m depth.

5.6.2.1 Scenario 1: Flushing in Sherwood Sandstone

^{4}He concentration profiles with depth over time is highlighted in Figure 5.7, with the end model ^{4}He concentrations with depth presented in Figure 5.8.

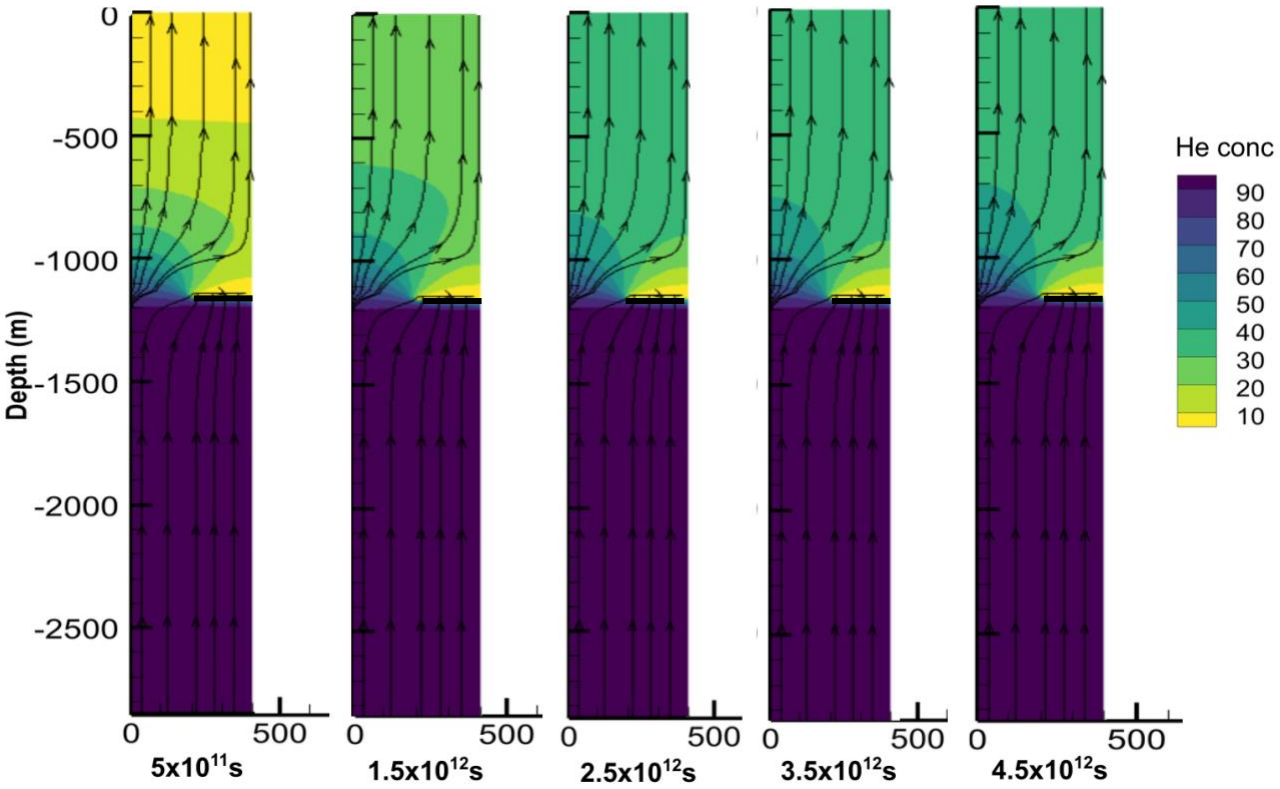

Figure 5-7: Modelled He concentration profiles in the subsurface over the five modelled time steps with fluid velocity vectors highlighted. The model presents the diffusion and dispersion of ^{4}He from thermogenic gas from depth, with groundwater flushing occurring at 1150m, releasing an ASW He signature into the model.

From the modelled results (Fig. 5.7), compared to the previous model, it is clear that groundwater flushing has an impact on He concentration, with He concentrations declining within 100m of the flushing to an ASW ^{4}He signature. It is evident that the modelled He signature more closely matches the measured He values at the Vale of Pickering compared to the diffusion/dispersion model. Modelled superficial values, whilst still higher than measured concentrations, are more reflective of a groundwater flushing signal. Again, it is apparent that the high ^{4}He signature observed in the Corallian aquifer cannot be accounted for through diffusion of KMB thermogenic gas. Due to the confined nature of the Corallian unit, it is

thought to be hydraulically disconnected from the overlying and underlying aquifer units, and so it is thought that it is not affected by groundwater flushing in the Sherwood Sandstone. Instead, the high ^{4}He values indicate the potential for a deeper external flux migrating from depth.

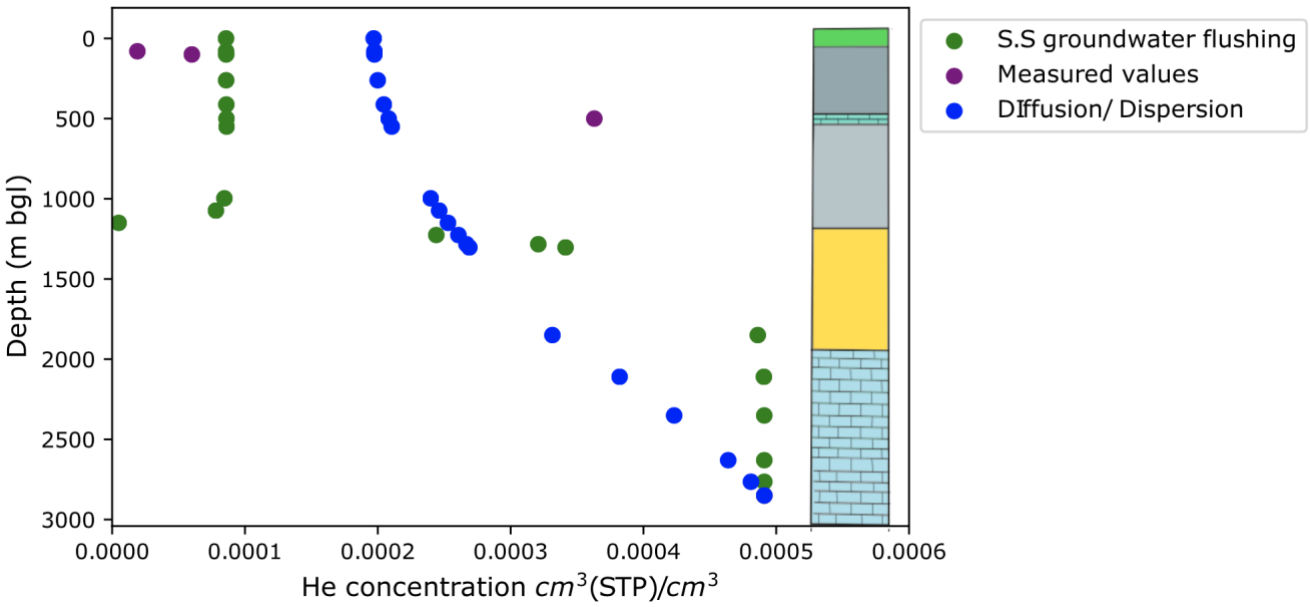

Figure *5-8:* Modelled result of ^{4}He concentration profile with depth via diffusion/dispersion of thermogenic gas (blue). Groundwater flushing is simulated at 1150m depth in the Sherwood Sandstone units, releasing an ASW signature into the subsurface (green). Measured ^{4}He concentrations collected from the Vale of Pickering (purple) are plotted for comparison. It is evident groundwater flushing has an impact on He concentration, with ^{4}He concentrations declining within 100m of the flushing to an ASW signature. Modelled superficial values, are more reflective of a groundwater flushing signal, though are still higher than measured concentrations. The high ^{4}He signature observed in the Corallian aquifer cannot be accounted for through diffusion and groundwater flushing of the KMB thermogenic gas. Due to the confined nature of the Corallian unit, it is thought to be hydraulically disconnected from the overlying and underlying aquifer units.

5.6.2.2 Scenario 2: Flushing in Superficial deposits

It is apparent that that confined Corallian aquifer is hydraulically disconnected from the overlying aquifer units, and so measured ^{4}He signatures from the Corallian are not affected from groundwater flushing within the subsurface. The model was set up to simulate shallow groundwater flushing within the unconfined superficial aquifer. ^{4}He concentration profiles with depth over time is highlighted in Figure 5.9, with the end model ^{4}He concentrations with depth presented in Figure 5.10.

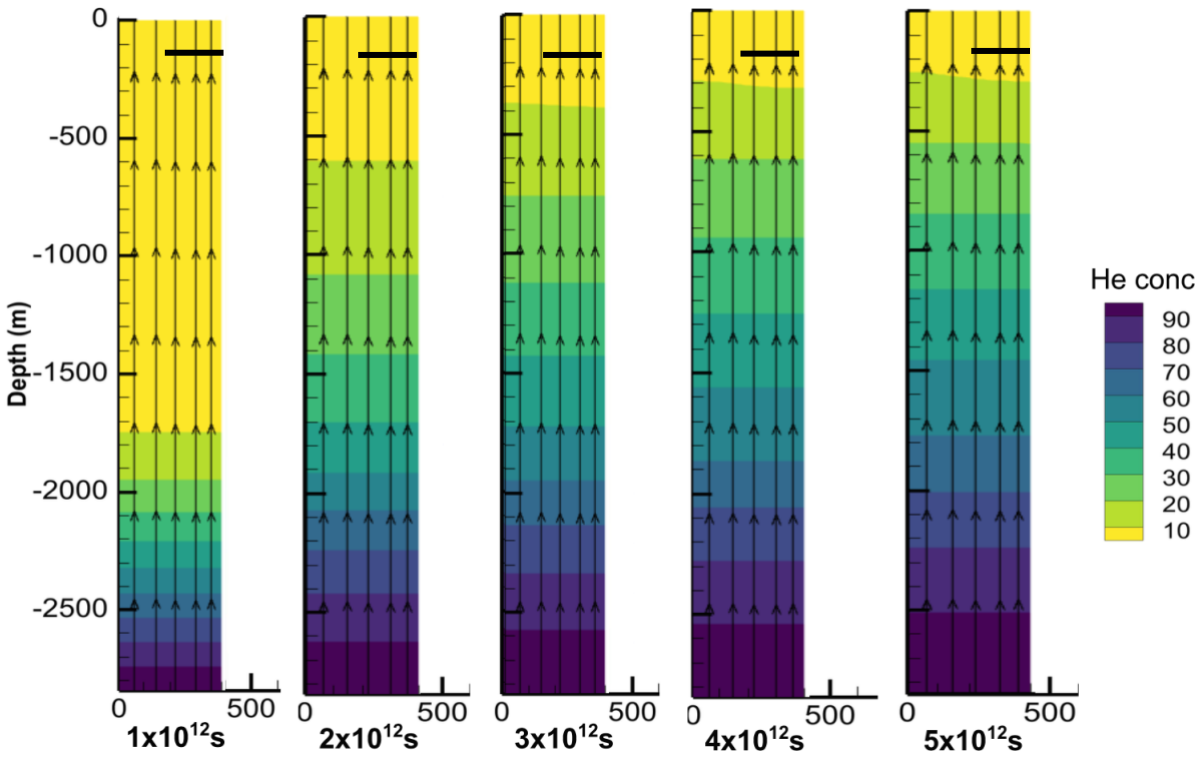

Figure 5-9: Modelled He concentration profiles in the subsurface over the five modelled time steps with fluid velocity vectors highlighted. The model presents the diffusion and dispersion of ^{4}He from thermogenic gas from depth, with groundwater flushing occurring within the shallow superficial deposits, within 100m of the surface (highlighted by the black line).

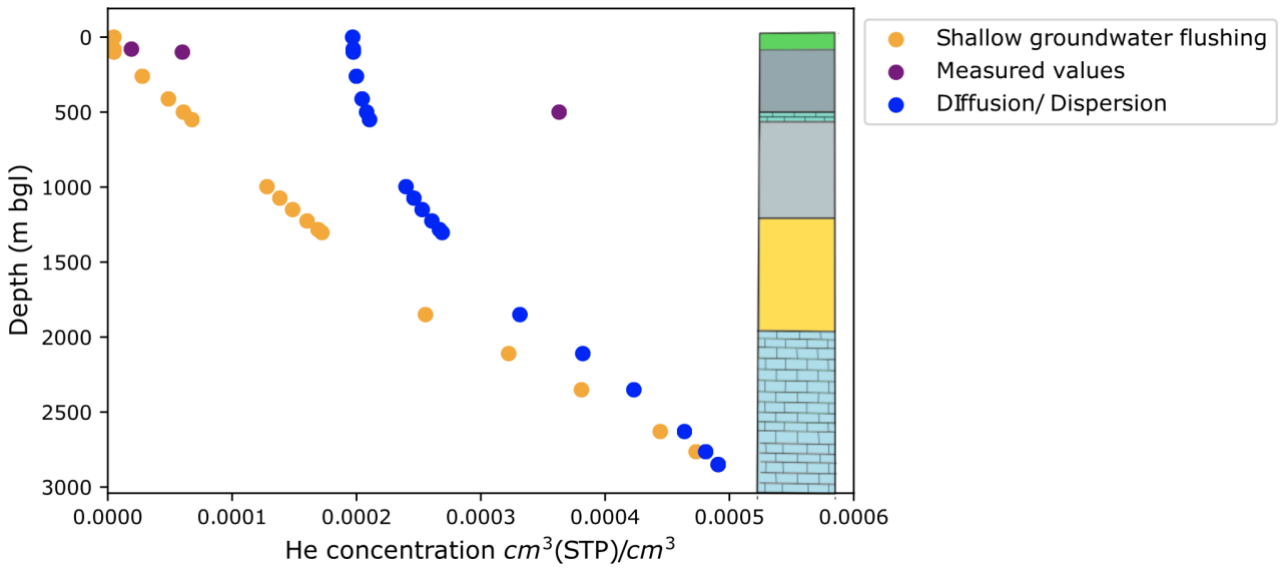

Figure 5-10: Modelled result of ^{4}He concentration profile with depth via diffusion/dispersion of thermogenic gas. Groundwater flushing is simulated in the shallow superficial deposits, within 100m of the surface. Measured ^{4}He concentrations collected from the Vale of Pickering (purple) are plotted for comparison. Shallow groundwater flushing within the superficial deposits closely match the measured ^{4}He concentrations in the Vale of Pickering groundwater. As such, it is thought that a deep ^{4}He external source is migrating from depth before shallow groundwater flushing results in a decrease in concentration to near ASW values.

From modelled ^{4}He profiles, shallow groundwater flushing within superficial deposits closely match the measured ^{4}He concentrations in shallow groundwater samples collected at the Vale of Pickering. Therefore, it is thought that a deep ^{4}He external source is migrating from depth before shallow groundwater flushing results in a decrease in concentration to near ASW values. From the modelled simulations, shallow groundwater flushing within the superficial deposits is assumed to be the more likely than flushing within the Sherwood Sandstone.

5.6.3 Model limitations and future work

This model simulates a simplified and generic steady state model, in order to initially investigate the ^{4}He signature within the Vale of Pickering subsurface. Assumptions such as material groups modelled as homogeneous and isotopic, storage not being considered (i.e. the model is at steady state), and estimations of material group model parameters such as

porosity and hydraulic conductivity values results in associated error and uncertainty in modelled results. Investigations into the potential effect of reducing the Kimmeridge Clay thickness from the regional 400m to a site-specific thickness of approximately 150m show that there is no effect on the ^{4}He diffusive profile with depth (Figure 5.11).

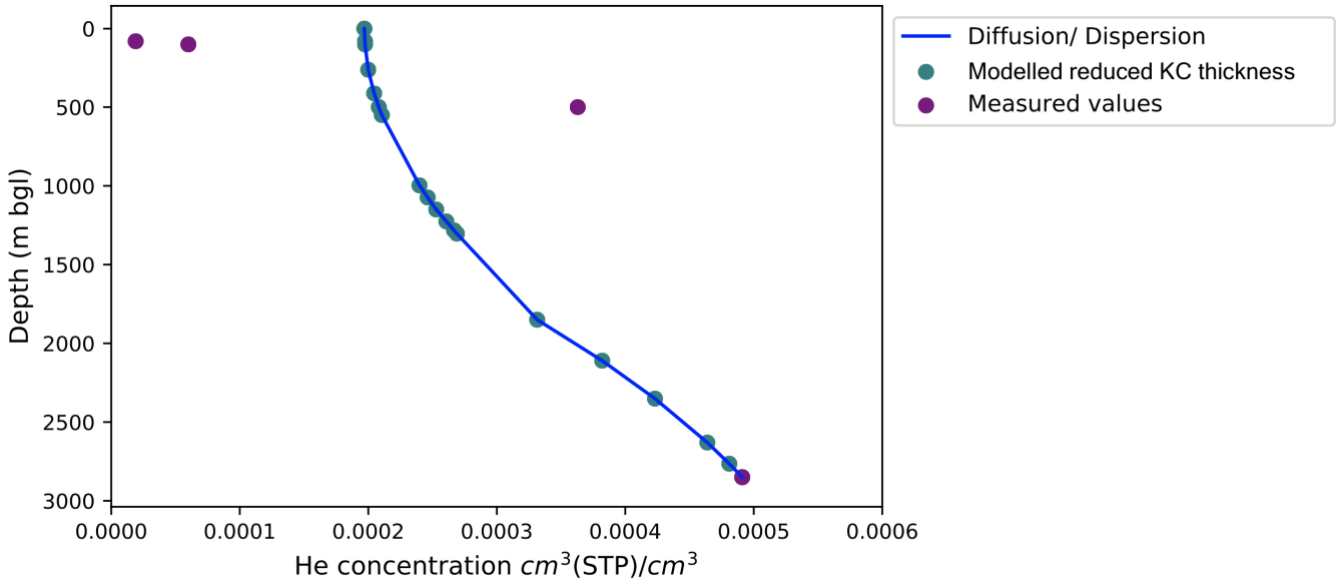

Figure 5-11: Modelled diffusion profile with reduced Kimmeridge Clay thickness (light blue dots) plotted against depth, alongside previous diffusive profile of increased Kimmeridge Clay thickness (blue line). As highlighted, there is no effect on the diffusive ^{4}He signature. Measured ^{4}He concentrations collected from the Vale of Pickering (purple) are plotted for comparison.

The hydro chemical model developed also does not take into account potential additional sources of ^{4}He within the subsurface (such as in situ generation), with the model simply modelling diffusion of ^{4}He from depth and subsequent groundwater flushing.

This model highlights the results of an initial investigation into the ^{4}He signatures of the Vale of Pickering, through the modelling of the migration of radiogenic ^{4}He with depth from thermogenic gases, and the effect of groundwater flushing of ^{4}He concentrations. The modelling results are restricted by the limited ^{4}He measured concentrations obtained with depth, which could be used to better discretise the high ^{4}He signature within the confined Corallian aquifer. Future work into developing the coupled hydro-chemical model could

include the modelling of additional ^{4}He sources within the subsurface, such as the in-situ generation of He from U and Th within the stratigraphy.

5.7 Discussion

5.7.1 Implications for the use of modelling and geochemical fingerprinting techniques

As part of the energy transition and development of geoenergy technologies, the use and importance of geochemical fingerprinting techniques to quantify the origin and migration of crustal fluids at various timescales has increased. Such geochemical tools are needed in order to address the associated environmental concerns over the potential for shallow aquifer contamination.

Through establishing a baseline for the Vale of Pickering site, it is evident that whilst there are two distinct sources of methane within the subsurface- shallow biogenic and deeper thermogenic derived from the Kirkham Abbey Formation, there is also evidence of elevated ^{4}He signatures compared to shallow ASW values. As such, through noble gas fingerprinting techniques, it is established that measured ^{4}He concentrations cannot be generated from the in-situ decay of U and Th alone, with the potential for mixing between deep thermogenic gas with atmospheric noble gases in the shallow subsurface. Coupled with hydro-chemical modelling, it is evident that crustal radiogenic ^{4}He is migrating from depth to the shallow subsurface, with the ^{4}He signature in the unconfined superficial aquifer being that of ASW due to groundwater flushing. The Corallian aquifer, hydraulically disconnected from the overlying units, still exhibits this high ^{4}He signature. Coupled process modelling also highlights that single phase flow cannot account for the high ^{4}He signature within the Corallian aquifer.

The Vale of Pickering's high ^{4}He signature and the potential of mixing between deep thermogenic gas with shallow biogenically derived methane highlights the complex gas interactions and gas migration within the subsurface, even prior to any geoenergy development. As such, this research highlights the need for an understanding of the fluid

migration pathways and use of coupled geochemical fingerprinting techniques in the establishment of environmental baselines, as characteristic 'key' geochemical tools, such as ^{4}He, that may be used as definitive evidence of fugitive gas migration, may be exhibiting the 'natural' geochemical baseline of the site pre-development.

5.8 Conclusions

Through the development of a coupled hydro-chemical model, ^{4}He gas concentrations and how they change within a simplified Vale of Pickering subsurface was investigated. From previous research discussed within Chapter 4, we show that $^{3}He/^{4}He$ and $^{4}He/^{20}Ne$ ratios are elevated in comparison to atmospheric values, and plot near or on the mixing line between the thermogenic gas end member and the atmosphere. From simple mixing models, the potential for mixing between deep thermogenic gas with atmospheric noble gases in the shallow subsurface was shown, with models showing an approximate 2 to 50% of radiogenic ^{4}He present in groundwater samples. Through calculating theoretical ^{4}He generation profiles for key units within the stratigraphy, we highlight that measured ^{4}He concentrations cannot be generated from the in-situ decay of U and Th alone and therefore ^{4}He must be sourced from an external radiogenic flux from depth.

In order to investigate the measured ^{4}He signature, three modelled scenarios were investigated. The diffusion and dispersion model of deep thermogenic ^{4}He gas migrating from depth to the surface did not produce He concentrations that matched measured sample values, with the Corallian aquifer having significantly larger concentrations than modelled, and the shallow superficial deposits having smaller measured concentrations. Through simulating groundwater flushing in the Sherwood Sandstone and the shallow superficial deposits, we show that shallow groundwater flushing reduces the ^{4}He signature migrating from depth to near an ASW He signature. High ^{4}He concentrations within the Corallian aquifer is thought to be a result of a deeper external source of radiogenic ^{4}He than is modelled, which is not affected by groundwater flushing due to its confined nature within the subsurface.

5.9 References

Allen, D.J., Brewerton, L.J., Coleby, L.M., Gibbs, B.R., Lewis, M.A., MacDonald, A.M., Wagstaff, S.J. and Williams, A.T., 1997. The physical properties of major aquifers in England and Wales.

Anderson, M.P., Woessner, W.W. and Hunt, R.J., 1992. Applied groundwater modeling: Simulation of flow and advective transport. *Academic Press Inc., San Diego, CA. Journal of Hydrology*, *140*, pp.393-395.

Ballentine, C. J., Burgess, R. and Marty, B. (2002) 'Tracing Fluid Origin, Transport and Interaction in the Crust', Reviews in Mineralogy and Geochemistry, 47(1), pp. 539–614. doi:10.2138/rmg.2002.47.13.

Ballentine, C. J. and Burnard, P. G. (2002) 'Production, Release and Transport of Noble Gases in the Continental Crust', Reviews in Mineralogy and Geochemistry, 47(1), pp. 481–538. doi:10.2138/rmg.2002.47.12

Barker, J.F. and Fritz, P., 1981. Carbon isotope fractionation during microbial methane oxidation. *Nature*, *293*(5830), pp.289-291.

Bearcock, J.M., Smedley, P.L. and Milne, C.J., 2015. Baseline groundwater chemistry: the Corallian of the Vale of Pickering, Yorkshire.

Burnard, P. (2013). *The Noble Gases as Geochemical Tracers* (p. 391). New York: Springer.

Byrne, D.J., Barry, P.H., Lawson, M. and Ballentine, C.J., 2018. Noble gases in conventional and unconventional petroleum systems. *Geological Society, London, Special Publications*, *468*(1), pp.127-149.

Darrah, T. H., Vengosh, a., Jackson, R. B., Warner, N. R. and Poreda, R. J. (2014) 'Noble gases identify the mechanisms of fugitive gas contamination in drinking-water wells overlying the

Marcellus and Barnett Shales', Proceedings of the National Academy of Sciences, 111(39), pp. 14076–14081.

Darrah, T.H., Jackson, R.B., Vengosh, A., Warner, N.R., Whyte, C.J., Walsh, T.B., Kondash, A.J., Poreda, R.J. 2015. The evolution of Devonian hydrocarbon gases in shallow aquifers of the northern Appalachian Basin: Insights from integrating noble gas and hydrocarbon geochemistry. Geochimica et Cosmochimica Acta, 170, 321–355, https://doi.org/10.1016/j.gca.2015.09.006.

Dembicki, H. (2016). *Practical petroleum geochemistry for exploration and production*. Elsevier.

Fraser, A.J. & Gawthorpe, R.L. 1990. Tectono-stratigraphic development and hydrocarbon habitat of the Carboniferous in northern England. In: HARDMAN, R.F.P. & BROOKS, J. (eds) Tectonic Events Responsible for Britain's Oil and Gas Reserves. Geological Society, London, Special Publi- cations, 55, 49–86,

Geuzaine, C., & Remacle, J. F. (2009). Gmsh: A 3-D finite element mesh generator with built-in pre-and post-processing facilities. *International journal for numerical methods in engineering*, *79*(11), 1309-1331.

Györe, D., Gilfillan, S.M. and Stuart, F.M., 2017. Tracking the interaction between injected CO2 and reservoir fluids using noble gas isotopes in an analogue of large-scale carbon capture and storage. Applied geochemistry, 78, pp.116-128.

Kipfer, R., Aeschbach-Hertig, W., Peeters, F., & Stute, M. (2002). Noble gases in lakes and ground waters. *Reviews in mineralogy and geochemistry*, *47(1), 615-700.*

Kolditz, O., Bauer, S., Bilke, L., Böttcher, N., Delfs, J. O., Fischer, T., ... & Park, C. H., 2012. OpenGeoSys: an open-source initiative for numerical simulation of thermo- hydro-mechanical/chemical (THM/C) processes in porous media. Environmental Earth Sciences, 67(2), 589-599.

Kruse, N.A. and Younger, P.L. 2009. Development of thermodynamically-based models for simulation of hydrogeochemical processes coupled to channel flow processes in abandoned underground mines. *Applied Geochemistry*, **24**, 1301–1311, https://doi.org/10.1016/j.apgeochem.2009.04.003.

LeDoux S.T, Szynkiewicz, A., Faiia, A.M., Mayes, M.A., McKinney, M.L. and Dean, W.G., 2016. Chemical and isotope compositions of shallow groundwater in areas impacted by hydraulic fracturing and surface mining in the Central Appalachian Basin, Eastern United States. Applied geochemistry, 71, pp.73-85.

Lollar, B.S. and Ballentine, C.J., 2009. Insights into deep carbon derived from noble gases. Nature Geoscience, 2(8), pp.543-547.

Molofsky, L.J., Connor, J.A., Wylie, A.S., Wagner, T. and Farhat, S.K., 2013. Evaluation of methane sources in groundwater in northeastern Pennsylvania. *Groundwater*, *51*(3), pp.333-349.

Osborn, Stephen G., Avner Vengosh, Nathaniel R. Warner, and Robert B. Jackson. "Methane contamination of drinking water accompanying gas-well drilling and hydraulic fracturing." *proceedings of the National Academy of Sciences* 108, no. 20 (2011): 8172-8176.

Ozima, M. and Podosek, F. A. (2001) Noble Gas Geochemistry. 2nd edn. Cambridge: Cambridge University Press

Schoell, M., 1980. The hydrogen and carbon isotopic composition of methane from natural gases of various origins. Geochimica et Cosmochimica Acta, 44(5), pp.649-661.

Schoell, M., 1988. Multiple origins of methane in the Earth. Chemical geology, 71(1-3), pp.1-10.

Shao, K.G.W.B. 2015. *Thermo-Hydro-Mechanical-Chemical Processes in Fractured Porous Media: Modelling and Benchmarking*. Kolditz, O., Shao, H., Wang, W. and Bauer, S. (eds). Terrestrial Environmental Sciences, https://doi.org/10.1007/978- 3-319-11894-9.

Stuart M.E. 2012. Potential groundwater impact from exploitation of shale gas in the UK. British Geological Survey Open Report, OR/12/001. 33pp

Tecplot. 2023. Tecplot CFD visualisation and analysis tools https://www.tecplot.com/.

Ward, R.S., Smedley, P.L., Allen, G., Baptie, B.J., Cave, M.R., Daraktchieva, Z., Fisher, R., Hawthorn, D., Jones, D.G., Lewis, A. and Lowry, D., 2018. Environmental baseline monitoring: Phase III final report (2017-2018).

Whiticar, M.J., Faber, E. and Schoell, M., 1986. Biogenic methane formation in marine and freshwater environments: CO2 reduction vs. acetate fermentation—isotope evidence. *Geochimica et Cosmochimica Acta*, *50*(5), pp.693-709.

Whiticar, M. J. (1999) 'Carbon and hydrogen isotope systematics of bacterial formation and oxidation of methane', Chemical Geology, 161(1–3), pp. 291–314.

Wilke, C. R., and Chang, P., 1955. Correlation of diffusion coefficients in dilute solutions. AIChE Journal, 1(2), 264-270.

6 Summary and Future work

6.1 Chapter 3: Constraining the Geochemical Fingerprints of Gases from the UK Carboniferous Coal Measures at the Glasgow Geoenergy Observatories Field Site, Scotland.

6.1.1 Chapter summary

This chapter presents the first CH_4 and CO_2 concentration-depth and stable isotope ($\delta^{13}C_{CH4}$, $\delta^{13}C_{CO2}$, and δD_{CH4}) profiles obtained from UK mine workings within the Glasgow Geoenergy Observatory field site, which were used to investigate the variability of gas fingerprints within unmined Carboniferous coal measures and coal mine workings. It is evident that methane contained within the Carboniferous coal measures was produced biogenically, with carbonate reduction being the primary production pathway, and the potential for mixing of CH_4 produced from methyl-type fermentation.

Results show that there is no correlation between gas concentration and depth, as both CH_4 and CO_2 gas concentration values are highly variable and are closely linked to individual stratigraphic horizons. Stable isotope compositions of CH_4 ($\delta^{13}C_{CH4}$= -73.4‰ to -14.3‰; $\delta^{13}C_{CO2}$= -29‰ to -6.1‰; δD_{CH4}= -277‰ to -88‰) provide evidence of a biogenic source, with carbonate reduction being the primary pathway of CH_4 production. Gas samples collected at depths of 63 to 79m exhibit enrichments in $^{13}C_{CH4}$ and ^{2}H, indicating the oxidative consumption of CH_4. This correlates with their proximity to the Glasgow Ell mine workings, which will have increased exposure to O_2 from the atmosphere as a result of mining activities. CO_2 gas is more abundant than CH_4 throughout the succession in all three boreholes, exhibiting high $\delta^{13}C_{CO2}$ values relative to the CH_4 present. Gases from unmined bedrock exhibit the highest $\delta^{13}C_{CO2}$ values, with samples from near-surface superficial deposits having the lowest $\delta^{13}C_{CO2}$ values. $\delta^{13}C_{CO2}$ values become progressively lower at shallower depths (above 90m), which can be explained by the increasing influence of shallow groundwaters containing a mixture of dissolved marine carbonate minerals (~0‰) and soil gas CO_2 (-26‰) as depth decreases.

The comparison of ground gas data with core and cutting gas measurements is critical for the monitoring of geothermal and other geoenergy activities, as it allows for the sensitive measuring and tracking of key hazardous gases that may arise from subsurface use (Monaghan et al., 2022). This study highlights that the CO_2 contained in the subsurface below 100m depth is geochemically distinct from that of the shallow subsurface (0-90m depth), meaning that an increase of CO_2 levels at the near-surface originating from deeper mine workings below 100m from any potential perturbation of the system may be detectable using $\delta^{13}C$ measurements. By comparing our results to determined ground gas signatures, it is apparent that there is no evidence of ground gas being impacted by gas migration at present from the Glasgow Observatory mine workings.

The findings presented in this study provide an insight into the variability of mine derived gases within 200m of the surface, and highlight the presence of distinct gas signatures that are linked to individual stratigraphic horizons.

6.1.2 Future work

In this study, a limited data set from two shallow monitoring wells and one seismic well was collected and analysed for gas composition and stable isotopes ($\delta^{13}C_{CO2}$, $\delta^{13}C_{CH4}$, δD) at designated intervals within the subsurface. Future work should ensure that any samples collected are investigated for the potential of secondary processes that could affect the geochemical signature of samples (for example, oxidation). Further investigation into the gas migration of the site could also be explored through the utilisation of noble gas analysis, as noble gases allow for the better characterisation of gas transport mechanisms and fate within the subsurface.

Our results also highlight that as the CO_2 contained in the subsurface below 100m depth is geochemically distinct from that of the shallow subsurface (0-90m depth), an increase of CO_2 levels at the near-surface originating from deeper mine workings from any potential perturbation of the system may be detectable using $\delta^{13}C$ measurements. However, further work is required to ascertain the detection limit, and if gas migration processes would significantly change the $\delta^{13}C$ signature of the migrating CO_2.

Future work could also be conducted in the continuation of establishing a geochemical baseline for the Glasgow Geoenergy Observatory, as these gas baseline signatures can be integrated into larger environmental datasets (Monaghan et al., 2022) in order to generate a "time zero" records of the site. Such records are key in the future of the development of subsurface utilising geoenergy technologies and are key to informing fit-for-purpose monitoring operations and developing efficient geothermal infrastructures.

6.2 Chapter 4: Stable isotope and noble gas characterisation of subsurface methane from the Vale of Pickering, Yorkshire

6.2.1 Chapter summary

This study presents the geochemical characterisation of the subsurface of the Vale of Pickering site, which was originally intended for unconventional gas extraction, but is now being considered for potential geoenergy technology development. Gas and groundwater samples collected from superficial deposits, the Corallian aquifer, and deep stratigraphic horizons highlight that methane is present within fluids throughout the stratigraphy and is the dominant gas in all samples. Two distinct sources of methane are identified: methane in both the shallow superficial and Corallian groundwater samples being produced biogenically by CO_2 reduction, and methane contained within the Third Energy gas samples produced thermogenically at depth. This study also evidences the potential for the oxidation of methane within groundwater samples, as some groundwater samples which display a more enriched $^{13}C_{CH4}$ signature, with a fractionation of <55% for $^{13}C_{CH4}$ relative to $^{13}CCO_2$.

Noble gas analyses indicates that $^{3}He/^{4}He$ and $^{4}He/^{20}Ne$ ratios are elevated in comparison to atmospheric values, and plot near or on the mixing line between the KM5 gas end member and the atmosphere. This highlights the potential mixing of deep thermogenic gas with atmospheric noble gases in the shallow subsurface, with an approximate 2 to 50% of radiogenic ^{4}He present in groundwater samples. From ^{4}He generation calculations, it is apparent that measured ^{4}He concentrations cannot be generated from the in-situ decay of U and Th within the Vale of Pickering stratigraphy alone. As such, ^{4}He values must be sourced from an external radiogenic flux. $CH_4/^{36}Ar$ ratios exceed saturation values and indicate that groundwater is equilibrating with a methane rich source at depth.

This study highlights the beneficial use of noble gas geochemistry in conjunction with gas composition and stable isotope ratio to allow for the robust characterisation of geochemical signatures within the subsurface at the Vale of Pickering, and the identification of different methane sources within the subsurface.

6.2.2 Future work

In this study, groundwater and gas samples were collected from a limited number of localities within the Vale of Pickering. Future work should ensure that any samples collected are investigated for the potential of secondary processes that could affect the geochemical signature of samples (for example, oxidation). Further investigation into the gas migration of the site could also be explored through the utilisation of $\delta^{13}C_{CO2}$ stable isotope analysis of any potentially migrating CO_2 gas.

Future work could also be conducted into the widening of this geochemical characterisation dataset for more sites and stratigraphic depths for the Vale of Pickering, as well as the continuation of monitoring of geochemical baseline signatures within the subsurface. Such as geochemical baseline of the subsurface is key for the potential development of the Vale of Pickering as a future geoenergy technology site, as there is a need for a better understanding of potential fluid migration pathways, and the subsequent development of contamination monitoring strategies.

6.3 Chapter 5: Hydrogeological and mass transport modelling of radiogenic ^{4}He noble gas within the Vale of Pickering subsurface

6.3.1 Chapter summary

This chapter presents the development of a hydro-chemical model of a simplified section of the Vale of Pickering subsurface in order to investigate how ^{4}He gas concentrations change within a simplified Vale of Pickering subsurface. Three modelled scenarios were investigated: a diffusion/ dispersion model of ^{4}He gas migrating to the surface, and two groundwater flushing scenarios within the Sherwood Sandstone and superficial deposits, respectively. The diffusion and dispersion model of thermogenic ^{4}He gas migrating from depth to the surface did not produce He concentrations that matched measured sample values, with the Corallian aquifer having significantly larger concentrations than modelled, and the shallow superficial deposits having smaller measured concentrations.

Simulated groundwater flushing within the Sherwood Sandstone and superficial deposits highlights that shallow groundwater flushing reduces the ^{4}He signature migrating from depth to near an ASW He signature. The High ^{4}He concentrations within the Corallian aquifer is thought to be a result of a deeper external flux of radiogenic ^{4}He, which is not affected by groundwater flushing due to its confined nature within the subsurface.

6.3.2 Future work

In this study, a limited set of model conditions were investigated into the nature of ^{4}He signatures within the Vale of Pickering subsurface. Future work on developing this initial model could be completed through the expansion of geochemical characterisation datasets for the Vale of Pickering. By collecting samples from more localities and at varied stratigraphic depths, a better understanding of the ^{4}He and other noble gas constituent profiles can be established. This in turn can feed into a better developed groundwater and mass transport model of the Vale of Pickering subsurface.

6.4 References

Monaghan, A.A., Starcher, V., Barron, H.F., Shorter, K., Walker-Verkuil, K., Elsome, J., Kearsey, T., Arkley, S., Hannis, S. and Callaghan, E., 2022. Drilling into mines for heat: geological synthesis of the UK Geoenergy Observatory in Glasgow and implications for mine water heat resources. Quarterly Journal of Engineering Geology and Hydrogeology, 55(1).

Appendix A- Full gas composition and stable isotope results

Table A.1: GGC01

Date sample obtained	**Type of storage of sample**	**Sample collected from drill depth start (m bgl)**	**Sample collected from drill depth end (m bgl)**	**SSK core sample number**	**IS (M) personal loan number**	**Gas Chromatography %**			**CH4 Data (‰)**		**CO2 Data (‰)**		
GGC01 Borehole						Air/N2	METHANE	CO2	$^{13}C_{vpdb}$	dD_{vsmow}	$^{13}C_{vpdb}$	$^{18}O_{vpdb}$	$^{18}O_{vsmow}$
28/11/2018	N_2 - isojar	44.88	44.93	105860	1198	99.1	0.0	0.9					
28/11/2018	De-ionised - isojar	44.88	44.93	105861	1198	99.0	0.0	1.0					
29/11/2018	N_2 - isojar	57.70	57.75	105872	1198	98.8	0.0	1.2					
29/11/2018	De-ionised - isojar	57.70	57.75	105873	1198	99.7	0.0	0.3					
29/11/2018	N_2 - isojar	68.30	68.35	105884	1198	100.0	0.0	0.0					

29/11/2018	De-ionised - isojar	68.30	68.35	105885	1198	100.0	0.0	0.0					
30/11/2018	N_2 - isojar	78.65	78.70	105468	1198	99.2	0.3	0.5					
30/11/2018	De-ionised - isojar	78.65	78.70	105469	1198	99.2	0.8	0.0					
30/11/2018	N_2 - isojar	88.77	88.82	105480	1198	99.3	0.4	0.3	-71.6	-249			
30/11/2018	De-ionised - isojar	88.77	88.82	105481	1198	96.1	1.4	2.5	-73.4	-251			
03/12/2018	N_2 - isojar	100.25	100.30	105492	1198	99.1	0.4	0.5			-6.1	-4.3	26.5
03/12/2018	De-ionised - isojar	100.25	100.30	105493	1198	96.2	1.0	2.7					
04/12/2018	N_2 - isojar	113.35	113.40	105508	1198	98.6	1.1	0.3					
04/12/2018	De-ionised - isojar	113.35	113.40	105509	1198	98.9	1.1	0.0					
04/12/2018	N_2 - isojar	123.16	123.21	105520	1198	97.7	0.4	1.8			-8.5	2.2	33.2

04/12/2018	De-ionised - isojar	123.16	123.21	105521	1198	97.2	0.9	1.9					
06/12/2018	N_2 - isojar	132.65	132.7	105528	1198	93.6	6.0	0.3	-68.3	-240			
06/12/2018	De-ionised - isojar	132.65	132.7	105529	1198	87.7	12.3	0.0	-68.3	-252			
07/12/2018	N_2 - isojar	143.16	143.21	105544	1198	98.7	1.0	0.4	-64.0	-242			
07/12/2018	De-ionised - isojar	143.16	143.21	105545	1198	97.3	2.6	0.2	-64.0	-277			
07/12/2018	N_2 - isojar	151.80	151.85	105552	1198	96.9	0.7	2.4					
07/12/2018	De-ionised - isojar	151.80	151.85	105553	1198	92.8	1.2	6.0					
10/12/2018	N_2 - isojar	161.69	161.74	105568	1198	97.8	1.7	0.5					
10/12/2018	De-ionised - isojar	161.69	161.74	105569	1198	95.8	3.3	1.0			-7.8	-0.4	30.5
11/12/2018	N_2 - isojar	174.80	174.85	105576	1198	98.8	1.0	0.2					

11/12/2018	De-ionised - isojar	174.80	174.85	105577	1198	97.8	2.2	0.0					
11/12/2018	N_2 - isojar	183.35	183.40	105592	1198	99.3	0.3	0.4			-12.7	-2.1	28.8
11/12/2018	De-ionised - isojar	183.35	183.40	105593	1198	99.1	0.9	0.1					
12/12/2018	N_2 - isojar	193.35	193.40	105604	1198	98.7	0.4	0.9					
12/12/2018	De-ionised - isojar	193.35	193.40	105605	1198	99.0	1.0	0.0					

Table A.2: GGA05

Date sample obtained	**Sample collected from drill depth start (m bgl)**	**Sample collected from drill depth end (m bgl)**	**SSK core sample number**	**Gas Chromatography %**				**CH4 Data (‰)**		**CO2 Data (‰)**		
GGA05 Borehole				Air/N2	METHANE	CO2	ETHANE	$^{13}C_{vpdb}$	dD_{vsmow}	$^{13}C_{vpdb}$	$^{18}O_{vpdb}$	$^{18}O_{vsmow}$
20/08/2019	18	19	105642	100.0	0.0	0.0	0.0					
20/08/2019	21	22	105643	99.3	0.0	0.7	0.0					
20/08/2019	24	25	105645	100.0	0.0	0.0	0.0					
22/08/2019	27	28	105646	100.0	0.0	0.0	0.0					
23/08/2019	30	31	105647	100.0	0.0	0.0	0.0					
04/09/2019	33	34	105657	98.5	0.0	1.5	0.0					
04/09/2019	36	37	105658	98.7	0.0	1.3	0.0			-22.49	2.21	33.183
05/09/2019	39	40	105659	99.0	0.0	1.0	0.0					
03/10/2019	42	43	105666	100.0	0.0	0.0	0.0					
04/10/2019	45	46	105667	100.0	0.0	0.0	0.0					
04/10/2019	48	49	105668	95.4	0.0	4.6	0.0			-11.06	4.05	35.088
04/10/2019	51	52	105671	99.8	0.0	0.2	0.0					
04/10/2019	54	55	105673	99.5	0.0	0.5	0.0					

04/10/2019	57	58	105674	54.4	45.4	0.0	0.1	-70	-182.4			
04/10/2019	60	61	105675	98.3	1.6	0.1	0.0	Too small				
07/10/2019	63	64	105676	97.1	2.6	0.3	0.0	-32.2	-122			
07/10/2019	66	67	105677	95.0	3.7	1.3	0.0	-14.3	17.3	-11.6	2.5	33.5
07/10/2019	69	70	105678	99.3	0.0	0.7	0.0					
07/10/2019	72	73	105683	97.6	0.0	2.4	0.0					
07/10/2019	75	76	105684	98.1	0.0	1.9	0.0					
08/10/2019	78	79	105685	99.5	0.0	0.5	0.0					
08/10/2019	81	82	105686	98.3	0.0	1.7	0.0			-10	2.59	33.584
08/10/2019	84	85	105689	99.1	0.0	0.9	0.0					
08/10/2019	87	88	105693	97.3	0.0	2.7	0.0			-29.03	-16.8	13.595

Table A.3: GGA08

Date sample obtained	**Sample collected from drill depth start (m bgl)**	**Sample collected from drill depth end (m bgl)**	**SSK core sample number**	**Gas Chromatography %**				**CH4 Data (‰)**		**CO2 Data (‰)**		
GGA08 Borehole				Air/N2	METHANE	CO2	ETHANE	$^{13}C_{vpdb}$	dD_{vsmow}	$^{13}C_{vpdb}$	$^{18}O_{vpdb}$	$^{18}O_{vsmow}$
29/08/2019	12	13	105648	100.0	0.0	0.0	0.0					
30/08/2019	15	16	105649	99.5	0.0	0.5	0.0					
02/09/2019	18	19	105651	98.4	0.0	1.6	0.0					
02/09/2019	21	22	105652	99.2	0.0	0.8	0.0					
02/09/2019	24	25	105653	98.6	0.0	1.4	0.0					
02/09/2019	27	28	105654	96.9	0.0	3.1	0.0			-25.46	-5.36	25.382
02/09/2019	30	31	105655	100.0	0.0	0.0	0.0					
02/09/2019	33	34	105656	97.0	0.0	3.0	0.0			-21.06	3.21	34.217
18/11/2019	36	37	105702	100.0	0.0	0.0	0.0					
18/11/2019	38	39	105701	95.4	4.6	0.0	0.1	-74.1	-259			
18/11/2019	39	40	105703	94.3	5.3	0.2	0.2	-70.5	-207.9			
18/11/2019	42	43	106024	100.0	0.0	0.0	0.0					
19/11/2019	45	46	106029	99.7	0.0	0.2	0.1					

19/11/2019	48	49	106031	99.7	0.0	0.3	0.0					
19/11/2019	51	52	106034	99.2	0.0	0.8	0.0					
19/11/2019	52	53	106032	92.7	0.8	6.6	0.0	too small		-18.3	2.2	33.2
19/11/2019	54	55	106033	98.4	0.0	1.6	0.0					
20/11/2019	57	58	106035	99.3	0.0	0.7	0.0					
20/11/2019	60	61	106037	99.3	0.0	0.7	0.0					
20/11/2019	63	64	105609	99.7	0.0	0.3	0.0					
21/11/2019	66	67	105610	98.6	1.2	0.2	0.0	-19.7	-94.7			
21/11/2019	69	70	105611	98.6	0.0	1.4	0.0			-15.24	-2.58	28.254
21/11/2019	72	73	105612	99.1	0.0	0.9	0.0					
21/11/2019	73	74	105613	96.6	0.0	3.4	0.0					
21/11/2019	75	76	105614	94.2	0.0	5.8	0.0			-12.93	3.72	34.748
21/11/2019	78	79	106041	98.0	1.5	0.5	0.1	-19.8	-87.8			
22/11/2019	81	82	106042	97.7	0.0	2.3	0.0					
22/11/2019	84	85	106043	100.0	0.0	0.0	0.0					
22/11/2019	87	88	106044	96.1	0.0	3.9	0.0			-11.43	3.79	34.816
22/11/2019	90	91	106045	97.1	0.0	2.9	0.0					

Table A.4: Measured C-H-O isotope values of CH_4 and CO_2 collected from GGERF site from boreholes GGC01, GGA05, and GGA08.

Borehole	Site	Sample Depths (m)	SSK Core sample No:	$\delta^{13}C_{CH4}$	δD_{CH4}	$\delta^{13}C_{CO2}$	$\delta^{18}O_{CO2\ (SMOW)}$
GGC01	GGERFS10	88	105480	-71.6	-249		
GGC01	GGERFS10	88	105481	-73.4	-251		
GGC01	GGERFS10	100	105492			-6.1	26.5
GGC01	GGERFS10	123	105520			-8.5	33.2
GGC01	GGERFS10	132	105528	-68.3	-240		
GGC01	GGERFS10	132	105529	-68.3	-252		
GGC01	GGERFS10	143	105544	-64.0	-242		
GGC01	GGERFS10	143	105545	-64.0	-277		
GGC01	GGERFS10	161	105569			-7.8	30.5
GGC01	GGERFS10	183	105592			-12.7	28.8
GGA05	GGERFS02	36-37	105658			-22.49	33.2
GGA05	GGERFS02	48-49	105668			-11.06	35.09
GGA05	GGERFS02	57-58	105674	-70.0	-182.4		
GGA05	GGERFS02	63-64	105676	-32.2	-122.0		
GGA05	GGERFS02	66-67	105677	-14.3	17.3	-11.6	33.5
GGA05	GGERFS02	81-82	105686			-10.0	33.58
GGA05	GGERFS02	87-88	105693			-29.03	13.6
GGA08	GGERFS03	27-28	105654			-25.46	25.38
GGA08	GGERFS03	33-34	105656			-21.06	34.22
GGA08	GGERFS03	38-39	105701	-74.1	-259		
GGA08	GGERFS03	39-40	105703	-70.5	-207.9		
GGA08	GGERFS03	52-53	106032			-18.3	33.2
GGA08	GGERFS03	66-67	105610	-19.7	-94.7		
GGA08	GGERFS03	69-70	105611			-15.24	28.25

GGA08	GGERFS03	75-76	105614			-12.93	34.75
GGA08	GGERFS03	78-79	106041	-19.8	-87.8		
GGA08	GGERFS03	87-88	106044			-11.43	34.82

Appendix B Model Theory

B1 Empirical Process Laws

B.1.1 Groundwater flow

In the1850's Henri Darcy established an empirical relationship of groundwater flow through the measuring of flux in sands. This relationship, known as Darcy's Law, states where the inflow into a control volume is equal to the outflow, there is a conservation of water. When a control volume has a cross-sectional area normal to the flow direction equal to *A* (m^2), Darcy velocity (q) can be calculated from volumetric flow rate (*Q* m^3/s) by:

$$\text{Darcy velocity} = q = \frac{Q}{A}$$

Equation B. 1

Darcy velocity (or specific discharge) has the units m/s, and was found to be directly proportional to changing hydraulic head (*h*) and inversely proportional to changing length (*l*). Hydraulic conductivity, K, is defined as a constant of proportionality and has the units m/s. K can be defined by the following equation:

$$K = \frac{q}{i}$$

Equation B.2

Where i is the hydraulic gradient. As such, by combining equations B.1 and B.2, the following equation can be written:

$$Q = AKi$$

Equation B.3

B1.2 Mass transport

Mathematical models of solute transport are based on the same principal of mass conservation which governs groundwater flow models. Applying this same principal to the control volume (Figure B.1), a transport model equation can be derived. Considering the mass stored in the control volume, dissolved mass equals $neΔxΔyΔzC$ where C is solute concentration. The sorbed mass is given by ΔxΔyΔz ρs with ρ = bulk density = mass of aquifer material divided by total volume [M/L3] and s = mass fraction of sorbed chemical. Therefore, the total mass of the chemical in the control volume:

$$neΔxΔyΔzC + ΔxΔyΔzρs$$

Equation B.4

Next, solute transport through the vertical faces of the control volume is considered. As solute mass is transported due to both advection and dispersion, there are two terms contributing to the mass flux F which is given by:

$$F=n_e vC\ n_e D-\mathrm{grad}C$$

Equation B.5

In this equation the first term represents the advective mass flux while the second term stands for the dispersive mass flux. The dispersive flux is assumed to be proportional to the concentration gradient (Fickian dispersion) and D is termed dispersion tensor. The negative sign indicates that the dispersive flux is oriented towards decreasing concentration values.

In order to quantify the net flux through the control volume, let F_x and $F_x + \frac{\partial F_x}{\partial x}\Delta x$ denote mass fluxes through faces perpendicular to the x-axis. This is identical to the assumptions used in groundwater flow.

Following the steps in the groundwater model, flux in minus flux out gives net flux of solute mass parallel to the x-axis:

$$F_x - \left(F_x + \frac{\partial F_x}{\partial x} \Delta x \right) = -\frac{\partial F_x}{\partial x} \Delta x$$

Equation B.6

Consequently, the net solute mass being transported through the vertical faces of the control volume within the time interval Δt [T] is given by:

$$-\left(\frac{\partial F_x}{\partial x} + \frac{\partial F_y}{\partial y} + \frac{\partial F_z}{\partial z} \right) \Delta x \Delta y \Delta z \Delta t \, .$$

Equation B.7

If there are no sources or sinks, the temporal change of mass in the control volume within the time interval Δt is the same as the net solute mass passing through the control volume. Therefore, we have mass balance:

$$\Delta x \Delta y \Delta z \left[\left(n_e C + \rho s \right)_{t+\Delta t} - \left(n_e C + \rho s \right)_t \right] = -\left(\frac{\partial F_x}{\partial x} + \frac{\partial F_y}{\partial y} + \frac{\partial F_z}{\partial z} \right) \Delta x \Delta y \Delta z \Delta t$$

Equation B.8

B.2 Groundwater flow equation derivation

Quantitative descriptions of groundwater flow are based on the conservation of water volume. In general, the conservation of volume is expressed by the relationship:

$$\frac{\Delta V_w}{\Delta t} = Q_{in} - Q_{out}$$

Equation B.9

The symbol Δ is used to represent a finite value, with V_w= volume of water contained within a control volume, Q_{in}= inflow into a control volume, and Q_{out}= outflow of the control volume. A control volume and this relationship is highlighted in Figure B.1. The equation above states that the temporal change of water volume in a certain time interval equals the difference of (total) inflow minus (total) outflow during the same time interval.

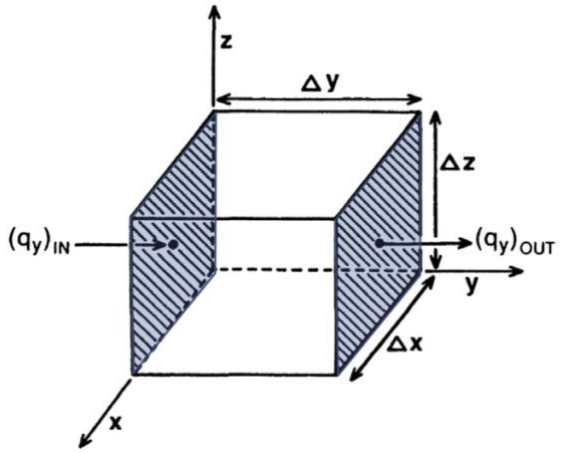

Figure B.1: Control volume ($\Delta x \Delta y \Delta z$) with inflows and outflows. Anderson et al., 2015.

The inflow for a control volume is given by:

$$Q_{in} = v_{fx}\Delta y\Delta z + v_{fy}\Delta x\Delta z + v_{fz}\Delta x\Delta y$$

Equation B.10

And the outflow of a control volume:

$$Q_{out} = \left(v_{fx} + \frac{\partial v_{fx}}{\partial x}\Delta x\right)\Delta y\Delta z + \left(v_{fy} + \frac{\partial v_{fy}}{\partial y}\Delta y\right)\Delta x\Delta z + \left(v_{fz} + \frac{\partial v_{fz}}{\partial z}\Delta z\right)\Delta x\Delta y$$

Equation B.11

Hence, the difference equals the net change of water volume within the control volume, which is equal to the change in storage:

$$Q_{in} - Q_{out} = -\frac{\partial v_{fx}}{\partial x}\Delta x \Delta y \Delta z - \frac{\partial v_{fy}}{\partial y}\Delta x \Delta y \Delta z - \frac{\partial v_{fz}}{\partial z}\Delta x \Delta y \Delta z$$

Equation B.12

The 3D groundwater flow equation for a confined aquifer can be written as:

$$S_s \frac{\partial h}{\partial t} = \frac{\partial}{\partial x}\left(K \frac{\partial h}{\partial x}\right) + \frac{\partial}{\partial y}\left(K \frac{\partial h}{\partial y}\right) + \frac{\partial}{\partial z}\left(K \frac{\partial h}{\partial z}\right) - Q$$

Equation B.13

Where Ss is defined as the specific storage, and Q= a source/sink term.